Turkish Journal of Civil Engineering

formerly
Teknik Dergi

Turkish Journal of Civil Engineering (formerly Teknik Dergi) Publication Principles

Turkish Journal of Civil Engineering (TJCE), a non-profit, open access scientific and technical periodical of UCTEA Chamber of Civil Engineers, publishes papers reporting original research work and major projects of interest in the area of civil engineering. TJCE annually publishes six issues and is open to papers in English and Turkish. It should be noted that TJCE (formerly, Teknik Dergi/ Technical Journal of Turkish Chamber of Civil Engineers) is being published regularly for more than 30 years since 1990. Main publication principles of TJCE are summarized below:

1. Articles reporting original scientific research and those reflecting interesting engineering applications are accepted for publication. To be classified as original, the work should either produce new scientific knowledge or add a genuinely new dimension to the existing knowledge or develop a totally new method or substantially improve an existing method.

2. Articles reporting preliminary results of scientific studies and those which do not qualify as full articles but provide useful information for the reader can be considered for publication as technical notes.

3. Discussions received from the readers of the published articles within three months from publication are reviewed by the Editorial Board and then published together with the closing remarks of the author.

4. Manuscripts submitted for publication are evaluated by two or three reviewers unknown to the authors. In the light of their reports, final decision to accept or decline is taken by the Editorial Board. General policy of the Board is to get the insufficient manuscripts improved in line with the reviewers' proposals. Articles that fail to reach the desired level are declined. Reasons behind decisions are not declared.

5. A signed statement is taken from the authors, declaring that the article has not been published as a "journal article or book chapter". In case the Editorial Board is in the opinion that the article has already been published elsewhere with minor changes or suspects plagiarism or a similar violation of ethics, then not only that article, but none of the articles of the same authors are published.

6. Papers reporting works presented as conference papers and developed further may be considered for publication. The conference it was presented to is given as a footnote in the first page.

7. Additionally, a document signed by all authors, transferring the copyright to UCTEA Chamber of Civil Engineers is submitted together with the manuscript.

Turkish Journal of Civil Engineering

formerly
Teknik Dergi

Turkish Journal of Civil Engineering (formerly Teknik Dergi)

Reviewers:

This list is renewed each year and includes reviewers who served in the last two years of publication.

CONTENTS

Behavior of Fiber Reinforced Concrete Beams with Inadequate Torsion Steel under Pure Torsion

Yılmaz Öğünç TETİK[1*]
Osman KAYA[2]

ABSTRACT

To investigate the relationship between reinforced concrete beams under pure torsion and steel fiber usage, 16 large-scaled reinforced concrete beams with inadequate torsion steel were designed and produced. For experiments, a new test setup was designed to allow specimens to have rotational movement on one end and axial movement on the other end. The variables were selected as reactangular beams with transverse reinforcement at 300 and 400 mm spacing of and steel fiber 0.0%, 0.3%, 0.6%, 0.9%, 1.2%, and 1.5% volumetric ratio of mixture as . Cracking torque, maximum torque and ultimate torque values were obtained experimentally, and torque-twist curves and energy dissipation capacities were determined. Findings were compared to indicate the relationship between variables. Results showed that certain values of steel fiber ratio as a replacement material for relevant spacing of transverse reinforcements.

Keywords: Reinforced concrete beam, pure torsional moment, steel fiber, energy dissipation capacity.

1. INTRODUCTION

Flexural moments and shear forces are primary considerations in the design of reinforced concrete (RC) beams. Although pure torsion rarely occurs in RC beams, the behavior of elements under pure torsion needs to be defined explicitly to understand their overall combined flexural and torsional response [1]. It is known that plain concrete beams under torsional loading typically fail in a brittle manner once tensile stresses exceed the tensile strength limit of the concrete. In torsional behavior, reinforcement contributes after the cracking, and it provides more ductile behavior. It is highlighted that reinforcement begins

1 Muğla Sıtkı Koçman University, Department of Civil Engineering, Muğla, Türkiye
   yilmazogunctetik@mu.edu.tr - https://orcid.org/0000-0002-0104-1555

2 Muğla Sıtkı Koçman University, Department of Civil Engineering, Muğla, Türkiye
   osmankaya@mu.edu.tr - https://orcid.org/0000-0003-3851-3082

* Corresponding author

to contribute to more ductile behavior after cracking, significantly influencing the torsional capacity of RC beams [2].

The researchers examined various factors affecting torsional behavior. The ratios of transverse and longitudinal reinforcement, known as the torsional reinforcement ratio, play a critical role [3], where excessive reinforcement can reduce torsional ductility [4]. Also, it is reported that the aspect ratio of the beam cross-section [5,6] and the compressive strength of the concrete have a considerable impact on designing [7]. Additional studies have observed that increases in compressive strength beyond a certain threshold lead to decreased twist angles and reduced ductility [8,9].

Steel fibers (SF) have been shown to enhance the crack resistance in reinforced concrete (RC) beams. SF contributes to a pseudo-ductile tensile response by transferring tensile stress across cracks and providing significant shear resistance [10]. It is also known that using steel fibers as shear reinforcements provides efficient ductility on RC beams [11]. Earlier experimental studies showed that concrete beams reinforced with steel fiber exhibit improved torsional strength [12]. When the behavior of plain concrete members reinforced with steel fibers was examined, it was observed that an increased steel fiber ratio provides greater torque capacity and enhances the first cracking load of the beam under pure torsion [13]. In other aspects, SF with a high-volume fraction in high-strength concrete (HSC) was observed to have a more ductile form [14]. Moreover, SF also enhances the ultimate torsional strength and torsional stiffness after the initial cracking, particularly in ultra-high-performance beams [15]. Besides, the impact of different types of steel fiber on ductility and toughness was also examined. Double-hooked and kinked steel fibers increased the flexural tensile strength of the beams at the maximum level [16]. Additionally, the effects of the SF ratio and the aspect ratio of SF on the behavior of reinforced concrete (RC) beams under torsional moments were investigated. It is seen that the torsional strength of the beams with a 0.6% volumetric ratio was enhanced by 10–60% [17,18].

Recent research has extended into exploring the behavior of various beam shapes under torsion, including not only traditional rectangular or circular beams [19] but also T and L-shaped beams [20]. In the experimental study that considered only longitudinal reinforcement, it was observed that the ductility capacity of steel fiber-reinforced rectangular beams was higher than that of the corresponding flanged beams [21].

In experimental studies, researchers preferred ACI318 [22], EC2 [23], CSA [24] and JSCE [25] standards for designing the beams [3,6]. However, torsional design equations given in these documents are generated by shear design and the modified forms of it. To determine the strength of SFRC beams under pure torsional loading, a model was developed by comparing 23 test results [26]. An empirical equation was proposed for estimating the torsional capacity of rectangular RC beams [27]. Also, the space truss analogy was modified to find the resisting capacities of the RC beams under pure torsion [28]. A simplified torsional strength model for SFRC beams was proposed based on the softened truss model and validated by test data obtained from the literature [29].

Despite experimental and analytic investigations displaying valuable results, the subject is still open for new findings and suggestions. This paper examines the behavior of RC beams designed according to the provisions of the Turkish Standard TS 500 [30]. The novelty of this experimental study consists of determining the behavior of beams designed according to

TS500, which have been strengthened with steel fibers. The study focuses on identifying an optimal steel fiber ratio as a potential replacement material for determined transverse reinforcement spacing. In the experimental study, 16 beams were tested for constant cross-sections. Volumetrically, five different steel fiber ratios and also two different stirrup spacing values were selected as parameters. To find the relationship between steel fiber and transverse reinforcement, torsional moments were determined. The torque-twist curves and energy dissipation curves were obtained based on the test results and findings were compared.

2. EXPERIMENTAL STUDY

2.1. Materials

To obtain identical concrete strength, ready-mixed concrete with 35 MPa characteristic strength was selected in the production stage of the specimens. During the casting process, ten cylindrical samples with the size of 100x200 mm were taken from the concrete with and without steel fibers. These samples were tested to determine the compressive strength of the concrete on the day when the experiments were conducted. The test results of the samples are given in Table 1. For all specimens, 12 mm diameter rebars and 8 mm diameter rebars were used as longitudinal and transverse reinforcements, respectively. The mean yield strength of both transverse and longitudinal reinforcement is found to be 583 and 506 MPa, respectively.

Table 1 - Compressive strengths of 100x200 samples

Fiber content (%)	Compressive strength (MPa)
0.0	36.41
0.0	30.95
0.0	37.35
0.0	29.04
0.0	48.22
0.3	43.07
0.6	30.85
0.9	36.06
1.2	36.56
1.5	36.08

Both sides bent Kemerix® 80/60 BG steel fiber used in the concrete is shown in Figure 1. The chosen fiber had an aspect ratio (l_f/d_f) of 80, length of 60 mm, and 0.75 mm diameter.[†] . The average yield strength of the steel fiber was f_{yf} = 1200 MPa, which was taken from the manufacturer's datasheet.

[†] Fibers were supplied by Kemerli Metal Pty Ltd., Turkey, and were used as a substitute for a commercially better known counterpart.
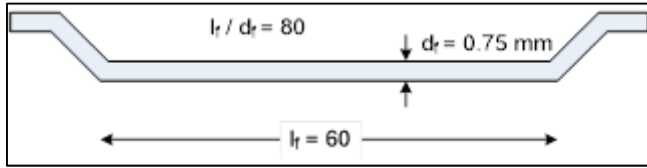
Figure 1 - Geometry of steel fibers

2.2. Specimen Details

The test specimens were designed according to the requirements defined in Turkish Standard TS500 [30]; however, the standard lacks a specification regarding pure torsion. To prevent brittle failure, Eq. 8.17 of TS500 is suggested. The requirements given in the standard are entirely related to combined torsion and shear forces. In most equations, a shear term is needed to obtain the results. However, the shear force is not to be considered when designing the specimen for pure torsion. To meet the requirements and avoid solving complicated equations, the design shear force (V_d) was assumed as 1 N in this study.

The mechanical properties of 16 beams fabricated were 300x300 mm in cross-sectional area and 2000 mm in length. 4Φ12 rebars were used as longitudinal reinforcements in all specimens. The dimensions of the test specimens and reinforcement layout are given in Figure 2. The specimens were designed with 300 mm and 400 mm stirrup spacing in the test regions. The main objective of this study was to explore the effects of steel fibers on torsional behavior. For this reason, two different transverse reinforcement ratios, both less than the requirements defined in Section 8.2.6 of the TS 500 standard, were selected. Therefore, as Table 2 shows, 8 specimens were produced with 300 mm spaced stirrups, and the remaining 8 were produced with 400 mm spaced stirrups. To prevent premature failure at the supports, a high amount of transverse reinforcement was used in these regions.

Another parameter was the volumetric fraction (V_f) of steel fibers. Many fiber aspect ratio variations are preferred according to beam type and its cross-section in previous studies [21, 31, 32, 33]. Loss of compressive strength and tensile toughness can be observed in high fiber ratios in beams [34, 35]. To determine a specific volume fraction, fiber ratios were chosen as 0.3%, 0.6%, 0.9%, 1.2%, and 1.5% by volume. The corresponding weight values and fiber contents were approximately determined as 4.2, 8.5, 12.7, 16.9, and 21.1 kg, respectively. It should also be considered that high fiber content might cause significant problems in casting operations especially if concrete composition is not well designed and controlled on-site. Essential attention was paid to preventing the formation of fiber balls in the mix and avoiding workability problems.

As for the designation of the specimens in this test, *s* indicated the spacing of transverse reinforcements in the test region, and V indicated the volume fraction of the steel fiber. When the 'V' block was null, it specified the specimens without steel fibers. Three identical specimens called I, II, and III were produced as no-fiber specimens for both 300 mm and 400 mm stirrup spacing. The classification of each specimen including all parameters is detailed in Table 2.
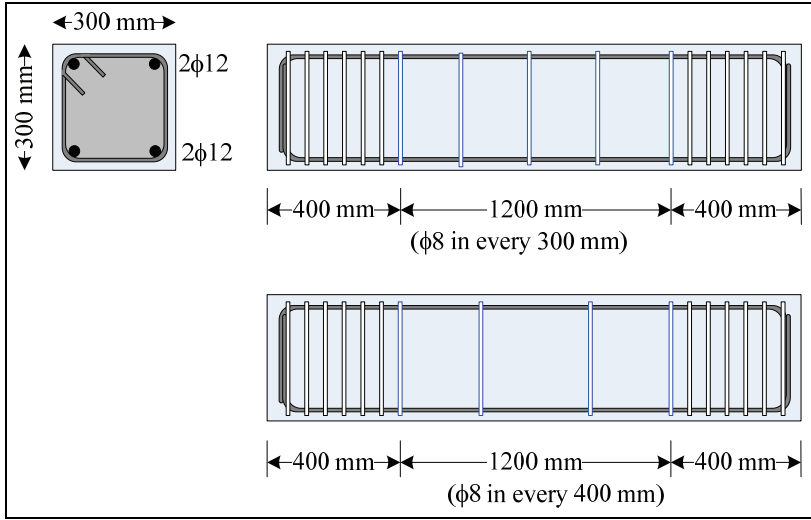
Figure 2 - Dimensions of test specimens and reinforcement details

Table 2 - Nomenclature and properties of specimens

Beam Designation	Φ8 transverse reinforcement spacing (cm)	Fiber volume fraction (%)
S30V00- I	30	**0**
S40V00- I	40	**0**
S30V00- II	30	**0**
S40V00- II	40	**0**
S30V00- III	30	**0**
S40V00- III	40	**0**
S30V03	30	**0.3**
S40V03	40	**0.3**
S30V06	30	**0.6**
S40V06	40	**0.6**
S30V09	30	**0.9**
S40V09	40	**0.9**
S30V12	30	**1.2**
S40V12	40	**1.2**
S30V15	30	**1.5**
S40V15	40	**1.5**

2.3. Test Setup and Instrumentation

The schematic depiction of the produced test setup is given in Figure 3 with front (a) and side (b) views. Unlike more conventional methods [36,37], the load was applied using a 100 kN hydraulic pump (actuator) from the ends
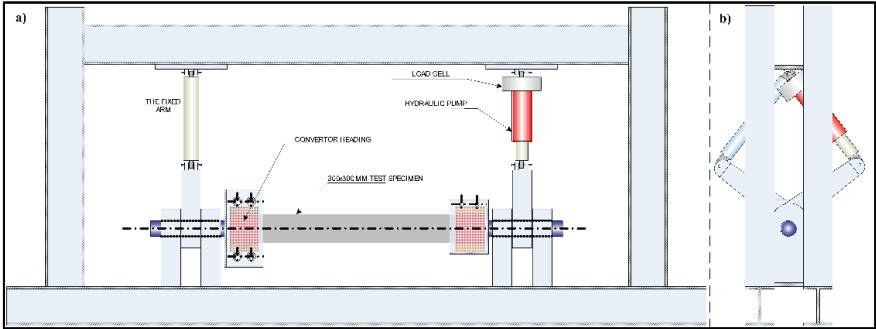
Figure 3 - Design of the test setup
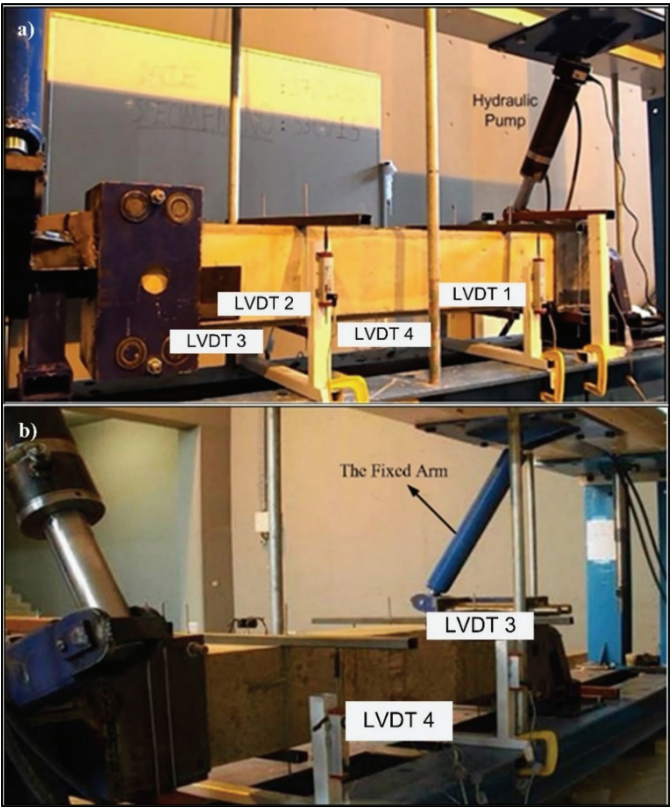
Figure 4 - The test setup, loading, and measurement systems (a) the backside of the setup (b)

The load was measured by a 200 kN capacity load cell mounted on the pump. The test specimen was located inside the test setup which involved specific support conditions. The force was applied by a rigid moment arm connected to the free support. The moment arm transferred the load to the RC beam as a pure torsional moment. To determine the twisting angle in the test region, four Linear Variable Displacement Transducers (LVDT) in total were placed on the front and back sides of the beam, as shown in Figures 4a and 4b. One end was rotationally fixed but free in the axial direction with the help of rollers inside the support to allow axial elongation. The other end was free to rotate. The side view of the test setup which is positioned during an experiment is shown in Figure 5a. Also, it is shown that rollers were placed inside the fixed support headpiece. For the elongation, on the fixed headpiece, a gap of approximately 5 cm was maintained between the outer face of the specimen and the inner plate, as shown in Figures 5b and 5c. Due to the gap and roller inside the support head, the axial resistant force becomes zero, allowing the specimen to elongate freely. The applied force was transferred to the specimen axis via the head support, which was restricted in the shear direction but free to rotate. Therefore, the specimen was not subjected to any shear forces.

Figure 5 - a) The side view of the test setup, b) Specimen in the headpiece, c) Details of the headpiece of the test setup for elongation

The load was progressively applied at a low rate, and the data from the LVDTs and loadcell were recorded every second by the data logger. L1 to L4 are the displacement readings from

the test region and D1 and D2 are the clear horizontal lengths between the LVDTs (Figure 6a). The calculation of rotation (θ) for each end of the test region is shown in Figure 6b and given in Eq. 1. Additionally, the angle of twist (φ) in the test region is calculated from Eq. 2.

$$\tan(\theta_i) = \frac{L_1 + L_4}{D_1} \quad \text{and} \quad \tan(\theta_j) = \left(\frac{L_2 + L_3}{D_2}\right) \tag{1}$$

$$\tan(\varphi) = \frac{(\theta_j) - (\theta_i)}{\ell_{average}} \tag{2}$$
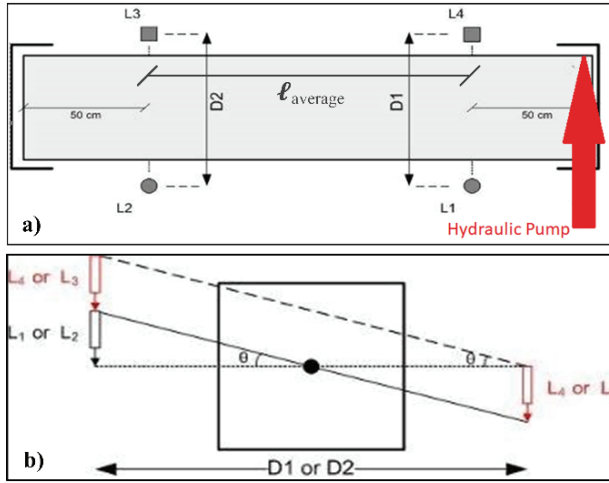
Figure 6 - Locations of LVDTs (a) rotation calculations (b)

As evident in literature data, smeared crack analysis is used for a rational estimation of torsional strengths and the elastic behavior of plain concrete members. However, the present study focuses only on experimental results of plain concrete as a reference point for the comparison of steel fiber-reinforced concrete's torsional values with the angle of twist [38].

3. TEST RESULTS AND DISCUSSION

Due to differences in code interpretation, specimens were designed with marginally inadequate torsion reinforcement, leading to ultimate torsion capacity lower than the cracking capacity. Consequently, a ductile torsion behavior could not be achieved. The discussion below is therefore restricted to non-ductile torsion behavior. Derived from the test results, the cracking torque (T_{cr}), maximum torque (T_{max}), and ultimate torque (T_u) values of each specimen are shown in Table 3 along with their corresponding angle of twist values (Φ_{cr}, Φ_{max} and Φ_u). Since the specimens without SF are similar in the experiments, only the test results of S30V00-I and S40V00-I are shown. The cracking, maximum, and ultimate torques indicate the torque value when the crack formed, the maximum resistance value (considered as the peak point) was achieved, and reinforcement was ruptured, respectively. The cracking strength of fiber reinforced concrete depends only on the strength of the concrete matrix. It

is observed that after the first crack developed in the experiments, the capacity of the beams continued to increase until they reached the peak and then started to decrease. Before reaching the T_u and experiencing a sudden decrease in torque capacity, beams demonstrated a post-cracking behavior. Also, it is observed that beams demonstrated a pseudo-ductile response through fibers, proceeding with energy absorption after the reinforcements separated. Therefore, the loading was sustained in accordance with the maximum twisting capacity of the test device, and it was observed that the twisting behavior of the beams continued.

Table 3 - Obtained test values

Beam Designation	Φ_{cr} (rad/m) $(*10^{-3})$	T_{cr} (kNm)	Φ_{max} (rad/m) $(*10^{-3})$	T_{max} (kNm)	Φ_u (rad/m) $(*10^{-3})$	T_u (kNm)	Φ_u/Φ_{cr}
S30V00	0.29	3.69	1.24	3.93	38.54	3.28	132.89
S30V03	0.61	3.22	1.80	3.69	73.55	2.95	120.57
S30V06	0.81	3.89	2.94	4.15	88.79	3.32	109.61
S30V09	0.66	3.93	1.93	4.22	85.67	3.38	129.80
S30V12	0.39	3.83	1.65	4.04	64.93	3.23	166.48
S30V15	0.94	3.39	1.75	3.71	154.10	2.97	163.93
S40V00	0.30	3.19	1.52	4.05	43.24	3.37	144.13
S40V03	0.51	3.48	1.60	4.00	57.78	3.20	113.29
S40V06	0.67	3.56	1.23	3.74	74.54	2.99	111.25
S40V09	0.44	3.40	1.57	3.75	59.47	3.00	135.15
S40V12	0.59	3.92	1.46	4.36	72.06	3.49	121.13
S40V15	0.68	3.54	2.01	4.06	56.20	3.25	82.67

The final twist value depends on the specimen twist capacity or actuator stroke capacity. This causes variation in ultimate twist and torque values. To be consistent, it is assumed that the failure of the specimen was developed when the torque was decreased by 20% of T_{max}. In Table 3, the ultimate torque and corresponding twist are given.

Regardless of fiber or steel content, the first cracking twist depends on the concrete type. As seen from Table 3, the maximum torques of specimens were low for low fiber contents and it was low again for higher fiber content for the S30 and S40 groups. For the S30 group, the decrease in T_{max} started after 0.9% fiber content, and it started after 1.2% fiber content for the S40 group. Figure 7 shows the Φ_u/Φ_{cr} ratios–variation concerning the fiber content. The Φ_u/Φ_{cr} ratios are almost same for lower fiber content for both S30 and S40 groups. However, the variation became scattered as the fiber content exceeded 9%. For S40 specimens, the Φ_u/Φ_{cr} ratios decreasing for higher SF contents. In this case, fibers might create weak points or reduce certain properties of the concrete due to the interaction between the steel fibers and the concrete matrix.
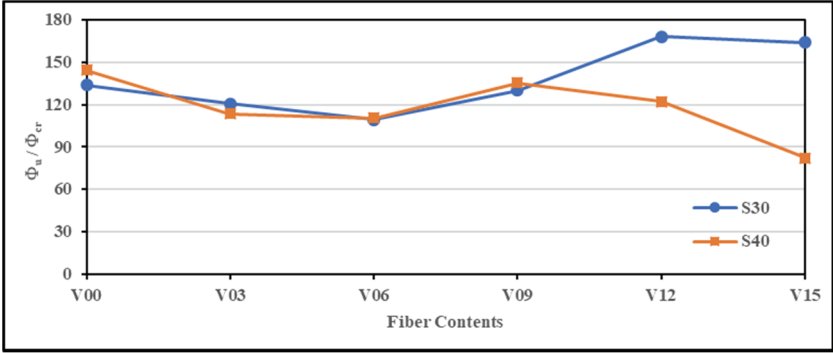
Figure 7 - Variation of Φ_u/Φ_{cr} ratios for S30 and S40 specimens' group

- In experiments, after the first crack was observed, the torsional moment continued to increase. It was also observed that number of cracks in the steel fiber beams was significantly higher than in non-fiberr ones. In the non-fiber beam tests, a few torsional diagonal cracks occurred, and with an increase in the load level, these cracks were propagated and widened. Due to generated local fractures, the beams are suddenly broke. However, in fiber beam tests, the cracks dispersed across all test regions, causing a pseudo-ductile behavior. Figure 8a and 8b show the typical crack patterns of beams without fiber (i) with moderate fiber (ii), and with an excessive fiber (iii) that are subjected to 300 mm and 400 mm spacing, respectively.

(a) S30V00 (i), S30V09 (ii) and S30V15 (iii)   (b) S40V00 (i), S40V12 (ii), and S40V15 (iii)
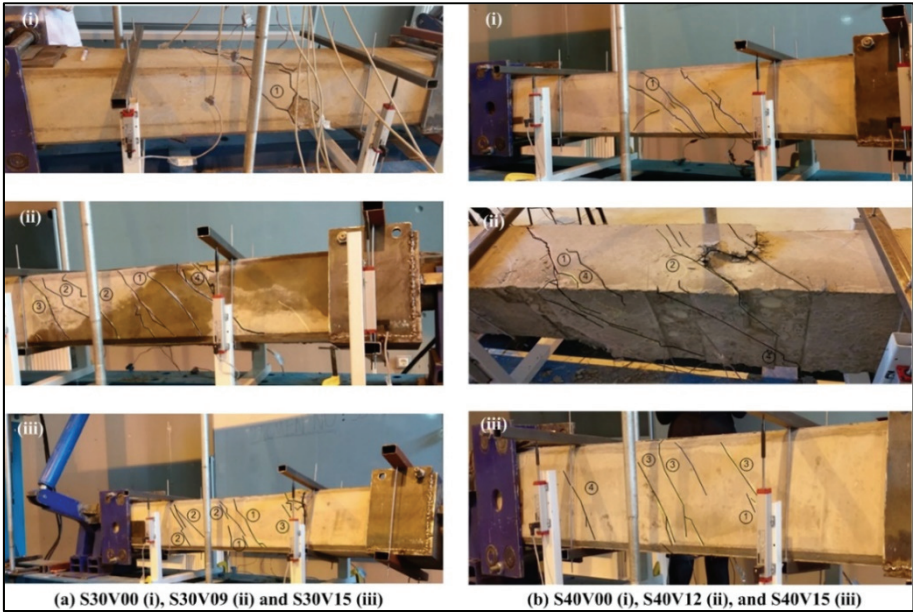
Figure 8 - Crack patterns

- The experimental results illustrate that S30 group beams predominantly displayed initial cracks within a load range of 6 kN to 7.28 kN, with beams S30V06, S30V09, and S30V12 notably demonstrating initial cracks at loads exceeding 7 kN, indicative of higher load capacities within this sub-set. For specimen S30V15, the first crack appeared at a 6.05 kN load and following cracks formed within very small intervals and continued to form until the maximum load was reached. The specimen failed from a point between the first and second crack. Similarly, the S40 group beams revealed initial cracks ranging from 5.94 kN to 7.28 kN, with S40V12 exhibiting the highest load resistance at 7.28 kN, reflecting the upper limit observed in this group. The first three cracks developed at 7.19, 7.22, and 7.28 kN, load respectively. The crack patterns of the S30V15 and S40V12 beams are also shown in Figures 9a and 9b.

Figure 9 - Crack pattern of S30V15 (a) and S40V12 (b) beams

- The post-cracking response of the beams continued up to a certain volume fraction of steel fiber. However, beams with relatively high amounts of SF displayed poor twisting ability during testing. Due to SFs exhibiting a bonding effect on the cracks, similar to stitches (Figure 10), the dispersing of the beams became difficult. It is proven that a high SF amount did not always increase the twisting angle due to the increased stiffness of the beams.

Figure 10 - SFs prevent the cracks

- During the testing of the beams, a dissociation was observed in the transverse reinforcements. The rupture in the S30V09 beam is shown in Figure 11.

Figure 11 - The rupture of transverse reinforcement (S30V09 beam)

- The reason for the rupture in the stirrup was the excessive use of SF. The intense utilization SFs might have caused the reinforcements to yield more than the estimated value. Consequently, the stirrup could no longer resist and ruptured at its weakest point. To state the findings clearly, the torque-twist curves are illustrated for the beams S30V12 and S40V15, respectively in Figures 12a and 12b. The stirrups of S30V12 and S40V15 ruptured at around 79.44×10^{-3} and 90.04×10^{-3} rad/m twist levels, respectively. As shown in the diagrams, the rupture of the stirrup caused a sudden decrease in torque and presented deformations due to the angle of twist.

- It was also observed that the twisting behavior of the beams continued even after the rupture of transverse reinforcement. Although the torque values are decreased, the

bearing capacity of the beams persists because SFs resist to keep the beam block together. At this point, however, it was unexpected for the beams to display a pseudo ductility manner even after the rupture, similar to post-cracking behavior.
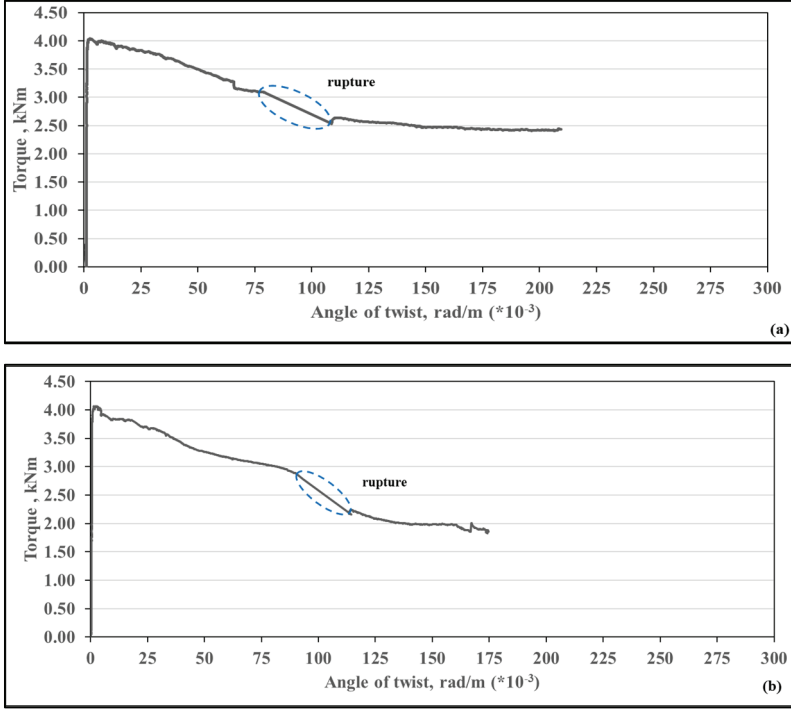
Figure 12 - Torque-twist curves of S30V12 (a) and S40V15 (b) beam

3.1. Comparison of Torque- Twist Curves and Energy Dissipation Capacities

To find out the similarity and discrepancy between the beams, the curves obtained from experiments were compared according to their twisting angles and energy dissipation capacities (EDC) under torsional loading.

The comparison of the torque-twist curves for the entire S30 group of experimental testing beams is illustrated in Figure 13a. Among them, beam S30V09 was clearly the most reasonable option for steel fiber utilization due to its reaching the maximum torque capacity. The torque-twist curve of the S40 group of testing beams is also shown in Figure 13b. As the figure summarizes, beam S40V12 was the most logical selection of all.

For better seismic performance in structural systems, a high energy dissipation capacity (EDC) in RC beams is desirable. According to the determined test results, the torsional EDCs of all beams were calculated by using the area under the torque–twist curves. Figure 14a and 14b indicate the respective cumulative EDCs of beams that have 300 mm and 400 mm transverse reinforcement spacing. The maximum EDCs of the beams and corresponding twist results are summarized in Table 4.
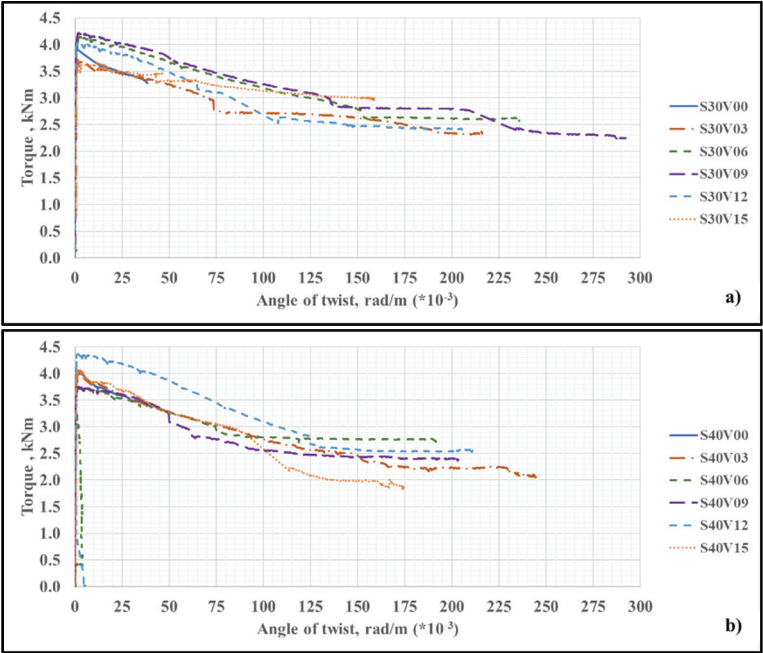
Figure 13 - Torque-twist curves of S30(a) and S40(b) group beams
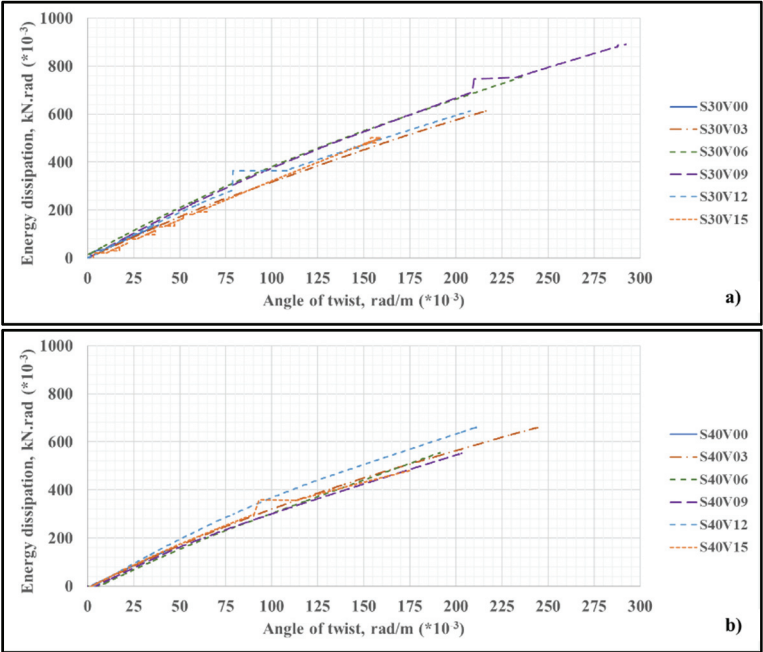
Figure 14 - Comparison of energy dissipation capacity: (a) S30 group beams and (b) S40 group beams

Table 4 - Comparison of the energy dissipation capacities of all fiber beams

Beam designation	Maximum energy dissipation capacity, kNrad ($*10^{-3}$)	Angle of twist, rad/m ($*10^{-3}$)
S30V03	612	216.74
S40V03	668	244.35
S30V06	754	241.77
S40V06	575	190.05
S30V09	890	292.64
S40V09	566	202.98
S30V12	614	210.09
S40V12	6.60	207.76
S30V15	5.23	168.87
S40V15	4.89	174.77

Since the EDCs of the non-fiber beams were almost identical, it is considered unnecessary to exhibit in Table 4. It was observed that specimens S30V00 and S40V00 exhibited slight twisting which corresponded to $38.65*10^{-3}$ and $43.27 *10^{-3}$ rad/m respectively, with corresponding EDCs $1.36*10^3$ and $1.41 *10^3$ kN.rad. To compare the EDCs of the beams, a limit value can be determined. For instance, the EDCs were almost the same for beams S30V03 and S40V03 in $150*10^{-3}$ rad/m twisting values. It is also seen that the maximum capacity for energy dissipation of the beam S40V03 was slightly higher than that of the S30V03 beam.

Contrary to expectations, the maximum energy capacities and dissipated energies at a $150*10^{-3}$ rad/m limit value for specimens S30V12 and S40V12 were distinctive. The EDC of the S40V12 beam was higher than that of the S30V12 beam, both for limit level and maximum capacity. The reason for less energy dissipation may have been due to the stirrup rupturing.

Except for beams S30V12 and S40V12, the energy dissipation capacities of all other beams in the S30 group were greater than those of their counterparts, both at the determined limit value and at maximum capacity.

4. CONCLUSION

In this study, the behavior of steel fiber reinforced concrete beams under pure torsional moment was investigated experimentally. 16 large-scaled reinforced concrete beams with inadequate torsion steel were designed and produced. Different transverse reinforcement ratios (based on the 300 and 400 mm spacing of the closed stirrups) and SF volume fractions (0.0%, 0.3%, 0.6%, 0.9%, 1.2%, and 1.5%) were selected as parameters. Torsional moments at cracking, maximum and ultimate values along with the corresponding angle of twist

behavioral curves were presented. Additionally, Φ_u/Φ_{cr} ratios of beams were given. Energy dissipation capacities (EDCs) were also examined to validate the corresponded torque capacities of beams and to describe the relationship of torque-twist values. The determination of specific SF ratios for two different transverse reinforcement spacing can be also regarded as the novelty of this experimental study.

Based on the test results, the following findings were drawn:

- For all types of beams, up to the first cracking, the torque - twist behavior was identical and can be accepted as linearly elastic. A similar situation was also seen in other studies [26].

- As expected, failure in non-fiber beams was due to a single crack in the test region, whereas many cracks spread out in fibercontaining beams, with the fibers tending to restrict these cracks and improve the twisting capacity of the beams. This has been observed in similar studies [18].

- It is concluded that torque-twist responses of beams clearly showed a pronounced softening behavior after cracking, however, higher amounts of SF increased stiffness and early cracking behavior in RC beams under pure torsional moment.

- Despite the larger distance in the spacing of the stirrups in an S40 group of RC beams, the maximum torque capacities were enhanced in 1.2% and 1.5% ratios of SF. This phenomenon can be explained by the SF behavior, which was similar to that of stirrups, especially at these levels. The use of SF showed a similar effect to the usage of torsional reinforcement in another study [39].

- In 0.6% and 0.9% SF ratios, the maximum EDC of the S30 group of RC beams is higher than that of the S40 group.

- EDC results showed that a certain amount of SF provides better twist capacity to beams. However, beams with SF ratios of under 0.3% and over 1.2% exhibited more rigid behavior. It is suggested by this experimental study that the implementation of SF in certain rations in RC beams results in greater EDCs under pure torsion.

- Test results showed that according to the T_{max} and determined EDCs, 0.9% and 1.2% volumetric ratios of SF were considered as the optimum value for the S30 and S40 group of RC beams, respectively. Besides, a high steel fiber amount (1.2% and 1.5%) caused less twist capacity in those groups.

In future studies, experiments can be conducted with different parameter preferences such as longitudinal reinforcement and variations in cross-section. Additionally, the range of the SF ratios could be increased, and more detailed results can be obtained with an increased number of beams. Findings can be compared to results in the literature that are designed according to provisions of other standards. Obtained results can be also supported by numerical studies.

References

[1] Nilson, A. H., Design of Concrete Structures, 12th ed., McGrawHill, New York. 1999. ISBN: 0-07-046586-X

[2] Hsu, T. T. Torsion of structural concrete-behavior of reinforced concrete rectangular members. Special Publication, 18, 261-306, 1968.

[3] Ju, H., Lee, D., Kim, J.R., Kim, K.S., Maximum torsional reinforcement ratio of reinforced concrete beams, Structures, 23, 481–493, 2020. https://doi.org/10.1016/j.istruc.2019.09.007

[4] Teixeira, M. M., Bernardo, L., Ductility of RC beams under torsion, Engineering Structures, 168, 759-769, 2018.. https://doi.org/10.1016/j.engstruct.2018.05.021

[5] Narayanan, R., Kareem-Palanjian, A. S., Torsion in beams reinforced with bars and fibers, Journal of Structural Engineering, 112(1), 53-66, 1968. https://doi.org/10.1061/(ASCE)0733-9445(1986)112:1(53)

[6] Kim, M.J., Kim H.G., Lee, Y.J., Kim, D.H., Lee, J.Y., Kim, H.E., Pure torsional behavior of RC beams in relation to the amount of torsional reinforcement and cross-sectional properties, Construction and Building Materials 260, 119801, 2020. https://doi.org/10.1016/j.conbuildmat.2020.119801

[7] Rasmussen, L., Baker, G., Torsion in reinforced normal and high-strength concrete beams part 1: Experimental test series, ACI Structural Journal, 92(1), 56-62, 1995.

[8] Waryosh, W. A., Mohaisen, S. K., Dkhel, R. H., Experimental study on torsional behavior of fiberious reinforced concrete beams with different concrete strength, IOP Conference Series: Materials Science and Engineering, 584, 2019. https://doi:10.1088/1757-899X/584/1/012052

[9] Kaya, S. Yalcin, C., Kaya, O. Experimental investigation of full-scale reinforced concrete beams under reversed-cyclic pure torsion, Structures, 51, 734-746, 2023. https://doi.org/10.1016/j.istruc.2023.03.079

[10] Facconi, L., Minelli, F., Ceresa, P, Plizzari, G. Steel fibers for replacing minimum reinforcement in beams under torsion, Materials and Structures, 54, 2021. https://doi.org/10.1617/s11527-021-01615-y

[11] Cucchiara, C., Mendola, L., Papia, M., Effectiveness of stirrups and steel fibres as shear reinforcement, Cement and Concrete Composites, 26(7), 777-786 2004. https://doi.org/10.1016/j.cemconcomp.2003.07.001

[12] Craig, R. J., Parr, J. A., Germain, E., Mosquera, V., Kamilares, S., Fiber reinforced beams in torsion, Journal Proceedings, 83(6), 934-942, 1986.

[13] Engin, S., Ozturk, O., Okay, F., Estimation of ultimate torque capacity of the SFRC beams using ANN, Structural Engineering and Mechanics, 53(5), 939-956, 2015. https://doi.org/10.12989/sem.2015.53.5.939

[14] Rao, T. G., Seshu, D. R., Torsion of steel fiber reinforced concrete members, Cement and Concrete Research, 33(11), 1783-1788, 2003. https://doi.org/10.1016/S0008-8846(03)00174-1

[15] Yang, I.-H., Joh, C., Lee, J. W., Kim, B.-S., Torsional behavior of ultra-high performance concrete squared beams, Engineering Structures, 56, 372-383, 2013. https://doi.org/10.1016/j.engstruct.2013.05.027

[16] Anandan, S., Effect of Steel fibre profile on the fracture characteristics of steel fibre reinforced concrete beams, Journal of Engineering Research, 7(2), 105-124, 2019

[17] Mansur, M. A., Nagataki, S., Lee, S. H., Oosumimoto, Y., Torsional response of fibrous concrete beams, ACI Structural Journal, 86(1), 36-44, 1989.

[18] Okay, F., Engin, S., Torsional behavior of steel fiber reinforced concrete beams, Construction and Building Materials, 28(1), 269-275. 2012. https://doi.org/10.1016/j.conbuildmat.2011.08.062

[19] Kamiski, M., Pawlak, W., Load capacity and stiffness of angular cross section reinforced concrete beams under torsion, Archives of Civil and Mechanical Engineering, 11(4), 885–903, 2011. https://doi.org/10.1016/s1644-9665(12)60085-5

[20] Salama, A.E., Kassem, M.E., Mahmoud, A.A., Torsional behavior of T- shaped reinforced concrete beams with large web openings, Journal of Building Engineering 18, 84-94, 2018. https://doi.org/10.1016/j.jobe.2018.02.004

[21] Chalioris, C. E., Karayinnis, C. G., Effectiveness of the use of steel fibers on the torsional behavior flanged concrete beams, Cement and Concrete Composites 31(5), 331-341, 2009 https://doi.org/10.1016/j.cemconcomp.2009.02.007

[22] ACI Committee 318. Building code requirements for reinforced concrete and commentary (ACI 318-14). American Concrete Institute, Detroit, MI, 2014.

[23] Comete European de Normalisation (CEN), Eurocode 2: design of concrete structures. Part 1-general rules and rules for buildings, pr EN 1992-1, 225, 2004.

[24] CSA Committee A23.3-14, Design of Concrete Structures (CAN/CSA-A23.3-14), Canadian Standards Association, Canada, 297, 2014.

[25] Japan Society of Civil Engineering, Standard Specifications for Concrete Structures, Japan Society of Civil Engineering, Japan, 2007.

[26] Amin, A., Bentz, E. C., Strength of steel fiber reinforced concrete beams in pure torsion, Structural Concrete, 19(3), 684-694, 2018. https://doi.org/10.1002/suco.201700183

[27] Ilkhani, M.H., Naderpour, H., Kheyroddin, A., A proposed novel approach for torsional strength prediction of RC beams, Journal of Building Engineering, 25, 2019. https://doi.org/10.1016/j.jobe.2019.100810

[28] Oettel, V. Steel fiber reinforced RC beams in pure torsion-Load-bearing behavior and modified space truss model, Structural Concrete, 24(1), 1348-1363, 2023. https://doi.org/10.1002/suco.202200031

[29] Kryzhanovskiy, K., Zhang, D., Ju, H. et al. Development of Torsional Strength Model for Steel Fiber Reinforced Concrete Beams with Transverse Reinforcement. Int J Civ Eng 21, 1123–1139, 2023. https://doi.org/10.1007/s40999-023-00816-6

[30] Turkish Standard TS500, Requirements for Design and Construction of Reinforced Concrete Structures. Turkish Standards Institution, Ankara, Turkey, 2000.

[31] Raut, L.L., Kulkarni, D.B., Torsional strengthening of under reinforced concrete beams using crimped steel fiber, International Journal of Research in Engineering and Technology 3(6), 2014. https://doi.org/10.15623/ijret.2014.0306087

[32] Narayanan, R., Darwish, I. S., Use of steel fibers as shear reinforcement, ACI Structural Journal 84(3), 216-27. 1987.

[33] Chalioris, C. E., Steel fibrous RC beams subjected to cyclic deformations under predominant shear, Engineering Structures, 49, 104-118, 2013. https://doi.org/10.1016/j.engstruct.2012.10.010

[34] Ju, H., Lee, D. H., Kim, K. S., Minimum torsional reinforcement ratio for reinforced concrete members with steel fibers, Composite Structures, 207, 460-470, 2019 https://doi.org/10.1016/j.compstruct.2018.09.068

[35] Naaman, A. E., Engineered steel fibers with optimal properties for reinforcement of cement composites, Journal of Advanced Concrete Technology, 1(3), 241-252, 2003. https://doi.org/10.3151/jact.1.241

[36] Hameed, A. A., Al-Sherrawi, M. H., Torsional strength of steel fiber reinforced concrete beams, International Journal of Civil Engineering and Technology 9(6), 1388–1396, 2018.

[37] Hanoon, A. N., Abdulhameed, A. A., Abdulhameed, H. A., Mohaisen, S. K., Energy absorption evaluation of CFRP-strengthened two-spans reinforced concrete beams under pure torsion, Civil Engineering Journal, 5(9), 2007-2018. 2019. http://dx.doi.org/10.28991/cej-2019-03091389

[38] Patil, S. P., Sangle, K. K., Tests of steel fiber reinforced concrete beams under predominant torsion, Journal of Building Engineering 6, 157-162, 2016. https://doi.org/10.1016/j.jobe.2016.02.004

[39] Ju, H., Han, S.-J., Zhang, D., Kim, J., Wu, W., Kim, K. S., Estimation of minimum torsional reinforcement of reinforced concrete members, Advances in Materials Science and Engineering, 1-10, 2019. https://doi.org/10.1155/2019/4595363

Using Sea Shell, Lime and Zeolite as Additives in the Stabilization of Expansive Soils

Senanur ÇELİK[1*]
Sabriye Banu İKİZLER[2]
Dina AQRA[3]
Zekai ANGIN[4]

ABSTRACT

Swelling soils are increasingly recognized as a critical issue in geotechnical engineering, as their presence can lead to substantial damage to built structures. When structures are built on such soils and free swelling is prevented, stresses can develop that may lead to significant damage to the structure. Soil stabilization through the use of additive materials has garnered considerable attention as an effective method for mitigating this problem. The objective of this study was to stabilize the clay soil (CH) with high swelling potential by using sea shell, lime and zeolite additives in two stages. In the initial phase, consistency limits were tested by mixing high plasticity clay soil mixed with 8-10-12-14-16% sea shell 0-3-5-6-8% lime (one of the most used soil stabilizer) and 0-5-10-15-20% zeolite by weight. The three mixtures and the two best percentages determined for each mixture were then combined. Upon completing these steps, five experimental sets were prepared by combining the percentages that yielded the best results. Compaction test, percent swelling test and swelling pressure tests were performed with these datas. According to the test results, adding 14% sea shell, 6% lime and 5% zeolite by weight (SS14L6Z5) gave the smallest swelling value as 1,07% and highes swelling pressure as 23 kPa. This study concludes that the combined use of these additives led to a substantial 96% increase in swelling pressure, along with a marked reduction in swelling potential.

Keywords: Swelling soils, soil stabilization, swelling pressure, swelling percentage, seashell, lime, zeolite.

1 Eskişehir Osmangazi University, Department of Civil Engineering, Eskişehir, Türkiye
senanurkologlu@gmail.com - https://orcid.org/0000-0003-2967-1206

2 Karadeniz Technical University, Department of Civil Engineering, Trabzon, Turkey
banuh@ktu.edu.tr - https://orcid.org/0000-0002-6820-5593

3 Karadeniz Technical University, Department of Civil Engineering, Trabzon, Turkey
dina-aqra@hotmail.com - https://orcid.org/0000-0002-5638-6171

4 Karadeniz Technical University, Department of Civil Engineering, Trabzon, Turkey
angin@ktu.edu.tr - https://orcid.org/0000-0002-6981-6396

* Corresponding author

1. INTRODUCTION

Expansive soils pose a significant challenge in numerous regions, particularly in countries characterized by arid and semi-arid climates. Inyang et al. argue that the shrink-swell performance of soils with wide moisture ranges, especially at low ground pressures and on large surface areas such as airports, accounts for more than half of the soil-related damage to structure [1].

The swelling mechanism in soils is typically categorized into two zones: interparticle or intercrystalline. In the interparticle zone, when clay is wetted, capillary tensions decrease causing the clay to swell. Intercrystalline swelling occurs in clays with weak bonds such as montmorillonite [2]. The study by El-Sohby and Mazen [3] claimed that mineralogical properties of clay also have a significant effect on swelling. Studies have shown (e.g., [4]) that the swelling percentage and capacity increase with added bentonite, while the swelling decreases as the water content of the mixture increases. During the swelling process, the soils volume expands, exerting high pressures on surrounding structures [4].

Various methods have been introduced to improve the geotechnical properties of such soils, [3] including mechanical and chemical stabilization. The purpose of mechanical stabilization is to convert two or more soils into a soil that meets the desired conditions by mixing them in appropriate proportions. This technique typically involves mixing coarse-grained soils with fine-grained soils. The earliest examples of this method can be seen on the roads of ancient Babylon and Rome [6, 7]. Stabilization of soil with additives is one of the oldest processes in geotechnical engineering. Type of chemical soil stabilization is a process by which several materials are added to soil to make better its engineering properties [10]. These materials enter between the grains of the soil, altering their chemical properties and resulting in the formation of a new soil with a different structure.

The effects of different materials, such as lime, fly ash, cement, which are known to be primarily effective in stabilizing expansive soils, have been the subject of investigation for a long time (e.g., [8, 9, 10, 11, 12]). Additionally, the use of eco-friendly additives is sensible approach for stabilizing expansive soils, as it conduce a sustainable and economic solution [13, 14] taken to safeguard the interest of natural environment [8].

Lime is the oldest traditional stabilizer used for soil stabilization [15, 5] and is employed to increase the bearing capacity of soil in various structures, such as airports, railway, and foundation bases [16, 17, 14]. The cations present in lime facilitate the agglomeration of clay particles by reducing the surface area and water absorption capacity of the soil sample [8]. Chandran and Soman [18] conducted a series of parametric studies on stabilizing swelling clays with lime and demonstrated that this method is a cost-effective method that can be used effectively to reduce the swelling problem. To stabilize a highly plastic clay soil, Özkan and Yenginar [32] used filter sludge, a waste material from the sugar industry. They observed that as the amount of filter sludge added to the soil increased, the plastic limit and optimum water content increased, while the liquid limit, plasticity index and maximum dry density decreased. Notably, when 15% sludge was incorporated into the samples, swelling decreased by 52,5%. Furthermore, this improvement was found to be positively correlated with curing time.

However, despite the important advantages of lime, certain disadvantages exist. Lime may lead to increased infiltration and swelling of untreated layers due to its higher hydraulic

conductivity [1]. For this reason, alternative solutions have been sought alongside lime. Taşçı [19] aimed to improve the engineering properties of a dispersive clay with high swelling potential by incorporating silica fume in addition to lime additive. By adding 3% lime and 10% silica fume to the sample, the swelling pressure was reduced by 95%. This study achieved significant improvement and contributed to the introduction of low-cost, optimal additives to the literature. Indiramma, Sudharani, and Needhidasan [8] used fly ash and lime, which are frequently preferred additives for stabilization, in their experimental studies. The free swelling index was initially 142%, but it decreased to 72% with 8% lime additives and to 70% with a combination of 10% fly ash and 8% lime additives.

To improve a soil sample with high dispersibility, Öztürk and Türköz [28] employed silica fume (SF) as an admixture. The standard Proctor test was conducted to determine the compressive properties of soil samples mixed with varying ratios of SF (0, 5, 10, 15, 20, 25, and 30 percent). In addition, the strength parameters of the samples were measured using unconsolidated undrained triaxial (UU) tests. The results of this experimental study indicated that silica fume is effective in stabilizing dispersive soils. Furthermore, significant increases in strength were observed as a function of curing time, attributed to the high silica content of silica fume.

Although there has been tremendous research such as lime and cement stabilization globally, the investigation of the effect of local materials, such as seashells, on soil stabilization should be expanded. Seashells, which are biomaterials containing approximately 90% calcium carbonate by weight, exhibit properties similar to those of lime. Mounika, Narayana, Manohar and Vardhan [20] aimed to stabilize the clay with high swelling potential by using varying percentages of seashell in their experimental study. The best results were obtained with 16% seashell additive. Similarly, Patel and Mishra [21] sought to enhance the properties of infrastructure soil by incorporating seashell powder, adding 12%, 15%, and 18% seashell by weight to the soil. They determined that a 15% seashell contribution to the infrastructure soil gave positive results.

One of the additives used for stabilization is zeolite. Components such as silicon oxides, particularly aluminum, make zeolite an effective type of pozzolanic material due to its high cation exchange capacity [22, 23]. Turkoz and Vural [24] claimed that the addition of clinoptilolite zeolite that is the type of zeolite used in most of the aforementioned research, increased the unconfined compressive strength of cement- stabilized clayey soil. Sharo, Shaqour, and Ayyad [23] observed a reduction in swell potential from 6,9% to 4,9% with the addition of 15% zeolite and 10% cement kiln dust.

Recent studies have increasingly focused on the application of chemical additives for soil stabilization, extending beyond traditional natural additives. GuhaRay, Syed, and Kar [14] demonstrated in their work that the addition of 10% and 15% alkali-activated binder (AAB) resulted in a reduction of swell percentage by 62% and 70%, respectively. AAB has been found to behave like a helpful cement binder with higher functionality performance with low ecological damage [25]. Lu, She, Duan, Yao, and Liu [26], in his article, transformed the soil into an almost non-swelling soil by using the Al/soil ratio above 0,10 mmol/g. They noted that this transformation was attributed to increased flocculation of soil particles, facilitated by the exchangeable cations between Al_{13} and the swelling soil. The treatment of expansive soil with the addition of Al_{13} shows greater potential durability than traditional stabilizers.

However, it is important to note that the presence of aluminum in PHA solutions may lead to aluminum toxicity, posing risks to living organisms.

Özkan and Çokça [29] reported that lime diffuses slowly into clay soil due to its low porosity. Thus, their study incorporated sodium lignosulphonate, a plasticiser commonly used in the concrete industry, into lime columns to enhance the diffusion of lime particles. These columns were filled with two different mixtures: water-lime and water-lime-sodium lignosulphonate, to investigate the effect of the addition of sodium lignosulphonate. Free swelling and compressive strength tests were carried out on undisturbed expansive clay samples obtained from the space between the columns. The experimental study revealed that the treated expansive clay samples placed between the lime columns containing sodium lignosulphonate had higher compressive strength than the untreated expansive clay samples. Consequently, it was found that adding sodium into lime columns yielded improved performance for the treatment of expansive clays compared to lime columns alone. Ertuğrul and Canoğulları [30] systematically reviewed the results of previous mechanical tests on fibre-cohesive soil mixtures. The results showed that the shear strength of the reinforced soil increased with the fibre content and that the consolidation settlement of clay soil mixed with polypropylene fibres decreased significantly.

In recent years, researchers have increasingly focused on the use of technology in soil improvement practices Narmandakh, Butscher, Ardejani, Yang, Nagel, and Taherdangkoo [31] to determine the swell potential of natural and artificial clay soils, it has developed advanced feed- and step-based neural network models trained using Levenberg-Marquardt and Bayesian optimization algorithms. The swelling potential experimental datasets collected from literature to develop network models were compared with empirical and semi-empirical correlations. The analysis revealed that the predictive performance of the Levenberg-Marquardt-trained feedforward neural network was satisfactory, demonstrating an acceptable fit to the experimental data.

Most studies on soil stabilization have not adequately addressed the effects of using seashells in combination with other additives (e.g., [20, 21, 27]).

The present study aims to determine the optimal additive ratios that result in the best performance by examining changes in geotechnical properties such as consistency limits, compaction, and swelling potential. This will be achieved using lime, seashell, and zeolite as source materials, sourced from the Denizbükü District of Ünye in Ordu province. The study introduces an innovative approach to utilizing seashells, a waste material, in combination with naturally available lime and zeolite. This strategy not only aids in preventing environmental pollution but also contributes economic value by strengthening the country's economy. Seashells, which form the exoskeleton of molluscs and are collected near the coast, contain up to 90% calcium carbonate, making them similar to lime in composition. Cause of seashells have properties akin to lime, they were chosen as an additive material and used in higher proportions than lime by weight to avoid the need for large amounts of lime. This decision was made in light of evidence indicating that lime can be detrimental to human health and may not be compatible with all types of clay [33]. The aim is to use shells as an alternative to lime and the use of zeolite will be a replacement for the cement additive.

Furthermore, this study combines widely recognized materials such as zeolite and lime, which have previously yielded positive results in research, with seashells, which have also

demonstrated efficacy when used independently. The chemical reactions that take place when these materials are used together have almost the same results as lime and cement additives; however, the damage to human health in comparison to lime and cement has not yet been clarified. This research examines the combined use of these materials on swelling soil as a new approach.

2. MATERIALS AND METHODS

2.1. Soil

The soil sample used in the study was collected as a disturbed sample from a depth of 1,5 meters from the Yazlak locality area of Denizbükü Neighborhood, within the Ünye district of Ordu. The soil is classified as CH (Clay of High Plasticity) according to the Unified Soil

(a)

(b)
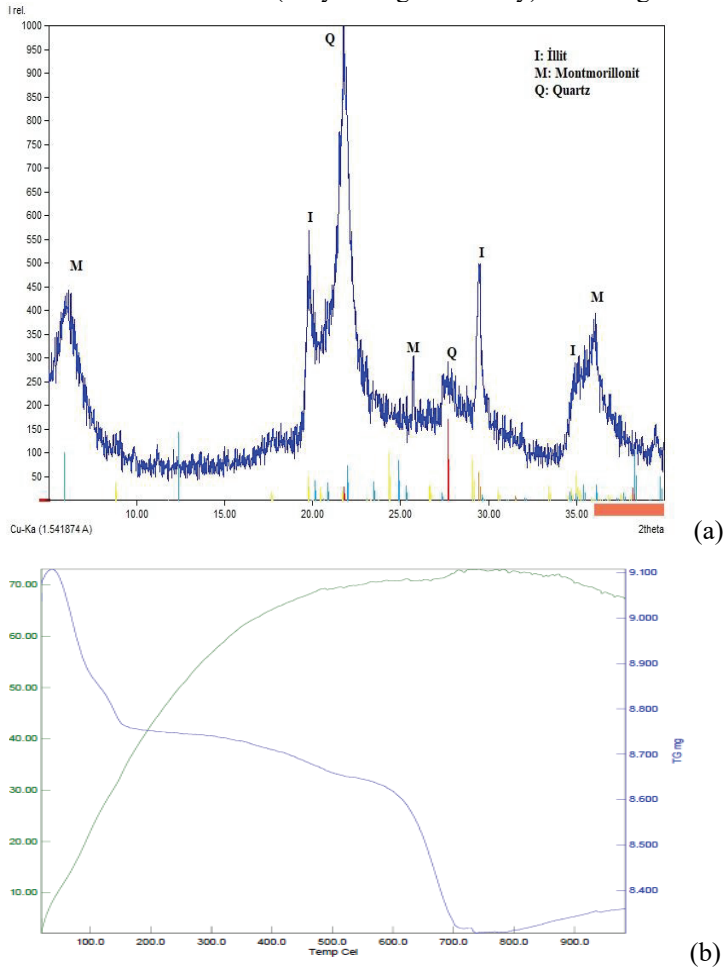
Figure 1 - Mineralogy properties of the soil: (a) X-ray diffraction result (b) Differential thermal analysis result

Classification System (USCS) and as A-7-5 based on the American Association of State Highway and Transportation Officials (AASHTO) classification system, based on consistency limits and particle size distribution results. Soil samples brought to the laboratory were first left to dry in air and then dried in an oven according to the conditions of the experiments to be applied. The index geotechnical characteristics of the soil are shown in Table 1. Differential thermal analysis (DTA) and X-ray diffraction (XRD) analysis were performed to make the mineralogical description of clays. The results of XRD analysis indicated that the main clay mineral of the soil sample is "montmorillonite" and the other contents are illite and mixed clay mineral as shown in Figure 1(a). The DTA technique was used to identify peaks in the curve drawn by the temperature differences resulting from phase changes and chemical reactions. This analysis confirmed that the primary mineral is "montmorillonite," while illite and mixed clay minerals also identified, as illustrated in Figure 1(b).

Table 1 - Physical and Index Properties of the Soil Sample

Properties	Quantity	Standart
Grain Size Distribution		
(a) Sand (%)	32	ASTM D422 (2007)
(b) Silt (%)	39	ASTM D422 (2007)
(c) Clay (%)	29	ASTM D422 (2007)
Specific gravity (g/cm³)	2,625	ASTM D857 (2014)
Liquid Limit (%)	143,6	ASTM D4318 (2017)
Plastic Limit (%)	38,8	ASTM D4318 (2017)
Plasticity Index (%)	104,8	ASTM D4318 (2017)
USCS	CH	ASTM D2487 (2017)
Maximum Dry Density (g/cm3)	1,23	ASTM D698 (2012)
Optimum Moisture Content (%)	37,4	ASTM D698 (2012)
Unconfined Compressive Streght (kPa)	327,17	ASTM D2166 (2016)
Swelling Percentage (%)	62,17	ASTM D4546 (2021)
Swelling Pressure (kPa)	580	ASTM D4546 (2021)

Table 2 - Physical properties of zeolite

Parameters	Value
Powder Density	1,42 g/cm²
Solid Density	2,143 g/cm²
Spill Density	0,54 g/cm²
Hardness	3,5 – 4,0 mohs
Specific Surface	14,500 cm/g
Colour	Ivory
Fluidization Temperature	1506 C°

2.2. Stabilizers

Within the scope of this study, seashells obtained from the Black Sea coasts in Trabzon were brought to the laboratory. Following collection, the seashells were washed and allowed to dry for 24 hours at 105°C in a furnace. Subsequently, they were ground using a mill to achieve a final weight of 1209,7 g, rendering them suitable for use in the experiments.

The zeolite used in this work is provided from Leonardit Bio Market, and the properties taken from the laboratory testing are furnished in Tables 2 and 3. CL 80 S slaked powder calcium lime was purchased from Barkisan Lime Factory. The particle size distribution of all materials is illustrated in Figure 2.
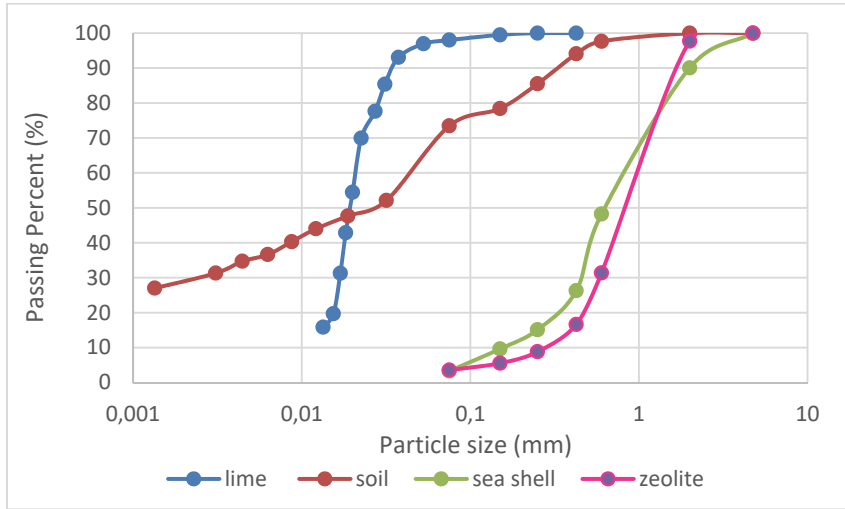
Figure 2 - Particle size distribution of the studied materials

Table 3 - Chemical Properties of zeolite

Parameters	% by Mass
SiO_2	69,2
Al_2O_3	10,81
TiO_2	0,08
Fe_2O_3	1,18
Na_2O	0,367
K_2O	2,78
CaO	2,98
MgO	1,48
P_2O_3	0,021
SO_2	0,036
Dry Matter (1500 C°)	10,21
Ph	7,0

2.3. Method

The laboratory experiments were carried out in two stages. In the first stage, liquid limit and plastic limit tests, which provide important information in the evaluation of the swelling potential of the soil, were carried out in relevance with the ASTM D4318 (2017) standard. In the stabilization of the high plasticity natural material, mixtures containing by weight 8, 10, 12, 14, 16% sea shell, 0, 3, 5, 6, 8% percent lime and 0, 5, 10, 15 and 20% percent zeolite were prepared (Table 5). The experimental studies conducted as part of this research were executed in two stages utilizing the optimization technique known as the Taguchi method. This method involves creating an orthogonal matrix based on the selected factors and levels, with the resulting experimental sets serving as a reference. The primary objective is to predict a greater number of experimental outcomes from a reduced set of experiments. The experimental sets employed in the Taguchi design were generated using an orthogonal array. The optimal five additive percentages, identified from the literature review, were designated as levels, while the three additive materials selected for use were defined as factors.

Following the soil mechanics experiments conducted to ascertain the mechanical and physical properties of the natural material, consistency limit experiments were performed to assess the swelling behavior of the soil. These experiments were carried out separately for 16 combination ratios using the Taguchi method, as outlined by the orthogonal matrix (L16). The data obtained from these experiments were subsequently analyzed using the Taguchi method, leading to the selection of the two percentages that yielded the best results for each additive based on the program's output. Thus, the first stage was completed. In the second stage of the study, these percentages were reassessed as five experimental sets according to the Taguchi analysis program. Compaction tests, swelling percentage assessments, and swelling pressure experiments were conducted for the five determined combination ratios. The plastic limit (PL) tests were performed using the material prepared for the liquid limit (LL) tests, with all experiments conducted at room temperature. The results indicated that the optimal seashell content ranged from 12% to 14% by weight, while the optimal lime content ranged from 5% to 6% by weight. For zeolite, the best results were obtained with an additive ratio of 5% to 10% by weight. Furthermore, the three mixtures, along with the two best percentages identified for each mixture, were combined. According to the combination result, 5 experimental sets were determined and mixture combinations were made to determine the behavior of these mixtures when used together (Table 4).

Table 4 - Mixtures used for stabilized soil.

Soil mixture	Symbol	Percentage			
		Seashell	**Lime**	**Zeolite**	**Soil**
12% Seashell + 6% Lime + 10% Zeolite	SS12L6Z10	12	6	10	72
14% Seashell + 6% Lime + 5% Zeolite	SS14L6Z5	14	6	5	75
12% Seashell + 5% Lime + 5% Zeolite	SS12L5Z5	12	5	5	78
14% Seashell + 5% Lime + 10% Zeolite	SS14L5Z10	14	5	10	71
14% Seashell + 6% Lime + 10% Zeolite	SS14L6Z10	14	6	10	70

When these abbreviations are classified;

In the expression that SS (1) L (2) Z (3)

S: soil, S; shell, L; lime, Z; zeolite and

(1); Percentage of seashell by dry weight in the total sample.

(2); Percentage of lime by dry weight in the total sample

(3); The percentage of zeolite by dry weight in the total sample are symbolized.

Table 5 - Only mixtures used for stabilized soil.

Soil mixture	Symbol	Additive percentace	Soil percentace
100% soil	S	0	100
8% seashell	SS8	8	92
10% seashell	SS10	10	90
12% seashell	SS12	12	88
14% seashell	SS14	14	86
16% seashell	SS16	16	82
3% lime	SL3	3	97
5% lime	SL5	5	95
6% lime	SL6	6	94
8% lime	SL8	8	92
5% zeolite	SZ5	5	95
10% zeolite	SZ10	10	90
15% zeolite	SZ15	15	85
20% zeolite	SZ20	20	80

In the second stage of the study, five experimental sets were prepared by combining the percentages that gave the best results. Compaction, swelling percentace and swelling pressure tests were performed for these five determined combination ratios. The Standard Proctor Test was carried out in accordance with ASTM D698 (2012).

To determine the swelling parameters of the mixture samples, experiments were carried out in accordance with the ASTM D4546 (2021) Standard. After a curing period of one day, the samples were placed in a conventional oedometer and subjected to swelling under a surcharge load of 1 kPa. Test data were taken and recorded during the experiment. Upon completion of the swelling process, vertical pressures were applied until the samples returned to their initial height. The pressure necessary for the samples to revert to their original height was recorded as the swelling pressure.

3. RESULTS AND DISCUSSION

3.1. Atterberg's Limits

Liquid limit (LL) and plastic limit (PL) tests were performed on different percentages of seashell (8%, 10%, 12%, 14%, 16% by dry weight of the soil), lime (3%, 5%, 6%, 8%) and zeolite (5%, 10%, 15%, 20%). The effects of additive ratios on consistency limits are shown in Figure 3, 4, and 5. In addition, LL and PL experiments results shown in Table 6 for the combination of additive percentages.
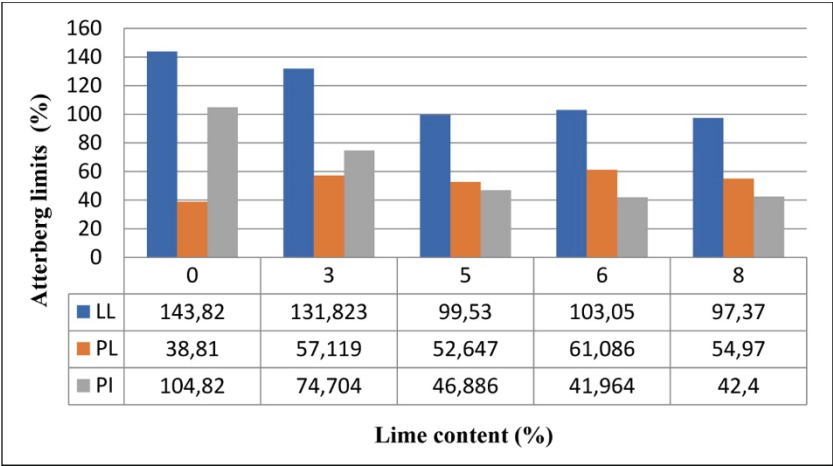
Figure 3 - Atterberg limits of natural soil-lime mixture
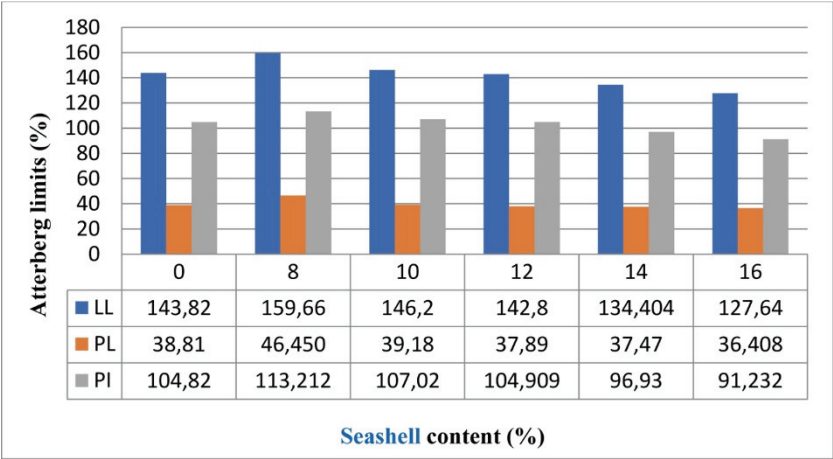
Figure 4 - Atterberg limits of natural soil-seashell mixture
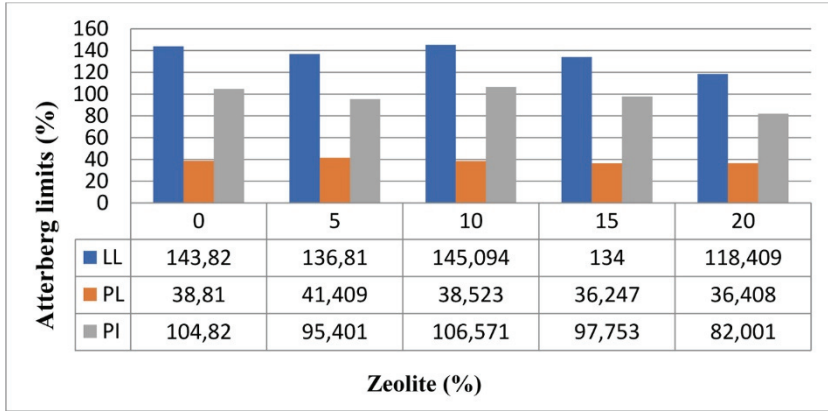
Figure 5 - Atterberg limits of natural soil-zeolite mixture

Table 6 - Results of Atterberg limits of mixtures

Soil mixture	LL	PL	PI
SS12L6Z10	82,32	57,56	24,73
SS14L6Z5	88,34	58,69	29,65
SS12L5Z5	83,74	36,25	47,49
SS14L5Z10	79,59	52,37	27,22
SS14L6Z10	74,45	49,21	25,24

3.2. Compaction Test

The compaction test was used to determine the impact of stabilizers on optimum water content and maximum dry density of the expansive soil. Mixtures were prepared according to five test sets and Standard Proctor test was performed in accordance with ASTM D698 (2012). Before starting the experiment, the water content of the soil and additives that were left to dry in the air was calculated. The water content calculated on the material mixture percentages was added and mixed by weight at the determined ratios. The compaction test commenced with the addition of approximately 20% water content to the air-dried soil sample, followed by incremental increases of approximately 3% in water content during subsequent stages. The compaction curves obtained at the end of the experiments are given in Figure 6. The minimum increase in maximum dry density and the minimum decrease in optimum water content were observed in SS12L5Z5 mixture. For all other mixtures, decreases in optimum water content (w_{opt}) and increases in maximum dry density were observed. The optimum water content for all mixtures was between 32%- 37% and the maximum dry density ranged between 1,27-1,31 kN / m^3. All additives reduced the optimum water content of the soil. Additionally, the results of the LL and PL experiments for the combinations of additive percentages are presented in Table 6.
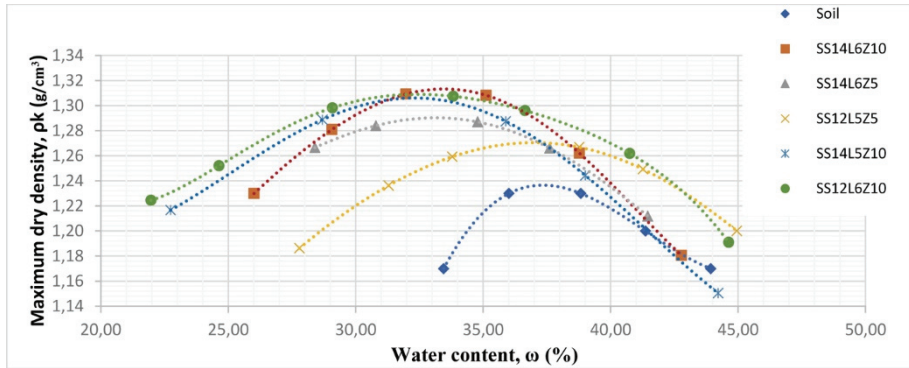
Figure 6 - Compaction curves of mixtures

3.3. Swelling Percent and Swelling Pressure Test

Accurately determining the swelling behavior of soils is crucial in geotechnical engineering, as damage is often inevitable in light structures built on expansive soils without proper precautions. Swelling behavior can sometimes occur not only with the change of water contens in the environment, but also with the decrease of the current load exposed to the ground over time. Therefore, to assess the swelling potential of a construction site, it is essential to carefully evaluate parameters such as the swelling percentage and swelling pressure during the project's planning phase.

In this study, swelling properties were determined in accordance with ASTM D4546 (2021) Standard. Samples prepared at the rates indicated in Table 5, were compressed with optimum water content and maximum dry unit weight. After a one-day curing period, the samples were allowed to swell under an surcharge load of 1 kPa in a conventional oedometer.

Measurements were taken and recorded during the experiment. After the swelling was completed, vertical pressures of 5, 10, 15, 20, 40, 80, kPa etc. were applied until the samples reached the initial height value. The pressure that allowed the samples to return to their initial height was recorded as the swelling pressure. The results obtained from the swelling pressure and swelling percentage experiments are given in Figure 7 and 8. As the amount of additive increased, a prominent reduce in swelling percentage and swelling pressure values was observed. This indicates that the combined application of seashell, zeolite, and lime effectively mitigates the swelling potential of clay soils.

The addition of 12% seashell, 6% lime, and 10% zeolite to the natural soil sample resulted in an 87% reduction in the swelling percentage, while the swelling pressure remained relatively stable. This is likely because the specified proportions of additives increased the strength of the treated soil, preventing vertical displacement. In a mixture with 12% seashell, 5% lime, and 5% zeolite, the swelling pressure was reduced by 88%, while the swelling percentage decreased by 98% compared to the untreated soil. Thus, the combination of 12% seashell, 5% lime, and 5% zeolite is sufficient to improve the swelling potential of the soil.
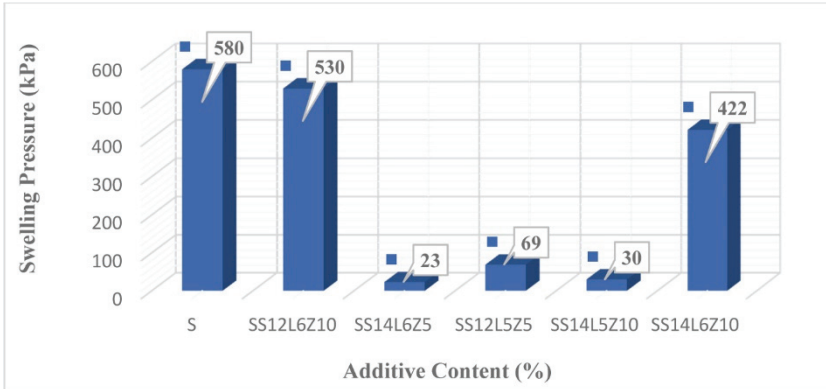
Figure 7 - Variation of swelling pressure with seashell, lime, and zeolite contents
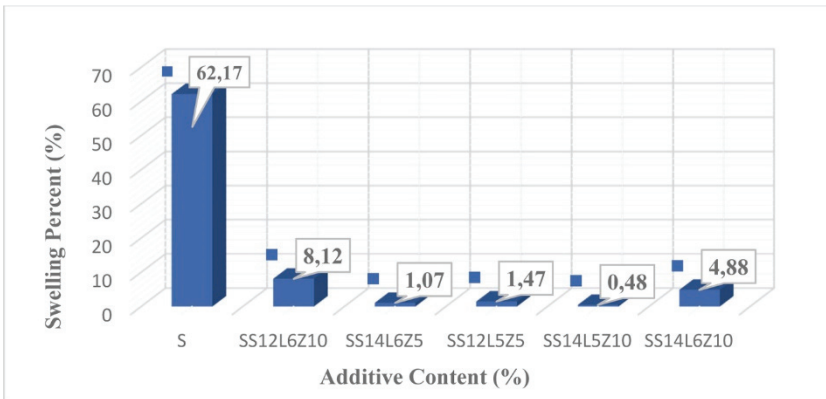
Figure 8 - Variation of swelling percent with seashell, lime, and zeolite contents

4. CONCULUSION

Soil swelling is a common problem in many regions of the world. Much research has been carried out in geotechnical engineering to solve this problem. Previous studies have evaluated the effect of additives such as sand, cement and lime on the swelling potential and the results obtained showed that the swelling properties were improved. In recent years the effect of new additives designed to replace these has been investigated. Specifically, the use of waste materials such as shells has increased in stabilising studies. In this study, the use of shells and alternative materials such as lime and zeolite in superficial soil stabilisation and the effects of these materials on the swelling problem of the soil were investigated. Experimental data from many previous studies in the literature were reviewed and the mix ratios used in this study were determined. To investigate the effect of alternative materials such as lime, shell and zeolite on soil stabilisation, mixtures were prepared by adding 8, 10, 12, 14 and 16 wt% shell, 0, 3, 5, 6, 8% lime and 0, 5, 10, 15, 20 wt% zeolite to natural soil. According to the

results of the Atterberg Limits, the best results were calculated for shells between 12 and 14 wt%, for lime between 5 and 6 wt% and for zeolite with an addition of 5 to 10 wt%.

The findings of this study may have significant implications for addressing soil stabilization issues by utilizing alternative materials such as lime, seashell, and zeolite. Based on the results of a series of Tests carried out the following conclusions can be drawn:

- While the liquid limit and plasticity index values of all mixtures in which additives are used together have decreased to a great extent, an increase has occurred in the plastic limit value. Since lime causes significant changes in the effective grain diameter and microstructure of the soil, it has been seems that the natural soil sample with lime added has started to show silty behavior.

- All additives added to the ground reduced the optimum water content of the soil. While the optimum water content of the natural soil was 37,4% and the maximum dry density weight was 1,23 g/cm^3, the optimum water content for all mixtures was between 32%-37% and the maximum dry density varied between 1,27- 1,31 g/ cm^3. The addition of materials with high unit volume weight such as seashell and zeolite also increased the maximum dry density of the soil.

- According to the swelling percentage tests performed on the samples prepared by adding additives to the natural soil, the mixture with 14% sea shell, 6% lime and 5% zeolite added by weight (SS14L6Z5) gave the smallest swelling value. The swelling percentage of the mixture added by weight was determined as 1,07%. The swelling percentage for this mixture was determined to be 1.07%, representing a 98% reduction compared to the natural soil sample. This helps in reducing the water retention abilities in the treated these rates.

- According to the swelling pressure tests performed on the samples prepared by mixing natural soil and additives, the minimum swelling pressure value was calculated as 23 kPa in the mixture with 14% sea shell, 6% lime and 5% zeolite (SS14L6Z5) by weight. The swelling pressure value of the mixture (SS14L6Z5) decreased by 986% compared to the swelling pressure value of the natural soil. However, unexpected high results of swell pressure were obtained for some mixtures which could be referred to their high strengths. The reason is probably the very high compressive strength of this compound.

   This study proposes an environmentally friendly solution that improves the geotechnical properties of the swelling soil by making use of available waste materials.

We hope that future studies, which consider the effectiveness of commercially available additives for the stabilization of expansive soils, will further validate our findings.

References

[1]   Scalia, J., Taher, Z., J and Bareither, C., A., Comparative assessment of expansive soil stabilization by commercially available polymers, *Transportation Geotechnics*, 24: 2214-3912, 2020.

[2] Popescu, M., E., A Comparison between the Behaviour of Swelling and of Collapsing Soils, *Engineering Geology*, 23: 145-163, 1986.,

[3] El-Sohby, M. A. and Mazen, O., Mineralogy and Swelling of Expansive Clayey Soils, 1983.

[4] Meshram, K., Singh, N. and Jain, P., K., Estimation of swelling characteristics of expansive soils with influence of clay mineralogy, *Acta Agrıculturae Scandınavıca, Sectıon B — Soıl & Plant Scıence*, 2021. https://doi.org/10.1080/09064710.2021.1872696.

[5] Al-Swaidani, A., Hammoud, I. and Meziab, A., Effect of adding natural pozzolana on geotechnical properties of lime-stabilized clayey soil, *Journal of Rock Mechanics and Geotechnical Engineering*, 8: 714-725, 2016.

[6] Ingles, O., G. and Metcalf, J., B., Soil Stabilization, John Wiley&Sons, New York. 1973.

[7] Çalık, Ü., Perlitin Puzolanik Katkı Olarak Kireç ile Birlikte Zemin Stabilizasyonunda Kullanımı, Doctoral Thesis, Karadeniz Technical University, Institute of Science and Technology, Trabzon, 2012.

[8] Indiramma, P., Sudharani, C., H. and Needhidasan, S., Utilization Of Fly Ash And Lime To Stabilize The Expansive Soil And To Sustain Pollution Free Environment, *Materials Today: Proceedings,* 22: 694 –700, 2019.

[9] Cokca, E., Use of class c fly ashes for the stabilization of an expansive soil, *J. Geotech. Geo Environ. Eng.,* 2001. https://doi.org/10.1061/(ASCE)1090-0241(2001)127:7(568)

[10] Kazemıkhosrowshahı, S., Stabılızatıon Of Expansıve Soıl Usıng Copolymer, Homopolymer Polypropylene, Fly Ash And Lım,. M.Sc. Thesıs, İ.T.Ü., Graduate School Of Scıence Engıneerıng And Technology, İstanbul, 2014.

[11] Rambabu, T., Rambabu, P., Prasad, R. and Indraja, P., Experimental Investigations on Expansive Soils Grouted with Additives, Advancements in Unsaturated Soil Mechanics, 127–141, 2019. https://doi.org/10.1007/978-3-030-34206-7_10.

[12] Taki, K., Choudhary, S., Gupta, S. and Kumar, M., Enhancement of geotechnical properties of municipal sewage sludge for sustainable utilization as engineering construction material, *Journal of Cleaner Production*, 251:0959-6526, 2020. https://doi.org/10.1016/j.jclepro.2019.119723.

[13] Pourakbar, S., Asadi, A., Huat, B., B. and Fasihnikoutalab, M., H., Soil stabilisation with alkali-activated agro-waste, *Environ Geotech*., 2:359–370, 2015.

[14] GuhaRay, A., Syed, M. and Kar, A., Stabilization of Expansive Clayey Soil with Alkali Activated Binders, *Geotech Geol Eng.,* 2020. https://doi.org/10.1007/s10706-020-01461-9.

[15] Mallela, J., Harold, V., Quintus, P. and Smith, K., L., Consideration of lime-stabilized layers inmechanistic-empirical pavement design, The National Lime Association, USA, 2004.

[16] Al-Mukhtar, M., Khattab, S. and Alcover, J. F., Microstructure and geotechnical properties of lime-treated expansive clayey soil, *J Eng Geol.,* 139:17–27, 2012.

[17] Jha, A., K. and Sivapullaiah, P., V., Susceptibility Of strength development by lime in gypsiferous soil-a micro mechanistic study, *Appl Clay Sci.,* 115:39–50, 2015.

[18] Chandran, G. and Soman, K., Heave control and strengthening of expansive soil using lime mixed GGBS column, *Int. J. Eng. Res. Technol. (IJERT)*, 5(8):469-474, 2016

[19] Taşçı, G., Problemli Kil Zeminin Geoteknik Özelliklerine Silis Dumanı ve Kireç Katkısının Etkisi, Master's Thesis, Eskişehir Osmangazi University, Institute of Science and Technology, Eşkişehir, 2011.

[20] Mounika, K., Narayana, B., Manohar, D. and Vardhan, K., Influence Of Sea Shells Powder On Black Cotton Soıl Durıng Stabılızatıon, *International Journal of Advances in Engineering & Technolog,* 7, 5: 1476-1482, 2014.

[21] Patel, A. and Mishr, C., B., Performance of Seashell Powder on Sub-grade Soil Stabilization, *Kalpa Publications in Civil Engineering*. 1: 150-156, 2017.

[22] Akimkhan, A. M., Structural and ion-exchange properties of natural Zeolite, In: Ion exchange technologies, InTech UK: 262-282, 2012.

[23] Sharo, A., Shaqour, F. and Ayyad, J., M., Maximizing Strength of CKD – Stabilized Expansive Clayey Soil Using Natural Zeolite*, Geotechnical Engineering,* 1226-7988, 2021. https://doi.org/10.1007/s12205-021-0786-2.

[24] Turkoz, M. and Vural, P., The effects of cement and natural zeolite additives on problematic clay soils, *Science and Engineering of Composite Materials,* 20(4):395-405, 2013. https://doi.org/10.1515/secm-2012-0104.

[25] Miao, S., Shen, Z., Wang, X., Luo, F., Huang, X. and Wei, C., Stabilization of highly expansive black cotton soils by means of geopolymerisation, *J Mater Civ Eng.* 29(10):04017170., 2017.

[26] Lu, Z., She, J., Duan, Y., Yao, H. and Liu, L., Experimental study on the engineering properties of expansive soil treated with Al13, *Scientific Reports,* 10:13930, 2020. https://doi.org/10.1038/s41598-020-70947-6.

[27] Bisanal, M. and Badiger, R., Study on Stabilization of Soil Using Sea Shell and Bitumen Emulsion, *International Journal of Innovative Research in Science. Engineering and Technology,* 4, 7: 5875-5882, 2015.

[28] Turkoz, M. and Öztürk, O., Effect of silica fume on the undrained strength parameters of dispersive soils, *Turkish Journal of Engineering*, 6(4); 293-299, 2022.

[29] Özkan, İ., and Çokça, O., The Investigation of the Addition of Sodium Lignosulfonate to Lime Column Used For Improving the Expansive Soils, *Turkish Journal of Engineering,* 770, 135-152, 2023. https://doi.org/10.18400/tjce.1209185.

[30] Ertuğrul, Ö., L., and Canoğulları, F., D., An investigation on the geomechanical properties of fiber reinforced cohesive soils, *Turkish Journal of Engineering*, 5(1); 15-19, 2021.

[31] Narmandakh, D., Butscher, C., Ardejani, F., D., Yang, H., Nagel, T., and Taherdangkoo, R., The use of feed-forward and cascade-forward neural networks to determine swelling potential of clayey soils, *Computers and Geotechnics*, 157, 105319, 2023. https://doi.org/10.1016/j.compgeo.2023.105319

[32] Özkan, İ., and Yenginar, Y., Improvement Of Hıgh Plastıcıty Clay By Usıng Fılter Sludge, *Konya Journal of Engineering Sciences*, 11(4), 973-985, 2023.

[33] Bell, F., G., Lime Stabilization of Clay Minerals and Soils, *Engineering Geology*, 42, 223-237, 1996.

Ülkemiz Mühendislik Uygulamalarında Çelik Çatı Sistemlerinin Optimum Tasarımına Dair İnceleme

Hasan ESER[1*]
Oğuzhan HASANÇEBİ[2]

ÖZ

Bu çalışmada, ülkemiz mühendislik uygulamalarında büyük açıklıklı çelik çatı sistemlerinin ne kadar optimum tasarlandığına dair bir inceleme yapılmaktadır. Bu amaçla, Türkiye'nin çeşitli bölgelerinde inşa edilmiş üç kapalı yüzme havuzuna ait çelik çatı sistemlerinin optimum boyutlandırılması, kaotik kapasite kontrollü arama (kaotik-KKA) yöntemi kullanılarak gerçekleştirilmiş ve elde edilen optimum tasarımlar bu sistemlerin daha önceden proje firmaları tarafından geleneksel mühendislik yöntemleri kullanılarak oluşturulan orijinal tasarımları ile karşılaştırılmıştır. Bu karşılaştırmalar neticesinde, büyük açıklıklı çelik çatı sistemlerinin tasarım aşamalarında yapı optimizasyonu yöntemlerinin kullanılması ile, yapı ağırlığında ve dolayısıyla maliyetinde, orijinal tasarımlara göre %10-40 oranında tasarruf sağlanabileceği tespit edilmiştir. Büyük açıklıklı çatı sistemlerinde çelik kullanımının azaltılması sadece malzeme masraflarını değil, aynı zamanda nakliye ve imalat maliyetlerini de düşürecektir. Bunun yanı sıra, çelik endüstrisinin çevresel zararlarını da azaltarak sürdürülebilirliğe katkı sağlayacaktır.

Anahtar Kelimeler: Çelik çatı sistemleri, yapı optimizasyonu, kaotik kapasite kontrollü arama yöntemi, endüstriyel uygulama, gerçek yapılar.

ABSTRACT

A Study on the Optimum Design of Steel Roof Systems in Turkish Engineering Practice

In this study, an investigation is conducted on how optimally large span steel roof systems are designed in Turkish engineering practice. For this purpose, the optimum sizing of the steel roofs of three indoor swimming pools constructed in different regions of Turkey was performed using the chaotic capacity controlled search (Chaotic-CCS) method and the

1 Orta Doğu Teknik Üniversitesi, İnşaat Mühendisliği Bölümü, Ankara, Türkiye
  heser@metu.edu.tr - https://orcid.org/0000-0001-8527-020X

2 Orta Doğu Teknik Üniversitesi, İnşaat Mühendisliği Bölümü, Ankara, Türkiye
  oguzhan@metu.edu.tr - https://orcid.org/0000-0002-5501-1079

* Sorumlu yazar

obtained optimum designs were compared with the original designs of these systems by design office engineers using conventional design approach. As a result, it was determined that the use of structural optimization methods in the design phase of large span steel roof systems will reduce structural weight about 10-40% and thus the cost of structures compared to the original designs. Reducing the use of steel in large span roof systems will not only reduce material costs, but also transportation and construction costs. It will also contribute to sustainability by reducing the impact of the steel industry on the environment.

Keywords: Steel roof systems, structural optimization, chaotic capacity controlled search, industrial application, real structures.

1. GİRİŞ

Modern inşaat mühendisliği uygulamalarının önemli bir parçasını oluşturan büyük açıklıklı çelik çatı sistemleri, geniş alanların desteklenmesi amacıyla kullanılan yapısal çözümlerdir. Bu sistemler, ekseriyetle spor salonları, alışveriş merkezleri, uçak hangarları, sergi salonları ve depolar gibi geniş iç mekanlar gerektiren yapılarda yaygın olarak kullanılırlar. Büyük açıklıklı çatı sistemlerinin tasarımı, yapının stabilitesi, güvenliği, estetiği ve ekonomisi açısından dikkatli bir mühendislik uygulaması gerektirir. Yapılara etki eden yüklerin doğru bir şekilde hesaplanması, yapının güvenliği ve dayanıklılığı için kritik öneme sahiptir.

Bu yapıların geleneksel yöntemlerle gerçekleştirilen tasarım sürecinde, tasarım mühendisi deneyimlerine, sezgilerine ve bazı yaklaşık hesaplamalara dayanarak bir ön tasarım oluşturur. Ardından bu tasarım analiz edilir. Analiz sonuçlarına göre, dayanımı yetersiz olan yapı elemanlarının kesitleri büyütülürken, gereğinden fazla dayanıma sahip elemanların kesitleri küçültülür. Bu süreç, tasarım koşullarını (deplasman, dayanım, vb.) sağlayan ilk uygun tasarım elde edilene kadar genellikle birkaç kez tekrarlanır. Böylece yapı için hem geçerli ve hem de ekonomik bir tasarım elde edilmeye çalışılır. Ancak, en küçük bir yapı probleminin tasarımında bile sonsuz sayıda geçerli (uygun) çözüm olduğu göz önünde bulundurulduğunda, bu geleneksel deneme-yanılma yaklaşımıyla elde edilen tasarımın, yapı için en ekonomik tasarım olmayacağı açıktır. Üstelik, bu yöntemle bazen gereğinden fazla ağır veya maliyetli tasarımların elde edilme olasılığı da vardır.

Yapı optimizasyonu, bir mühendislik yapısının sonsuz sayıda uygun tasarımı arasından ağırlık veya maliyet açısından en iyi (optimum) çözümü bulmayı amaçlar. Temelleri 1960'lı yıllara dayanan ve o tarihten itibaren sürekli bir gelişim içerisinde olan bu disiplinde, inşaat mühendisliği yapılarının optimum tasarımları için ilkin matematiksel programlama ve optimumluk kriteri yöntemleri kullanılmıştır [1-3]. Ancak, bu yöntemlerde kullanılan türeve dayalı algoritmaların tasarım değişkenlerini sürekli-değerli kabul etme zorunluluğu, bu yöntemlerle gerçekçi ve uygulanabilir çözümlerin elde edilmesini oldukça zorlaştırmaktadır. Bu sebeple, söz konusu yöntemler zamanla terk edilmiş ve yeni algoritmalar geliştirilmeye çalışılmıştır [4-8].

1990'lı yılların başından itibaren, diğer tüm disiplinlerde olduğu gibi yapı optimizasyonu literatüründe de meta-sezgisel (metaheuristic) olarak adlandırılan optimizasyon algoritmalarının ön plana çıktığı ve yaygın olarak kullanılmaya başlandığı görülmüştür. Doğadaki oluşumların taklit edilerek nümerik bir arama algoritmasına dönüştürülmesi esasına göre geliştirilen bu yöntemlerin ortak özellikleri, türeve dayalı arama metodolojilerini

reddetmeleri ve ayrık-değerli tasarım değişkenleri içeren optimizasyon problemleri için çözüm üretebilmeleridir. Ayrıca, bu yöntemlerin türeve dayalı olmayan arama metodolojileri, kötü lokal optimum çözümlere yakalanmadan tasarım uzayının kapsamlı bir şekilde taranmasına olanak vermektedir. Yapı optimizasyonu literatüründe, yeni meta-sezgisel optimizasyon yöntemlerinin geliştirilmesi, bu yöntemlerin çeşitli uyarlamaları, birbirleriyle karşılaştırmaları ve farklı yapı türlerine uygulanmaları konularında çok sayıda çalışma mevcuttur [9-17]. Öte taraftan, bu yöntemlerin yakınsama hızları oldukça düşüktür. Global optimum çözüme veya iyi bir lokal optimum çözüme yakınsamadan önce, problem boyutuna bağlı olarak binlerce, on binlerce ve hatta yüz binlerce iterasyona ihtiyaç duyabilirler. Ancak, tasarım için harcanan zamanın önemli bir unsur olarak görülmesi sebebiyle, meta-sezgisel yöntemlerin proje ofisleri tarafından benimsenerek gerçek mühendislik yapılarının tasarımında kullanılması çok muhtemel gözükmemektedir. Dahası, performansa dayalı, doğrusal olmayan yapısal analiz yöntemlerinin tasarım şartnamelerinde yer almaya başlaması ile birlikte yapı analiz sürelerinin uzaması, çok sayıda iterasyon gerektiren meta-sezgisel yöntemlerin gerçek mühendislik uygulamalarında kullanımını zaman yönünden daha da elverişsiz hale getirmektedir [18].

Son dönemlerde tasarım-odaklı (design-driven) yöntemler, yapı optimizasyonunda öne çıkmaktadır. Bu yöntemler önceki iterasyonlardaki analiz ve tasarım aşamalarından elde edilen alan bilgisinden (domain knowledge) yararlanarak arama sürecini daha etkin bir şekilde yönlendiren algoritmalar kullanırlar [19-22]. Bu nedenle, olasılıksal geçiş kurallarını kullanan meta-sezgisel yöntemlerden birkaç kat daha hızlı çalışırlar ve gerçek mühendislik uygulamalarında kullanılma potansiyelleri daha yüksektir.

Yapı optimizasyonunda kullanılan yöntemlerin yukarıdaki paragraflarda bahsedilen dezavantajları, bu yöntemlerin proje ofisleri tarafından yapı tasarımı uygulamalarında yaygın olarak kullanılmasını kısıtlamıştır. Ancak, bu alanda yapılan akademik ve bilimsel çalışmalarda da konunun güncel mühendislik uygulamalarına kazandırılması yönünde özel bir çaba gösterilmediği de bir gerçektir. Nitekim, yapı optimizasyonu üzerine yapılan araştırmalarda gerçek uygulamalara yer veren çalışmalar oldukça sınırlıdır [23-28]. Bu alanda yayınlanan akademik ve bilimsel çalışmalardaki sayısal uygulamalar ekseriyetle küçük ölçekli veya idealize edilmiş yapı sistemleri kullanılarak gerçekleştirilmiştir. Bazı çalışmalarda binlerce elemandan oluşan büyük ve gerçek boyutlu yapılar kullanılmış olsa da bu problemler yükleme durumlarının sadeleştirilmesi veya gerçek mühendislik problemlerinde göz önüne alınması gereken tasarım kriterlerinin göz ardı edilmesiyle nispeten basitleştirilerek kullanılmıştır. Böyle olunca, yapı optimizasyonu alanının akademik dünyadaki gelişimi ile mühendislik uygulamalarındaki kullanımı arasında oluşan boşluk bir türlü kapatılamamıştır.

Şüphesiz, yapı optimizasyonunun mühendislik uygulamalarına yeterince entegre edilememesinin tek sebebi, bu alanda kullanılan yöntemlerin belirtilen dezavantajlarından kaynaklanmamaktadır. Yapı optimizasyonu yöntemleri ve uygulamaları konularında proje ofislerinin yeterli bilgiye sahip olmamaları, yapı optimizasyonun maliyet avantajları konusunda yapı sahiplerinin (kişi, özel teşebbüs veya kamu kurum ve kuruluşları) farkındalıklarının bulunmaması, kamu kurum ve kuruluşları tarafından ihale edilen işlerde yapıların proje ofisleri tarafından ne kadar ekonomik tasarlandığının idarelerce incelenmemesi, ilave malzeme kullanımı ile daha güvenli bir tasarım oluşturduğuna dair yanlış inanışlar, yapım maliyetlerinin kamu kurum ve kuruluşları tarafından karşılanması

sebebiyle, proje ofislerinin maliyet azaltma konusuna yeterince önem vermemesi gibi faktörler, bu sorunun diğer nedenleri arasında sayılabilir.

Bu çalışmada, bir kamu idaresi tarafından ihale edilerek Türkiye'nin çeşitli bölgelerinde inşa edilmiş üç kapalı yüzme havuzuna ait çelik çatı sistemlerinin tasarım odaklı bir optimizasyon tekniği olan kaotik kapasite kontrollü arama (Kaotik-KKA) yöntemi ile optimum boyutlandırılması gerçekleştirilmiştir. Sonrasında bu sistemler için elde edilen optimum tasarımlar yapıların daha önceden proje firmaları tarafından geleneksel mühendislik yöntemleri kullanılarak oluşturulan orijinal tasarımları ile karşılaştırılmıştır. Çalışmanın amacı, ülkemiz mühendislik uygulamalarında büyük açıklıklı çelik çatı sistemlerinin ne derece ekonomik tasarlandığını incelemek ve yapı optimizasyonu ile elde edilebilecek maliyet avantajlarını ortaya koyarak, bu yöntemlerin ülkemiz mühendislik uygulamalarında kullanılmasını teşvik etmektir.

Makalenin diğer bölümleri şu şekilde düzenlenmiştir. İkinci bölümde, yapı optimizasyonu probleminin tanımı ve matematiksel formülasyonu ele alınmıştır. Üçüncü bölümde, bu çalışmada kullanılan Kaotik-KKA yöntemi ve algoritması özetlenmiştir. Dördüncü bölümde, çalışmada kullanılan yapı optimizasyonu problemleri tanıtılmış ve bu yapılar için elde edilen optimum tasarımlar, yapıların orijinal tasarımları ile karşılaştırılmıştır. Beşinci ve son bölümde ise, elde edilen sonuçlar özetlenmiş ve yapı optimizasyonunun bir tasarım rutini haline getirilmesinin gerekliliği ve maliyet avantajları vurgulanmıştır.

2. YAPI OPTİMİZASYONU PROBLEMİNİN FORMÜLASYONU

Bir çelik yapının tasarımında yapı elemanları, kesit havuzu veya profil listesi olarak tanımlanan hazır (ayrık) kesitler arasından seçilerek boyutlandırılmalıdır. Bir profil listesindeki kesitler artan kesit alanına göre sıralanırlar ve her kesite 1'den başlanarak bir sıra numarası verilir. Böylelikle, listedeki en küçük kesit alanına sahip olan kesitin sıra numarası 1'e, en büyük kesit alanına sahip kesitin sıra numarası ise toplam kesit sayısına eşitlenir. İmalat ve montaj kolaylığı açısından, yapı genelinde çok fazla sayıda farklı kesit kullanılması tercih edilmez. Bu sebeple, tasarım aşamasında yapı elemanları genellikle belirli sayıda (N_g) eleman grubuna ayrılır ve bir gruba ait tüm elemanlar için aynı kesit ataması yapılır. Bu bilgiler ışığında, bir çelik yapı için ayrık boyutlandırma optimizasyon problemi (kesit optimizasyonu) şu şekilde formüle edilir:

Yapı optimizasyonu işleminde amaç, bir yapının ağırlığını (W) tasarım sınırlayıcılarına (g_k) uygun olarak minimize eden tasarım değişkenleri vektörünü (**I**) elde etmektir.

$$\mathbf{I^T} = \begin{bmatrix} I_1, I_2, \dots, I_{N_g} \end{bmatrix} \tag{1}$$

$$W = \sum_{i=1}^{N_g} \gamma_i A_i \sum_{j=1}^{N_{m,i}} L_{j,i} \tag{2}$$

$$g_k \leq 0, \quad k = 1, 2, \dots, N_c \tag{3}$$

Denklem (1-3)'te, tasarım değişkeni vektörü (**I**), kesit havuzundan N_g eleman grubuna atanan kesitlerin sıra numaralarını; γ_i ve A_i sırasıyla bir eleman grubuna atanan ayrık bir kesitin

birim ağırlığını ve alanını; $N_{m,i}$, i'nci eleman grubundaki toplam eleman sayısını; $L_{j,i}$, i'nci eleman grubundaki j'inci elemanın uzunluğunu; g_k, k'inci normalize edilmiş tasarım sınırlayıcısını ve N_c toplam tasarım sınırlayıcı sayısını ifade etmektedir.

Optimizasyon işlemi sonunda elde edilecek uygun bir tasarımın, yapı tasarım şartnameleri ve yapım uygulamaları gereği yerine getirmesi gereken tüm koşullar ve hükümler, optimizasyon probleminin sınırlayıcıları olarak tanımlanır. Ülkemizde çelik yapıların tasarımı için Çevre, Şehircilik ve İklim Değişikliği Bakanlığı tarafından hazırlanan "Çelik yapıların tasarım, hesap ve yapımına dair esaslar" [29] şartnamesi kullanılmaktadır. Bu şartnameye göre, çelik yapı elemanlarının aşağıdaki dayanım sınırlayıcılarını sağlamaları gerekmektedir.

Eğilme momenti ve eksenel kuvvet etkisindeki çift ve tek simetri eksenli elemanlar için:

$$\left(\frac{P_r}{P_c}\right)_j \geq 0.2 \text{ ise } g_1 = \left(\frac{P_r}{P_c}\right)_j + \frac{8}{9}\left(\frac{M_{rx}}{M_{cx}} + \frac{M_{ry}}{M_{cy}}\right)_j - 1.0 \leq 0 \tag{4}$$

$$\left(\frac{P_r}{P_c}\right)_j < 0.2 \text{ ise } g_1 = \left(\frac{P_r}{2P_c}\right)_j + \left(\frac{M_{rx}}{M_{cx}} + \frac{M_{ry}}{M_{cy}}\right)_j - 1.0 \leq 0 \tag{5}$$

Kesme kuvveti etkisi altındaki elemanlar için:

$$g_2 = \left(\frac{V_r}{V_c}\right)_j - 1 \leq 0 \tag{6}$$

Burulma, kesme kuvveti, eğilme ve eksenel kuvvetin ortak etkisindeki boru ve kutu enkesitli elemanlar için:

$$\left(\frac{T_r}{T_c}\right)_j \geq 0.2 \text{ ise } g_3 = \left(\frac{P_r}{P_c} + \frac{M_{rx}}{M_{cx}} + \frac{M_{ry}}{M_{cy}}\right)_j + \left(\frac{V_{rx}}{V_{cx}} + \frac{V_{ry}}{V_{cy}} + \frac{T_r}{T_c}\right)_j^2 - 1 \leq 0 \tag{7}$$

Bu denklemlerde, g_1, eğilme momenti ve eksenel kuvvet etkisindeki çift ve tek simetri eksenli elemanlar için; g_2, kesme kuvveti etkisi altındaki elemanlar için; g_3, eğilme ve eksenel kuvvetin ortak etkisindeki boru ve kutu enkesitli elemanlar için dikkate alınan dayanım sınırlayıcılarıdır. Herhangi (j numaralı) bir yapı elemanı için P_r, M_r, V_r ve T_r sırasıyla gerekli eksenel kuvvet, eğilme momenti, kesme kuvveti ve burulma momenti dayanımlarını; P_c, M_c, V_c ve T_c sırasıyla ilgili şartname hükümlerine göre belirlenen mevcut eksenel kuvvet, eğilme momenti, kesme kuvveti ve burulma momenti dayanımlarını; x ve y ise sırasıyla elemanın güçlü ve zayıf eksenlerini ifade etmektedir.

Büyük açıklıklı çelik yapı sistemlerinde elemanların dayanım gereksinimleri yanı sıra, çatı makaslarında oluşacak sehimin de sınırlandırılması gerekmektedir. Buna ilişkin olarak, aşağıdaki sehim sınırlayıcıları tanımlanır:

$$g_4 = \frac{\Delta_i^{max}}{\Delta_i^a} - 1 \leq 0 \tag{8}$$

Denklem (8)'de, g_4, çatı makaslarının altında oluşan sehimin sınırlandırılması için dikkate

alınan deplasman sınırlayıcısıdır. Δ_i^{max}, i'nci çatı makası için belirli yük kombinasyonları altında hesaplanan azami sehimi, Δ_i^a ise izin verilen sehim limitini ifade eder.

2.1. Ceza Fonksiyonu Yaklaşımı

Bu çalışmada, optimizasyon problemindeki sınırlayıcıların yönetimi için harici ceza fonksiyonu yaklaşımı uygulanmıştır. Bu yaklaşımda, optimizasyon işlemi süresince üretilen tasarımlar arasında sınırlayıcıları ihlal eden geçersiz (uygun olmayan) tasarımlar için ceza uygulanmakta ve bu tasarımların amaç fonksiyon değerleri Denklem (9) kullanılarak elde edilmektedir.

$$\phi = W[1 + ceza(\mathbf{I})] = W\left[1 + r_o\left(\sum_{k=1}^{N_c} \max(0, g_k)\right)\right] \tag{9}$$

Bu denklemde, ϕ, uygun olmayan bir $\mathbf{I}$ tasarım için hesaplanan cezalandırılmış (kısıtlı) amaç fonksiyonu değerini; g_k, k'inci normalize edilmiş tasarım sınırlayıcısını; ve N_c ise toplam tasarım sınırlayıcı sayısını ifade etmektedir, Ayrıca bu denklemde r_o ile gösterilen statik ceza katsayısı, cezanın şiddetini genel olarak ayarlamak için kullanılır ve bu çalışmada 1.0 olarak belirlenmiştir.

Optimizasyon süreci sonunda, süreç boyunca elde edilen tasarımlar arasından, tüm tasarım sınırlayıcılarını sağlayan en hafif tasarım, optimum tasarım olarak kabul edilir. Diğer yandan, amaç fonksiyonu değeri daha düşük olsa bile, bir veya birden fazla tasarım sınırlayıcısını ihlal eden tasarımlar optimum tasarım olarak değerlendirilmez.

3. OPTİMİZASYON YÖNTEMİ

Kapasite kontrollü arama (KKA) algoritması yazarlar tarafından son dönemlerde geliştirilmiş olan bir optimizasyon yöntemidir [30]. KKA tasarım odaklı bir yöntem olduğundan, meta-sezgisel yöntemlere kıyasla optimum çözüme çok daha hızlı yakınsamaktadır. Bu yöntemde temel olarak her tasarım grubu için talep/kapasite (T/K) oranının mümkün olan en yüksek değere çıkarılması ve böylece yapı elemanlarının verimli bir şekilde kullanılması hedeflenir. Ayrıca, deplasman sınırlayıcılarının olasılıksal bir yaklaşımla ele alınarak sağlanması amaçlanır. Bu çalışmada, KKA algoritmasının kaos tabanlı bir varyantı olan Kaotik-KKA metodu geliştirilmiş ve kullanılmıştır. Kaotik-KKA, orjinal KKA algoritmasının tüm temel özelliklerini taşırken; eleman gruplarının seçilmesi ve bu gruplara yeni kesitlerin atanması aşamasında düzgün dağılımlı rastgele sayılar yerine kaotik rastgele sayılar kullanılmasıyla ayrışmaktadır. Kaotik-KKA yönteminin uygulama adımları aşağıda özetlenmiştir:

I. Başlangıç: Optimizasyon işlemine başlanmadan önce, her eleman grubu için bir kesit havuzu (profil listesi) belirlenir. Yapı genelinde kullanılan eleman tipine bağlı olarak, bir problemde birden fazla profil listesi tanımlanabilir. Bir profil listesinde yer alan kesitler, kesit alanlarına göre küçükten büyüğe doğru sıralanmalıdır. Genellikle, başlangıç tasarımı, her eleman grubuna bağlı olduğu profil listesindeki en büyük kesitin atanmasıyla oluşturulur. Ancak, eğer yapı için daha önce geleneksel yöntemlerle geçerli bir tasarım oluşturulmuşsa, bu tasarım da başlangıç tasarımı olarak kullanılabilir. Daha sonra, başlangıç tasarımı için yapı analizi gerçekleştirilerek her bir eleman grubu için maksimum T/K oranı belirlenir ve iterasyon sayacı bir olarak ayarlanır.

II. Pertürbasyon için Eleman Gruplarının Seçimi: Mevcut tasarımın iyileştirilmesi amacıyla aday bir tasarım oluşturulur. Bu tasarım, mevcut tasarımdaki bazı eleman gruplarının seçilmesi ve bu gruplara yeni kesitlerin atanması yoluyla gerçekleştirilir. Yapı optimizasyonunun formülasyonu kapsamında, bu işlem bazı tasarım değişkenlerinin seçilmesi ve bu değişkenlere yeni değerlerin atanmasını ifade eder. Tasarım değişkenlerinin seçimi, eleman gruplarının mevcut tasarımdaki T/K oranları kullanılması ile Denklem (10) doğrultusunda gerçekleştirilir.

$$max(P_{min}, |1 - DCR_i|^u) \geq \xi_n \tag{10}$$

$$\xi_{n+1} = 4\xi_n(1 - \xi_n), \ \xi_0 = 0.49 \tag{11}$$

Denklem (10) ve (11)'de, DCR_i i'inci eleman grubu (tasarım değişkeni) için maksimum T/K oranını; u seçilme olasılığını ayarlamaya yarayan bir katsayıyı, ξ_n logistik kaos haritası kullanılarak 0 ile 1 arasında üretilen rastgele bir sayıyı ve P_{min} ise bir tasarım değişkeni için belirlenmiş asgari seçilme olasılığını ifade etmektedir. Bir tasarım değişkeni için bu denklemin sağlanması durumunda, değişken bir sonraki aşamada yapılacak pertürbasyon (değişiklik) için seçilir ve güncellenir. Aksi takdirde bu değişken seçilmez ve mevcut tasarımdaki değeri aday tasarımda da korunur.

III. Pertürbasyon: Seçilen bir tasarım değişkeninin pertürbasyonu, değişkenin mevcut değeri çevresinde tanımlanan bir aralık içerisinde eleman grubuna yeni bir kesitin rastgele atanması suretiyle gerçekleştirilir. Pertürbasyon aralığının genişliği, önce Denklem (12) ve (13) kullanılarak uyarlamalı aralık genişliği (nw_a) şemasına göre belirlenir:

$$nw_{a,i} = round\left(\sqrt{N_{sec,i} - 1}\right) \cdot (min(1, |1 - DCR_i|)^\rho) \tag{12}$$

$$nw_{min} \leq nw_{a,i} \tag{13}$$

Denklem (12) ve (13)'de, $N_{sec,i}$, i'inci eleman grubu için kesit havuzundaki toplam kesit sayısını; ρ aralığın genişliğindeki azalma oranını ayarlamak için kullanılan bir parametreyi; ve nw_{min} minimum aralık genişliğini ifade eder. Daha sonra, Denklem (14) ve (15) kullanılarak pertürbasyon aralığı ($nw_{a,i}$) içerisinde rastgele belirlenen yeni kesit, eleman grubuna atanır.

$$I_i^{iter+1} = I_i^{iter} + \beta \cdot round\left(max\left(1, |Randn_i| \cdot nw_{a,i}\right)\right) \tag{14}$$

$$\beta = sign\left((DCR_i - 1)(\tau - \xi_n)\right) \tag{15}$$

Denklem (14) ve (15)'te, I_i eleman grubu için atanan kesitin sıra (indeks) numarasını; β eleman grubuna daha küçük veya daha büyük bir kesitin atanıp atanmayacağını belirleyen olasılıksal bir parametreyi; τ, β'yı ayarlamak için kullanılan bir sabiti; $Randn_i$ ortalaması 0 ve standart sapması 1 olan normal dağılıma sahip rastgele bir sayıyı ifade etmektedir.

IV. Aday Tasarımın Değerlendirilmesi: Sıradaki adım aday tasarımın amaç fonksiyonu değerini hesaplamaktır. Aday tasarımın amaç fonksiyonu değeri, ilkin yapısal analiz

gerçekleştirilmeksizin sadece yapısal ağırlığı dikkate alınarak, Denklem (9) ile hesaplanır. Yapısal analiz öncesinde aday tasarımın hesaplanan amaç fonksiyon değerine, analiz öncesi amaç fonksiyonu denir. Bu değer, mevcut tasarımın amaç fonksiyonu değerinden yüksekse, aday tasarım otomatik olarak reddedilir ve algoritma ikinci adıma geri döner. Aksi takdirde, aday tasarım için yapısal analiz gerçekleştirilir ve tüm sınırlayıcı ihlalleri dikkate alınarak amaç fonksiyonu değeri Denklem (9)'e göre yeniden hesaplanır. Eğer aday tasarım, mevcut tasarımdan daha düşük bir amaç fonksiyonu değerine sahip ise mevcut tasarım aday tasarımla değiştirilir; aksi takdirde aday tasarım reddedilir.

V. Duraklama Kontrolü: Sonraki adım algoritmanın duraklama kontrolünü yapmaktır. Mevcut tasarımın, önceden belirlenmiş bir iterasyon sayısı boyunca iyileştirilememesi, algoritmanın lokal bir optimum çözüme yakalandığı ve bu sebeple optimizasyon işleminde bir duraklama veya tıkanma sürecinin yaşandığı anlamına gelir. Böyle bir durumda, algoritmanın yakalandığı bu lokal çözümden kaçabilmesi için duraklamadan kaçış dönemi DKD başlatılır. DKD önceden belirlenen bir sayıda iterasyondan oluşur. DKD'nin başlamasıyla birlikte, sadece bir kereye mahsus olmak üzere elitizm kuralı askıya alınır ve mevcut tasarıma kıyasla daha yüksek bir amaç fonksiyonuna sahip bir aday tasarımın mevcut tasarımın yerine geçmesine izin verilir (yukarı doğru hareket). Ancak, bu olurken çok kötü bir çözüme geçişi engellemek için, aday tasarımın amaç fonksiyonu değerinin mevcut tasarımın amaç fonksiyonu değerine oranının önceden belirlenmiş bir oranı (α_u) aşmaması koşulu aranır. DKD, mevcut tasarımdan daha iyi bir aday tasarım bulunduğunda sona erer.

VI. Sonlandırma: Algoritma, maksimum iterasyon sayısına ($iter^{max}$) ulaştığında veya mevcut tasarımın belirli bir iterasyon sayısı boyunca ($iter^{ni}$) iyileştirilmemesi durumunda sonlandırılır. Bu iki kriterden biri karşılanmadığı sürece, iterasyon sayısı bir artırılır ve ikinci adıma geri dönülür.

4. SAYISAL ÖRNEKLER

Çalışmanın bu bölümünde, ülkemiz mühendislik uygulamalarında büyük açıklıklı çelik çatı sistemlerinin ne derece ekonomik tasarlandığı ve yapı optimizasyonu ile elde edilebilecek maliyet avantajları sayısal olarak incelenmektedir. Bu amaçla, bir kamu idaresi tarafından ihale edilerek Türkiye'nin farklı bölgelerinde inşa edilen üç kapalı yüzme havuzuna ait çelik çatı sistemleri, örnek yapı problemi olarak kullanılmıştır. Burada vurgulanması gereken önemli bir husus, bu çalışma kapsamında gerçekleştirilen yapı optimizasyonu ile, yapıların detaylı tasarımları öncesi ön boyutlandırma işlemi yapılmaktadır. Birleşim noktalarının tasarımları ve birleşimlerin teşkili nedeniyle oluşan enkesit kayıplarının yapı elemanlarında dayanım azalmasına veya ilave yapısal yetmezlik modlarına sebebiyet verip vermeyeceği, ön tasarım aşamasını müteakiben detaylı tasarım aşamasında yapılması gereken tahkiklerdir. Bu yaklaşım, mühendislik yapılarının tasarım süreçlerinde yaygın olarak uygulanan bir yöntemdir; çünkü birleşim noktalarının detaylandırılması ve birleşimlerden kaynaklanan taşıma gücü kontrolleri, ön boyutlandırma sonrasında yapılacak daha kapsamlı analizler ve hesaplamalar gerektirmektedir. Netice olarak, bu çalışma kapsamında gerçekleştirilen yapı optimizasyonu ile çelik çatı sistemlerinin ön boyutlandırma işlemleri gerçekleştirilmekte olup çekme elemanları için blok kırılma dayanımı gibi detaylı tasarım aşamalarında yapılması gereken tahkikler, bu çalışma kapsamında yer almamaktadır.

Bu problemler şunlardır:

(1) 1263-elemanlı kapalı yüzme havuzu çatısı

(2) 1567-elemanlı kapalı yüzme havuzu çatısı

(3) 1634-elemanlı kapalı yüzme havuzu çatısı

Bu çatı sistemlerinin proje firmaları tarafından gerçekleştirilen yapısal modelleme, analiz ve tasarım işlemlerinde SAP2000 [31] yazılımı kullanılmıştır. Tasarım aşamasında yapı elemanlarının dayanım tahkikleri, ülkemiz şartnamesi [29] ile uyumlu olan, ASCE 360-10 [32] şartnamesinin, Yük ve Dayanım Katsayılarına göre tasarım (YDKT) yöntemi kullanılarak gerçekleştirilmiştir. Çelik elemanlarının enkesitlerin narinlik koşulları gerek orijinal tasarımlarda gerekse bu yapıların optimum tasarım sürecinde sınırlayıcı olarak doğrudan dikkate alınmamıştır, ancak bu koşulların (3 no'lu örnekteki yapma kolon kesiti - eleman grubu no. 3- dışında) her üç örnekteki tüm çelik elemanlar için sağlandığı tespit edilmiştir. Ayrıca, sehim hesaplamaları için tanımlanan yük kombinasyonları altında çatı makaslarındaki düşey deplasmanlar, açıklığın 1/300'ü ile sınırlandırılmıştır. Yapıların optimum tasarımları elde edilirken, orijinal tasarımlarda esas alınan tüm bu hüküm ve kısıtlara tam anlamıyla uyulmuştur.

Tablo 1 - Kaotik-KKA algoritmasının parametre değerleri

u	ρ	τ	nw_{min}	α_u	DKD	$iter^{ni}$	$iter^{max}$
2	3	0.8	2	1.1	20	80	500
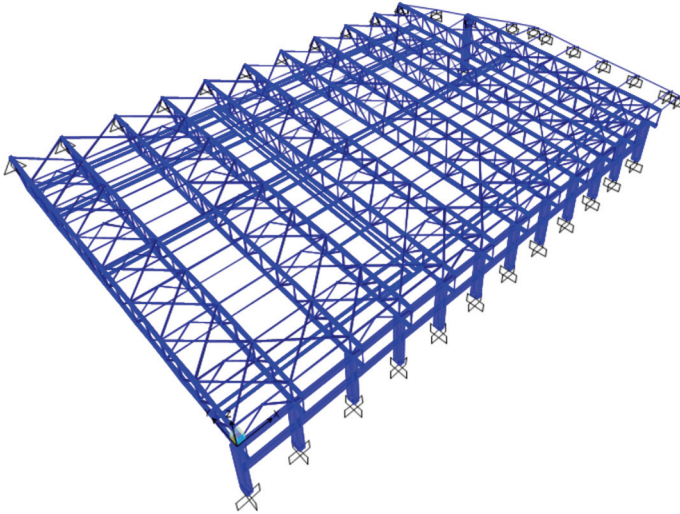
Şekil 1 - 1263-elemanlı kapalı yüzme havuzu çatısı SAP2000 modeli.

Çalışmada kullanılan optimizasyon algoritması MATLAB [33] ile kodlanmış ve yapısal analizler ve tasarım kontrolleri için SAP2000 programının OAPI altyapısı kullanılmıştır. Analizler, Intel i7-12700H mobil CPU ve 32 GB DDR5 RAM'e sahip kişisel bir bilgisayar kullanılarak gerçekleştirilmiştir. Kullanılan optimizasyon yönteminin (Kaotik-KKA) kısmen stokastik yapıda olması sebebiyle, her problem için algoritma birden fazla kez bağımsız olarak çalıştırılmış ve elde edilen en hafif tasarım, o yapının optimum tasarımı olarak kabul edilmiştir. Kaotik-KKA algoritmasın bu çalışmada kullanılan parametre değerleri Tablo 1'de özetlenmektedir.

4.1. 1263-Elemanlı Kapalı Yüzme Havuzu Çatısı

İlk örnek problem olarak, 1263-elemanlı bir yüzme havuzu çatısının optimum tasarımı ele alınmıştır (Şekil 1). Çatı, x-yönünde 79.10 metre, y-yönünde ise 53.99 metre uzunluğa sahip olup, çatı makaslarının yüksekliği (dikme uzunluğu) 3.25 metredir. Çelik elemanlar, yapının orijinal tasarımındaki gruplandırmaya uygun olarak 14-eleman grubuna ayrılmıştır. Bu eleman gruplarına kesit ataması yapmak üzere S275 sınıfındaki H kesitlerden ve S235 ve S355 sınıfındaki boru kesitlerden oluşan 2 farklı profil listesi kullanılmıştır. Yapının tasarımı

Tablo 2 - 1263-elemanlı kapalı yüzme havuzu çatısı - orijinal ve optimum tasarımların karşılaştırması

#	Eleman Grubu	Orijinal Tasarım		Optimum Tasarım	
		Kesitler	T/K Oranı	Kesitler	T/K Oranı
1	ALT BAŞLIK	HE360B	0.9427	HE340B	0.9775
2	ALT YATAY1	BORU 139.7x3.0-S355	0.6614	BORU 127.0x3.0-S235	0.9579
3	ALT YATAY2	HE220A	0.7666	HE200A	0.9871
4	DİKEY ÇAPRAZ1	BORU 139.7x3.0-S355	0.4851	BORU 114.3x3.0-S355	0.8423
5	DİKEY ÇAPRAZ2	BORU 168.3x4.0-S355	0.6784	BORU 165.1x4.0-S235	0.8319
6	DİYAGONALLER1	BORU 139.7x3.0-S355	0.0833	BORU 76.1x3.0-S235	0.5440
7	DİYAGONALLER2	BORU 168.3x4.0-S355	0.7594	BORU 168.3x4.0-S355	0.7718
8	DİYAGONALLER3	BORU 219.1x5.0-S355	0.8403	BORU 193.7x5.0-S355	0.9707
9	DİYAGONALLER4	BORU 244.5x6.0-S355	0.7822	BORU 244.5x6.0-S355	0.7661
10	KEDİYOLU	HE200A	0.5291	HE180A	0.7472
11	ÜST BAŞLIK	HE360B	0.8924	HE320B	0.9666
12	ÜST YATAY1	BORU 168.3x4.0-S355	0.8033	BORU 165.1x4.0-S235	0.8672
13	ÜST YATAY2	BORU 219.1x5.0-S355	0.5349	BORU 193.7x5.0-S355	0.7154
14	YATAY ÇAPRAZ	BORU 219.1x5.0-S355	0.8225	BORU 219.1x4.0-S235	0.9901
	Tasarım Ağırlığı (ton)	307.81		277.27	
	Tasarruf (%)	-		9.92	
	Max. Düşey Deplasman (cm)	12.34		13.24	
	Global Temel Periyot (s)	0.32		0.33	
	Analiz Sayısı ve Süresi	-		71 Analiz (1 saat, 39 dakika)	

için toplamda 162 adet yük kombinasyonu tanımlanmış olup, bu yük kombinasyonlardan 159'u elemanların dayanım tahkikleri için, 3'ü ise makasların sehim kontrolleri için kullanılmıştır. Sehim hesaplamaları için tanımlanmış yük kombinasyonları altında çatı makaslarında oluşan düşey deplasmanlar 18.0 cm ile sınırlandırılmıştır.

Çatının bir proje firması tarafından geleneksel mühendislik yöntemleri kullanılarak elde edilen orijinal tasarımının ağırlığı 307.81 ton olarak belirlenmiştir. Kaotik-KKA yöntemi kullanılarak yapılan optimizasyon sonucunda, bu ağırlık %9.92 oranında bir azalma göstererek 277.27 tona düşürülmüştür. Optimizasyon işleminde başlangıç tasarımı olarak yapının orijinal tasarımı kullanılmıştır. Optimizasyon işlemi süresince 71 analiz yapılmış olup, algoritmanın toplam hesaplama süresi 1 saat 39 dakika olarak kaydedilmiştir Yapının orijinal ve optimum tasarımları, yapı ağırlıkları, eleman gruplarına atanan kesitler, eleman grupları için hesaplanan en büyük T/K oranları, çatı makaslarında hesaplanan maksimum sehimler ve global temel periyotları açısından Tablo 2'de karşılaştırılmıştır. Her iki tasarım da sehim sınırlayıcılarını sağlamaktadır. Tablodaki global temel periyot değerleri, kütle katılımının en fazla olduğu modu temsil etmektedir. Orijinal ve optimum tasarımlarda global temel periyotların yakın olması, optimizasyon işlemi sonucunda yapının rijitliğinin yapının ağırlığı ile orantılı olarak azaldığını göstermektedir. Şekil 2'de tasarım modeli üzerinde grup bazında T/K oranları görselleştirilmiş ve karşılaştırılmıştır. Bu görselleştirmeden optimum tasarım yöntemine göre boyutlandırılmış yapı elemanlarının, orijinal tasarıma kıyasla daha verimli kullanıldığı görülmektedir.
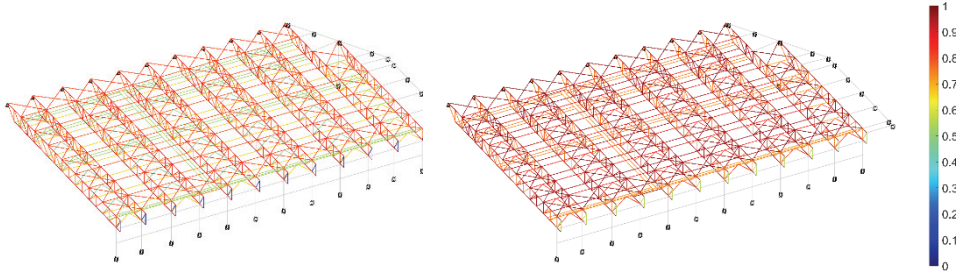
Şekil 2 - 1263-elemanlı kapalı yüzme havuzu çatısı grup bazında talep/kapasite oranları (orijinal tasarım solda, optimum tasarım sağda)

4.2. 1567-Elemanlı Kapalı Yüzme Havuzu Çatısı

İkinci örnek problem olarak, 1567-elemanlı bir yüzme havuzu çatısının optimum tasarımı ele alınmıştır (Şekil 3). X-yönünde 76.80 metre uzunluğa, y-yönünde 49.40 metre uzunluğa sahip olan çatının, maksimum çatı makası yüksekliği (dikme uzunluğu) 4.25 metredir. Çelik elemanlar, yapının orijinal tasarımındaki gruplandırmaya uygun olarak 20-eleman grubuna ayrılmıştır. Bu eleman gruplarına kesit ataması yapmak üzere S275 sınıfındaki H kesitlerden, S275 sınıfındaki I kesitlerden, S235 sınıfındaki kutu kesitlerden ve S235 sınıfındaki boru kesitlerden oluşan 4 farklı profil listesi kullanılmıştır. Yapının tasarımı için toplamda 121 adet yük kombinasyonu tanımlanmış olup, bu yük kombinasyonlardan 115'i elemanların dayanım tahkikleri için, 6'sı ise makasların sehim kontrolleri için kullanılmıştır. Sehim

hesaplamaları için tanımlanmış yük kombinasyonları altında çatı makaslarında oluşan düşey deplasmanlar 16.47 cm ile sınırlandırılmıştır.

Şekil 3 - 1567-elemanlı kapalı yüzme havuzu çatısı SAP2000 modeli.

Çatının orijinal tasarımında yapı ağırlığı 240.55 ton olarak belirtilmiştir. Çatı elemanlarının optimum boyutlandırılması ile elde edilen tasarımının ağırlığı ise bu tasarıma kıyasla %17.95 daha hafif olup, sadece 197.37 tondur. Optimizasyon işleminde başlangıç tasarımı olarak yapının orijinal tasarımı kullanılmıştır. Optimizasyon işlemi süresince 257 analiz yapılmış olup, algoritmanın toplam hesaplama süresi 5 saat 55 dakika olarak kaydedilmiştir. Yapının orijinal ve optimum tasarımları Tablo 3'de karşılaştırılmıştır. Bu tablodan her iki tasarımın da sehim kısıtlarını sağladığı görülmektedir. Optimizasyon işlemi sonucunda yapının periyodu biraz artmış olsa da orijinal ile optimum tasarımların periyotlarının yakın olması yapının kütlesinin yapının rijitliğine olan oranının fazla değişmediğini ortaya koymaktadır. Şekil 3'de ise tasarım modeli üzerinde grup bazında T/K oranları görselleştirilerek karşılaştırılmıştır. Bu görselleştirmeden, optimum tasarım yöntemine göre boyutlandırılmış yapı elemanlarının orijinal tasarıma kıyasla daha verimli kullanıldığı açıkça görülmektedir.

Tablo 3 - 1567-elemanlı kapalı yüzme havuzu çatısı - orijinal ve optimum tasarımların karşılaştırması.

#	Eleman Grubu	Orijinal Tasarım		Optimum Tasarım	
		Kesitler	T/K Oranı	Kesitler	T/K Oranı
1	ALT BAŞLIK	HE300A	0.7671	HE260A	0.9386
2	ARA YATAYLAR1	BORU 139.7x3.0-S235	0.7240	BORU 127.0x3.0-S235	0.9779
3	ARA YATAYLAR2	BORU 168.3x4.0-S235	0.7023	BORU 159.0x3.0-S235	0.9290
4	DİKEY ÇAPRAZ1	BORU 168.3x4.0-S235	0.6300	BORU 133.0x3.0-S235	0.9357

Tablo 3 - 1567-elemanlı kapalı yüzme havuzu çatısı - orijinal ve optimum tasarımların karşılaştırması. (devam)

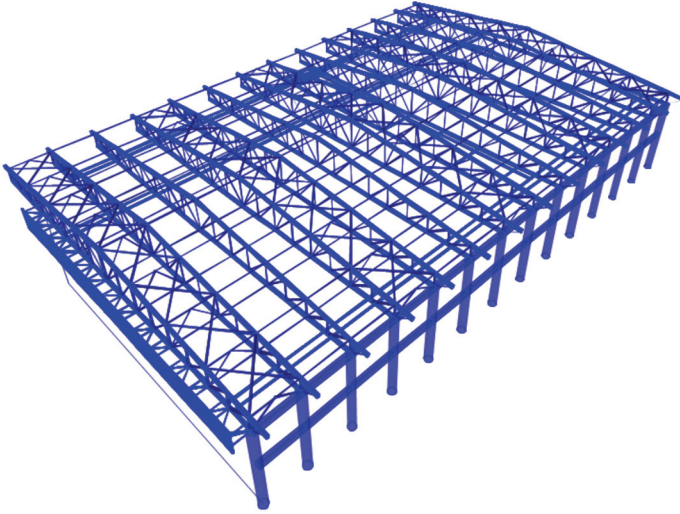| #	Eleman Grubu	Orijinal Tasarım		Optimum Tasarım	
		Kesitler	T/K Oranı	Kesitler	T/K Oranı
5	DİKEY ÇAPRAZ2	BORU 139.7x3.0-S235	0.8058	BORU 127.0x3.0-S235	0.9638
6	DİKEY DÜZ1	BORU 139.7x3.0-S235	0.7052	BORU 127.0x3.0-S235	0.9068
7	DİKEY DÜZ2	BORU 168.3x4.0-S235	0.7158	BORU 139.7x3.0-S235	0.9984
8	DİYAGONALLER1	BORU 139.7x3.0-S235	0.4963	BORU 101.6x3.0-S235	0.9688
9	DİYAGONALLER2	BORU 168.3x4.0-S235	0.6733	BORU 159.0x3.0-S235	0.8959
10	DİYAGONALLER3	BORU 219.1x4.0-S235	0.7536	BORU 165.1x4.0-S235	0.9564
11	DİYAGONALLER4	BORU 244.5x5.0-S235	0.6457	BORU 193.7x4.0-S235	0.9998
12	DİYAGONALLER5	BORU 273.0x8.0-S235	0.7303	BORU 323.9x6.0-S235	0.7842
13	DİYAGONALLER6	BORU 88.9x3.0-S235	0.0914	BORU 60.3x3.0-S235	0.3440
14	KEDİYOLU	IPE220	0.7573	IPE220	0.8555
15	PARAPET ÇAPRAZ	KUTU 60x4.0-S235	0.8149	KUTU 60x4.0-S235	0.9437
16	PARAPET DİKEY	KUTU 100x4.0-S235	0.6197	KUTU 80x4.0-S235	0.8652
17	PARAPET TAŞIYICI	KUTU 60x4.0-S235	0.3385	KUTU 60x4.0-S235	0.3416
18	PARAPET YATAY	KUTU 80x4.0-S235	0.6393	KUTU 80x4.0-S235	0.7381
19	ÜST BAŞLIK	HE320B	0.8146	HE340A	0.9778
20	YATAY ÇAPRAZ	BORU 219.1x4.0-S235	0.7215	BORU 193.7x4.0-S235	0.8304
Tasarım Ağırlığı (ton)		240.55		197.37	
Tasarruf (%)		-		17.95	
Max. Düşey Deplasman (cm)		6.91		8.16	
Global Temel Periyot (s)		0.49		0.52	
Analiz Sayısı ve Süresi		-		257 Analiz (5 saat, 55 dakika)	
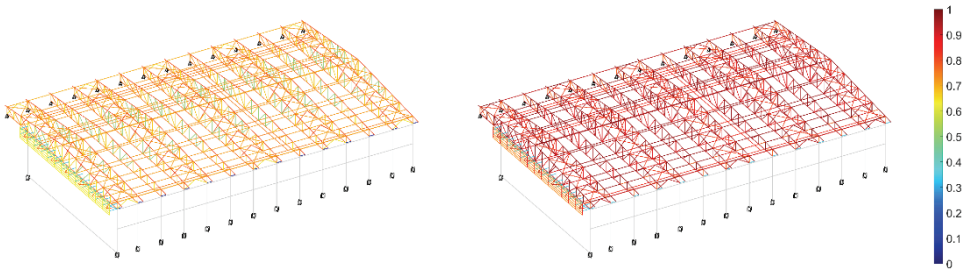
Şekil 4 - 1567-elemanlı kapalı yüzme havuzu çatısı grup bazında talep/kapasite oranları (orijinal tasarım solda, optimum tasarım sağda).
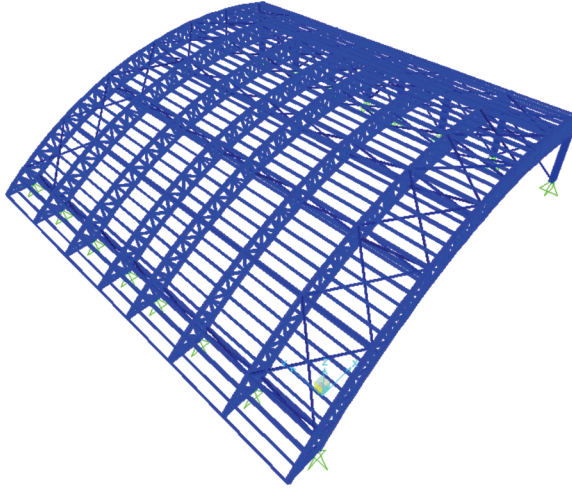
Şekil 5 - 1634-elemanlı kapalı yüzme havuzu çatısı SAP2000 modeli.

4.3. 1634-Elemanlı Kapalı Yüzme Havuzu Çatısı

Üçüncü ve son örnek problemde, 1634-elemanlı bir yüzme havuzu çatısının optimum tasarımı ele alınmıştır (Şekil 5). Ark şeklinde makaslardan oluşan çatı, x-yönünde 35.65 metre, y-yönünde ise 41.95 metre plan uzunluğuna sahip olup, çatı makaslarının yüksekliği (dikme uzunluğu) 2 metredir. Yapının çelik elemanları, orijinal tasarımdaki gruplandırmaya uygun olarak 13-tasarım grubuna ayrılmıştır. Bu eleman gruplarına kesit ataması yapmak üzere S275 sınıfındaki H kesitlerden, S235 sınıfındaki boru kesitlerden ve S235 sınıfındaki UPN kesitlerden oluşan 3 farklı profil listesi kullanılmıştır. 3 numaralı eleman grubu için ise orijinal tasarımda kullanılan yapma kolon kesiti (Y900IST) olduğu gibi kullanılmıştır.

Bu örnek problem için iki farklı optimizasyon senaryosu oluşturulmuştur. İlk senaryoda, yapı eleman gruplarının kesit tipleri orijinal tasarıma uygun olarak belirlenmiştir. İkinci senaryoda ise, bazı eleman gruplarının kesit tiplerinde değişiklik yapılmış ve bu gruplar için daha elverişli olduğu düşünülen kesit tipleri kullanılmıştır. Bu değişiklikler şunları içermektedir: (1) 5. gruptaki diyagonaller için HEA/B profilleri yerine boru profiller kullanılmıştır, (2) 9. gruptaki aşıklar için HEA/B profilleri yerine UPN profiller kullanılmıştır, (3) 11. ve 12. gruptaki dikmeler için HEA/B profilleri yerine boru profiller kullanılmıştır. Yapının tasarımı için toplamda 59 adet yük kombinasyonu tanımlanmış olup, bu yük kombinasyonlardan 56'sı elemanların dayanım tahkikleri için, 3'ü ise makasların sehim kontrolleri için kullanılmıştır. Sehim hesaplamaları için tanımlanmış yük kombinasyonları altında çatı makaslarında oluşan düşey deplasmanlar 11.88 cm ile sınırlandırılmıştır.

Çatının geleneksel mühendislik yöntemleri kullanılarak elde edilen orijinal tasarımının ağırlığı 244.67 tondur. İlk senaryoda, yani eleman grupları için kesit tiplerinin orijinal tasarıma uygun olarak seçildiği durumda, yapılan optimizasyon sonucunda yapı ağırlığı %33.80 oranında azaltılarak 161.97 tona düşürülmüştür. Bu senaryoda, başlangıç tasarımı, her eleman grubuna bağlı olduğu profil listesindeki en büyük kesitin atanmasıyla

oluşturulmuştur. Optimizasyon işlemi süresince 308 analiz yapılmış olup, algoritmanın toplam hesaplama süresi 1 saat 40 dakika olarak kaydedilmiştir. İkinci senaryoda, yani kesit tiplerinde yapılan değişikliklerle gerçekleştirilen optimizasyon işleminde yapı ağırlığı orijinal tasarıma göre %40.52 azaltılarak, 145.54 tona düşürülmüştür. İlk senaryoda olduğu gibi bu senaryoda da, başlangıç tasarımı, her eleman grubuna bağlı olduğu profil listesindeki en büyük kesitin atanmasıyla oluşturulmuştur ve optimum tasarıma toplamda 55 dakika süren 171 analiz ile ulaşılmıştır.

Tablo 4 - 1634-elemanlı kapalı yüzme havuzu çatısı - orijinal ve optimum tasarımların karşılaştırması

#	Eleman Grubu	Orijinal Tasarım		Optimum Tasarım (ilk senaryo)		Optimum Tasarım (ikinci senaryo)	
		Kesitler	T/K Oranı	Kesitler	T/K Oranı	Kesitler	T/K Oranı
1	ALT BAŞLIK	HE300A	0.7869	HE260A	0.8616	HE240A	0.9397
2	ALT BAŞLIK2	HE160A	0.0263	HE100A	0.0748	HE100A	0.0748
3	YAPMA KOLONLAR	Y900IST	0.8177	Y900IST	0.9329	Y900IST	0.9268
4	DİKEY ÇAPRAZLAR	BORU 168.3x6.0	0.6438	BORU 159.0x3.0	0.8481	BORU 159.0x3.0	0.8038
5	DİYAGONALLER	HE160A	0.3701	HE100A	0.6707	BORU 127.0x3.0	0.9343
6	YATAY ÇAPRAZLAR	BORU 193x12.0	0.9624	BORU 219.1x4.0	0.9821	BORU 219.1x4.0	0.9934
7	ARA YATAYLAR	HE240A	0.5464	HE200A	0.6959	HE200A	0.6598
8	AŞIKLAR1	UPN220	0.7980	UPN200	0.9999	UPN200	0.9946
9	AŞIKLAR2	HE240A	0.2702	HE160A	0.6905	UPN260	0.8883
10	ÜST BAŞLIK	HE300A	0.4720	HE120B	0.8593	HE120A	0.9929
11	DİKMELER1	HE180A	0.0676	HE100A	0.0652	BORU 60.3x3.0	0.5103
12	DİKMELER2	HE300A	0.3580	HE100A	0.6476	BORU 127.0x3.0	0.9856
13	KOLON ÇAPRAZLARI	BORU 168.3x6.0	1.1321	BORU 177.8x4.0	0.9330	BORU 177.8x4.0	0.9178
Tasarım Ağırlığı (ton)		244.67		161.97		145.54	
Kazanç (%)		-		33.80		40.52	
Max. Düşey Deplasman (cm)				2.33		2.58	
Global Temel Periyot (s)		0.42		0.64		0.69	
Analiz Sayısı ve Süresi				308 Analiz (1 saat 40 dk.)		171 Analiz (55 dakika)	

Yapının orijinal ve optimum tasarımlarının (her iki senaryo altında) karşılaştırması Tablo 4'de verilmiştir. Bu tablodan, orijinal tasarımda 13. grupta bir dayanım ihlali olduğu görülmektedir. Öte taraftan, orijinal ve her iki optimizasyon senaryosunda elde edilen optimum tasarımlar sehim kısıtlarını başarıyla karşılamaktadır. Optimizasyon işlemleri sonucunda yapı periyodunda gözlemlenen artış, eleman kesitlerinin küçülmesi ile birlikte yapının daha esnek hale geldiğine işaret etmektedir. Ancak, bu durum bu herhangi bir sorun teşkil etmemektedir. Zira optimum tasarımlar, sehim kriterleri de dahil olmak üzere tüm tasarım sınırlayıcılarını sağlarken, orijinal tasarımda dayanım sınırlayıcısı ihlali bulunmaktadır. Şekil 6'da tasarım modeli üzerinde grup bazında T/K oranları görselleştirilerek karşılaştırılmıştır. Bu görselleştirmeden, optimum tasarım yöntemine göre

boyutlandırılmış yapı elemanlarının, orijinal tasarıma kıyasla çok daha verimli kullanıldığı açıkça gözlemlenmektedir.
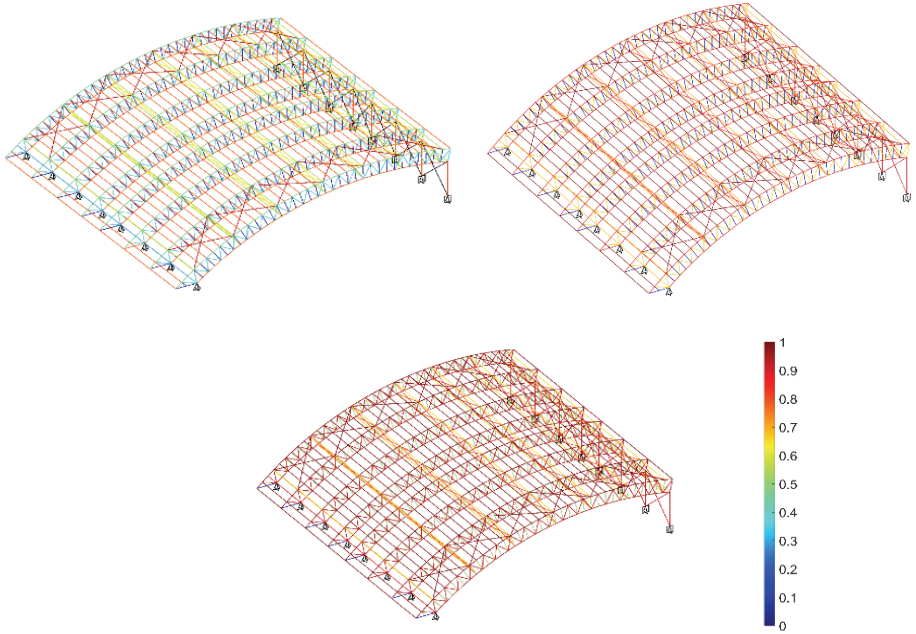
Şekil 6 - 1634-elemanlı kapalı yüzme havuzu çatısı - grup bazında talep/kapasite oranları (başlangıç tasarımı sol üstte, ilk senaryoya göre optimum tasarım üstte sağda, ikinci senaryoya göre optimum tasarım altta)

5. SONUÇ

Bu çalışmada ülkemiz mühendislik uygulamalarında büyük açıklıklı çelik çatı sistemlerinin ne derece ekonomik tasarlandığı araştırılmış ve yapı optimizasyonu ile elde edilebilecek maliyet avantajları ortaya koyulmuştur. Bu amaçla, bir kamu idaresi tarafından ihale edilerek Türkiye'nin farklı bölgelerinde inşa edilmiş üç kapalı yüzme havuzuna ait çelik çatı sistemlerinin optimum boyutlandırılması gerçekleştirilmiş ve bu sistemler için elde edilen optimum tasarımlar yapıların daha önceden geleneksel mühendislik yöntemleri kullanılarak oluşturulan orijinal tasarımları ile karşılaştırılmıştır. Bu karşılaştırmalar neticesinde, büyük açıklıklı çelik çatı sistemlerinin tasarım aşamasında yapı optimizasyonu yöntemlerinin kullanılmasının, yapı ağırlığını ve dolayısıyla yapı maliyetini, %10-40 oranında azaltabileceği tespit edilmiştir. Ayrıca, eleman grupları için uygun kesit tipi seçilmesinin yapı maliyetinin düşürülmesinde önemli bir etken olduğu gösterilmiştir.

Çalışmada, ayrıca tasarım odaklı bir optimizasyon tekniği olan kaotik kapasite kontrollü arama (Kaotik-KKA) yönteminin ülkemizde inşa edilecek mühendislik yapılarının optimum boyutlandırılarak tasarlanması için önemli bir potansiyel barındırdığı gösterilmiştir. Kaotik-

KKA yönteminin basitliği ve az sayıda analizle optimum çözüme hızlı bir şekilde ulaşabilme yeteneği, bu yöntemi gerçek mühendislik uygulamalarında kullanışlı ve cazip kılmaktadır. Nitekim, bu çalışma kapsamında ele alınan gerçek yapı problemleri için optimum tasarımlara 71-308 analiz ile ulaşılmış ve optimizasyon süreci standart donanıma sahip bir kişisel bilgisayar ile birkaç saat içinde tamamlanmıştır. Yapısal çelik kullanımının azaltılması, yalnızca malzeme maliyetlerini düşürmekle kalmayıp, nakliye ve imalat maliyetlerinde de ilave tasarruf sağlayacaktır. Ayrıca, çelik endüstrisinin çevresel etkilerini azaltarak daha sürdürülebilir ve çevre dostu bir dünyaya katkıda bulunacaktır.

Teşekkür

Kaynaklar

[1] Erbatur, F., Al-Hussainy, M. M. Optimum Design of Frames. Computers & Structures, 45, 887-91, 1992.

[2] Tabak E. I., Wright, P. M. Optimality Criteria Method for Building Frames. Journal of Structural Division, ASCE, 107, 1327–1342, 1981.

[3] Saka, M. P. Optimum Design of Steel Frames with Stability Constraints. Computers & Structures, 41, 1365-1377, 1991.

[4] Goldberg, D. E. Samtani M. P., Engineering Optimization via Genetic Algorithm. In: Proceeding of the Ninth Conference on Electronic Computation, ASCE, 471-482, 1986.

[5] Kirkpatrick, S., Gerlatt, C. D., Vecchi, M.P. Optimization by Simulated Annealing. Science, 220, 671-80, 1983.

[6] Kennedy, J., Eberhart, R. Particle Swarm Optimization. In: IEEE İnternational Conference on Neural Networks, IEEE Press, 1942-1948, 1995.

[7] Colorni A., Dorigo, M., Maniezzo, V. Distributed Optimization by Ant Colony. In: Proceedings of the First European Conference on Artificial Life, USA, 134-142, 1991.

[8] Lee, K. S., Geem, Z. W. A New Structural Optimization Method Based On The Harmony Search Algorithm. Computers & Structures, 82, 781-798, 2004.

[9] Toğan, V., Daloğlu, A. Genetik Algoritma ile Üç Boyutlu Kafes Sistemlerin Şekil ve Boyut Optimizasyonu. Teknik Dergi, 17(82), 3809-3825, 2006.

[10] Hasançebi, O., Azad, S. K. An Exponential Big Bang-Big Crunch Algorithm For Discrete Design Optimization of Steel Frames. Computers & Structures, 110, 167-179, 2012.

[11] Gandomi, A. H., Yang, X. S., Alavi, A. H. Cuckoo Search Algorithm: A Metaheuristic Approach to Solve Structural Optimization Problems. Engineering with Computers, 29, 17-35, 2013.

[12] Artar, M., Daloğlu, A. Çok Katlı Kompozit Çelik Çerçevelerin Genetik Algoritma ile Dinamik Sınırlayıcılı Optimizasyonu. Teknik Dergi, 26(2), 2015.

[13] Askarzadeh, A. A Novel Metaheuristic Method for Solving Constrained Engineering Optimization Problems: Crow Search Algorithm. Computers & Structures, 169, 1-12, 2016.

[14] Mirjalili, S., Lewis, A. The Whale Optimization Algorithm. Advances in Engineering Software, 95, 51-67, 2016.

[15] Karabörk, T., Sönmez, M., Aydın, E., Çelik, T., Bölükbaş, Y. Çelik Yapılarda Kullanılan Diyagonal Çelik Çaprazların Yapay Arı Koloni Algoritması ile Optimizasyonu. Uludağ Üniversitesi Mühendislik Fakültesi Dergisi, 23(1), 51-64, 2018.

[16] Degertekin, S. O., Lamberti, L., Ugur, I. B. Sizing, Layout and Topology Design Optimization of Truss Structures Using the Jaya Algorithm. Applied Soft Computing, 70, 903-928, 2018.

[17] Bekdaş, G., Yucel, M., Nigdeli, S. M. Evaluation of Metaheuristic-Based Methods for Optimization of Truss Structures via Various Algorithms And Lèvy Flight Modification. Buildings, 11(2), 49, 2021.

[18] Chan, C. M. Optimal Lateral Stiffness Design of Tall Buildings of Mixed Steel and Concrete Construction. Structural Design of Tall Buildings, 10(3), 155–77, 2001.

[19] Elvin A, Walls R, Cromberge D. Optimising Structures Using the Principle of Virtual Work. Journal of the South African Institution of Civil Engineering, 51(2), 11–9, 2009.

[20] Azad, S. K., Hasançebi, O. Computationally Efficient Discrete Sizing of Steel Frames via Guided Stochastic Search Heuristic. Computers & Structures, 156, 12-28, 2015.

[21] Walls R, Elvin A. Optimizing Structures Subject to Multiple Deflection Constraints and Load Cases Using the Principle Of Virtual Work. Journal of Structural Engineering, 136(11), 1444–52, 2010.

[22] Flager, F., Soremekun, G., Adya, A., Shea, K., Haymaker, J., Fischer, M. Fully Constrained Design: A General and Scalable Method for Discrete Member Sizing Optimization of Steel Truss Structures. Computers & Structures, 140, 55-65, 2014.

[23] Kociecki, M., Adeli, H. Two-Phase Genetic Algorithm for Size Optimization of Free-Form Steel Space-Frame Roof Structures. Journal of Constructional Steel Research, 90, 283-296, 2013.

[24] Dillen, W., Lombaert, G., Mertens, R., Van Beurden, H., Jaspaert, D., Schevenels, M. Optimization in A Realistic Structural Engineering Context: Redesign of The Market Hall in Ghent. Engineering Structures, 228, 111473, 2021.

[25] De Souza, R. R., Miguel, L. F. F., Lopez, R. H., Miguel, L. F. F., Torii, A. J. A Procedure for the Size, Shape and Topology Optimization of Transmission Line Tower Structures. Engineering Structures, 111, 162-184, 2016.

[26] Luna, F., Zavala, G. R., Nebro, A. J., Durillo, J. J., Coello, C. A. C. Distributed Multi-Objective Metaheuristics for Real-World Structural Optimization Problems. The Computer Journal, 59(6), 777-792, 2016.

[27] Lagaros, N. D. A General Purpose Real-World Structural Design Optimization Computing Platform. Structural and Multidisciplinary Optimization, 49, 1047-1066, 2014.

[28] Eser, H., Hasançebi, O., Gholizadeh, S. Optimizing Real-World Steel Structures: A Comparison with Design Office Solutions. Practice Periodical on Structural Design and Construction, ASCE, Under Review, 2024.

[29] T. C. Çevre, Şehircilik ve İklim Değişikliği Bakanlığı. Çelik Yapıların Tasarım, Hesap ve Yapımına Dair Esaslar, 2018.

[30] Eser, H., Hasançebi, O. Capacity Controlled Search: A New and Efficient Design-Driven Method for Discrete Size Optimization of Steel Frames. Computers & Structures, 275, 106937, 2023.

[31] Computers and Structures Inc. SAP2000 version: 21.0.2. Berkeley, California, 2019.

[32] AISC 360-10. Specification for Structural Steel Buildings. American Institute of Steel Construction. Chicago, Illinois, 2010.

[33] MathWorks Inc. MATLAB version: 9.14.0 (R2023a), Natick, Massachusetts, 2023.

A Review of Punching Shear Strength in FRP-Reinforced Concrete Slab-Column Connections

Ragheb SALIM[1*]

ABSTRACT

This review explores the use of Fiber Reinforced Polymer (FRP) bars to reinforce concrete slab-column connections, highlighting their potential to extend service life, reduce maintenance costs, and improve life-cycle cost efficiency. FRP bars offer a more environmentally friendly alternative to traditional steel reinforcement. The shear behavior of reinforced concrete structural members, which depends on complex internal load-carrying mechanisms, remains an active area of research. This article provides a comprehensive overview of the punching shear strength and behavior of FRP-reinforced concrete (FRP-RC) slab-column connections, both with and without FRP stirrups for shear reinforcement. It examines the mechanisms of punching shear in FRP-RC slab-column connections and reviews existing codes, proposed or modified models, and machine learning approaches for predicting the punching shear strength of these connections.

Keywords: Slab-column connection, punching shear capacity, FRP bar, machine learning, design model.

1. INTRODUCTION

The corrosion of steel reinforcement stands out as a primary durability issue in reinforced concrete (RC) structures, posing a significant threat to their longevity and incurring substantial maintenance costs. In severe instances, corrosion can precipitate unforeseen and severe failures in RC structures. This deterioration is compounded by the degradation of the bond between concrete and steel reinforcement as corrosion progresses, further weakening the structure [1-2]. Moreover, corrosion might result in a reduction in the steel reinforcement's cross-sectional area, which lowers its tensile strength and ductility [3-4]. As a result, several strategies to reduce the danger of corrosion have been proposed and developed. These include of using low-permeable or impermeable concrete, adding thickness to the concrete cover, utilizing coated or stainless steel bars, and putting waterproofing

measures in place [5-7]. One possible solution to corrosion problems in concrete structures is the adoption of modern composite materials, like fiber-reinforced polymer (FRP) bars, which have gained increased popularity in recent times. Utilizing FRP bars offers multiple advantages; besides their exceptional resistance to corrosion in harsh environmental conditions (such as salt exposure for deicing, freeze-thaw cycles, and wet-dry cycles), they boast a high strength-to-weight ratio and are non-magnetic [8]. The use of FRP bars as flexural and shear reinforcement in concrete structures has been the subject of several experimental studies with the goal of improving knowledge of their effects on the structural performance of FRP-reinforced concrete (FRP-RC) elements such as beams, slabs, and columns [9-11]. Because punching shear failure in concrete slab-column connections is usually abrupt and brittle, and frequently happens suddenly, a great deal of attention has been focused on researching it. Such failures might cause partial floor damage or possibly collapse structurally [12-13]. According to Matthys and Taerwe [14], assuming equivalent flexural stiffness, concrete slabs reinforced using carbon fiber reinforced polymer (CFRP) grids for flexural reinforcement showed a punching shear capacity similar to that of conventional concrete slabs reinforced with steel. According to research by Ospina et al. [15], the flexural stiffness of the FRP reinforcement and the strength of the bond between the concrete and the FRP are the two main elements determining the punched shear strength of FRP-RC slab-column connections. Furthermore, it was noted that the punching shear capabilities of concrete connections reinforced with FRP bars and grids varied. These variations were ascribed to variations in bonding characteristics and stress distribution at the FRP grid intersections. Lee et al. [16,17] demonstrated that boosting the glass fiber reinforced polymer (GFRP) reinforcement ratio within 1.5 times the slab thickness (denoted as 'h') from the column face enhances the punching shear strength of concrete slabs. Nevertheless, it was discovered that adding more GFRP reinforcement than 3% will not increase the GFRP-RC slabs' punching shear capability [16]. Dulude et al. [18] observed a notable increase in the punching shear strength of FRP-RC slabs with larger slab thicknesses and column sizes. Likewise, employing higher strength concrete yielded a similar enhancement [19].

Concrete slab-column connections' punching shear strength may be greatly increased by adding steel shear reinforcement, as is well known [20, 21]. Previous studies reporting the use of FRP bars as shear reinforcement have shown similar findings [22–26]. A range of shear reinforcing methods, such as CFRP shear bands [22], CFRP rods [23], CFRP shear rails [24], GFRP and CFRP spiral stirrups [25], and double-head GFRP bars used as shear studs [26], have been presented by research investigations to improve the punching shear strength of FRP-RC slabs. By minimizing bond-slip and postponing the propagation of cracks around column faces, these reinforcing techniques successfully avoid punching shear failure at lower load values [27]. Punching shear strength can be further increased by using FRP stirrups that are properly secured [28].

To calculate the punching shear strength of connections between FRP-RC slabs and columns, a number of design equations have been put forth. These formulae were obtained in two ways: either by modifying the design formulas already in use for traditional RC slabs reinforced with steel [14, 29–31], or by conducting restricted tests [15]. Several analytical models have been introduced, such as Theodorakopoulos and Swamy's [32] model, which is based on moment-shear interaction. This model aims to forecast the punching shear strength of FRP-RC slab-column connections. The depth of the compression zone, which is influenced by the FRP reinforcement's tensile strength and elastic modulus as well as the

bonding properties between the concrete and the reinforcement, is the main emphasis of the model. A semi-empirical fracture mechanics-based model was devised by Nguyen-Minh and Rovnak [33] to assess the punching shear resistance of internal GFRP-RC slab-column connections. This model takes into account many aspects, including the anchorage effect of flexural reinforcement, the span-to-depth ratio (L/d), and the size impact. Moreover, a number of other design formulae for FRP-RC slabs with FRP shear reinforcement are available in the literature. To allow for FRP shear reinforcement, Gouda and El-Salakawy [26] and Salama et al. [31] suggested changes to the CSA/S806-12 [34] code. According to Gouda and El-Salakawy [26], concrete contributes 75% of what FRP-reinforced concrete components lacking shear reinforcement do within the shear-reinforced zone. On the other hand, Salama et al. [31] recommended, contrary to CSA/S806-12 [34], that the shear strength be calculated taking into account the shear reinforcement with a maximum strain limit of 0.005, as well as half the shear strength given by concrete inside the shear-reinforced zone. Similarly, Hassan et al. [35] proposed that, compared to concrete lacking shear reinforcement, the shear strength contributed by concrete in the area reinforced for shear should be halved. Furthermore, they recommended using the allowable stress for FRP shear reinforcement to determine the shear strength provided by the shear reinforcement.

Despite the wealth of research on resistance to punching shear in FRP-reinforced concrete slab-column connection, there remains a notable gap in the literature: a comprehensive synthesis of findings consolidated into a single resource. This study endeavors to fill this gap by undertaking a thorough examination of various aspects, including FRP properties, the mechanics behind punching shear failure, and the efficacy of FRP shear reinforcement in enhancing punching shear strength. In particular, it looks into two main situations: the punching shear resistance of FRP-RC slab-column connection lacking FRP shear reinforcement, and those incorporating such reinforcement. Additionally, the study scrutinizes mathematical and numerical models aimed at predicting punching shear strength. Drawing from a meticulous review of approximately one hundred research papers, this analysis aims to provide a consolidated understanding of punching shear strength in FRP-reinforced concrete slab-column connections.

2. FRP COMPOSITE MATERIALS

In 1975, the earliest application of fiber reinforced polymer (FRP) was seen in Russia, specifically in the form of reinforcement bars [36,37]. Fiber reinforced plastic, or FRP, is a category of materials that use natural or synthetic fibers to naturally increase the strength and stiffness of a polymer matrix [37]. FRPs utilized for strengthening and reinforcing structures boast immense strength, being rated as eight times stronger than traditional steel reinforcement bars [38]. Glass fiber reinforced polymer (GFRP) is employed as prestressing tendons to enhance the strength of a 9-meter-long wooden bridge that is securely fastened [39]. In Europe, research on the potential of fiber-reinforced polymers (FRPs) as a substitute for steel plate bonding in bridge repair and reinforcement began in the 1980s. On the other hand, FRP composites have been used for structural strengthening in the US for around 25 years [40]. Throughout this timeframe, the acceptance of FRP composite as a prevalent construction material rose in tandem with the increasing number of successful FRP strengthening projects. Among design consultants, the adoption of FRP for strengthening, rehabilitation, and retrofitting gained significant traction, surpassing traditional methods like

installing additional structural steel frames and components [41]. FRP is primarily utilized as internal reinforcement, such as rebar, or externally bonded reinforcement to enhance the strength of concrete, timber, steel, and masonry structures [42]. During the 1990s in Japan, FRP bars garnered considerable attention due to their involvement in the study of notably elevated train support structures [43]. Not only does FRP weigh only 25% of steel, but it also has a unique tensile strength attribute that exceeds steel's [36–43]. The Japanese group was the first to publish design recommendations for using fiber reinforced polymer (FRP) to strengthen reinforced concrete (RC) buildings in 1996 [43, 44]. Since then, the use of FRP as a structural reinforcement has grown exponentially, leading official organizations all over the world to create design supervision and guidance guidelines [45, 46]. Design regulations for seismic upgrades of structures have long supported the use of externally bonded fiber reinforced polymer (FRP) reinforcement for reinforcing structural elements, particularly when using high-strength CFRP. Notably, there has been a recent surge in interest towards developing economical and efficient methods for repairing, upgrading, strengthening, or reinforcing existing RC bridges [47, 48]. Rebuilding an existing RC bridge is usually driven by two primary concerns: the need to address deterioration that has accumulated over years of use and the need to increase the bridge's strength to keep up with increases in the weight of contemporary vehicles [49–55]. FRP reinforcements can be used to increase an element's structural load-bearing capability [38,56,57].
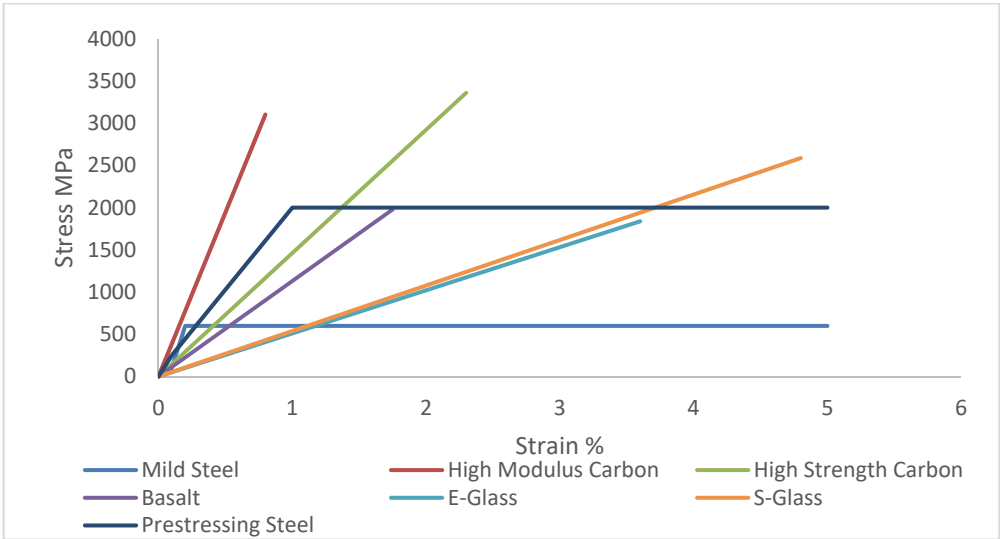
Figure 1 - Comparative analysis between FRP materials and steel [39]

The most widely used FRP composite reinforcements in civil engineering are made by pultruding carbon fiber (CFRP), glass fiber (GFRP), basalt fiber (BFRP), and aramid fiber (AFRP) [58,59]. Among structural FRPs, E-GFRP stands out as the most economical material and consequently enjoys the highest consumption rate [60]. In contrast to E-GFRP, BFRP carries a higher cost due to limited manufacturing capacity. Nevertheless, its price is justified by its superior strength compared to GFRP, along with its resistance to alkalis and

its nearly inexhaustible resource base [38]. With an emphasis on their stress-strain characteristics, Figure 1 presents a thorough comparison of FRP materials and steel reinforcements. Because of its high cost and limited compressive strength independent of the direction of fiber alignment, AFRP is not commonly used as a structural bar, despite its promise [61, 62]. Aramid fiber stands out as the optimal choice for ballistic-resistant fabrics, as it effectively absorbs impact energy [63]. CFRP exhibits the highest strength among FRP materials and boasts the widest range of strengths available [64]. This diversity arises from differences in carbon sources and manufacturing methods. Comparing CFRP to other FRP materials, however, CFRP shows a higher resilience to fatigue and creep failure [65]. Due of its remarkable strength and resistance to fatigue and cycle failures, CFRP is more expensive than other materials [66–68].

Materials of FRP bars are often classified and identified based on their mechanical properties. Table 1 provides an overview of the mechanical properties of the most commonly available FRP bars on the market.

Table 1 - Overview of mechanical properties for various types of FRP materials [41]

Material type	Density (kg/m³)	Tensile strength (MPa)	Young's modulus (GPa)	Elongation (%)
CFRP	1500-2100	600-3920	37-784	0.5-1.8
GFRP	1250-2500	483-4580	35-86	1.2-5.0
AFRP	1250-1450	1720-3620	41-175	1.4-4.4
BFRP	1900-2100	600-1500	50-65	1.2-2.6
Steel	7850	483-690	200	6.0-12.0

Fiber-reinforced polymer (FRP) composite materials exhibit notable durability [69–71] and offer a reasonable fatigue life [72,73]. Their high strength-to-weight ratios make them adaptable to various shapes and sizes of structures with ease. Additionally, FRPs demonstrate corrosion resistance and robust weather resilience. They excel in chemical resistance across a spectrum of substances. Furthermore, their lightweight nature significantly reduces labor costs. As the composite industry continues to advance, focusing on high-performance materials for aging civil engineering infrastructure, FRP stands poised to significantly extend the service life of global infrastructure throughout this century.

3. PUNCHING BEHAVIOR OF STEEL-REINFORCED CONCRETE (RC) SLABS

Punching shear failure in reinforced concrete flat slabs happens locally around the support regions due to intense shear and bending stresses. This type of failure is characterized by the development of a truncated cone shape, which results in a rapid and substantial decrease in the slabs' load-bearing capacity [74]. The evolution of the process leading to punching failure unfolds through several stages as illustrated in Figure 2 [75]: Initially, an approximately circular crack initiates around the column edge on the tension surface of the slab, penetrating deeply in the direction of the compression area. Afterward, a fresh lateral and flexural crack

appears. Next, an inclined shear crack develops near the midpoint of the slab depth, often occurring when the load approaches approximately half to two-thirds of its load-carrying capacity. As the loading persists, these diagonal cracks extend across both the areas experiencing tension and compression, typically at angles varying between 25 and 45 degrees. Ultimately, the diagonal cracks advance to the juncture where the slab meets the support, indicating the failure point at the punching load. The ability of slabs to withstand punching shear is commonly affected by particular factors concerning geometry and material characteristics. These factors include the size of the support cross-section, depth of the slab, strength of the concrete, and the proportion of longitudinal reinforcement [76].
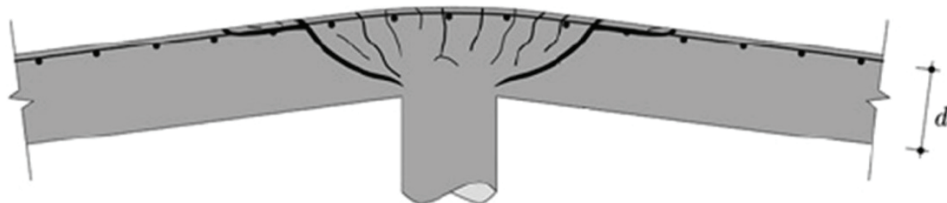
Figure 2 - Punching shear failure mechanism observed in reinforced concrete flat slabs [75]

In the absence of shear reinforcement, inclined cracks trigger the resistance of shear stresses through five key elements of concrete shear strength, as identified by the ASCE-ACI Committee 426 [77]. These factors include: (1) Vc denotes the shear resistance within the compression zone, where the concrete remains uncracked.; (2) Va pertains to the interlocking of aggregates along the surfaces of cracks; (3) Vd relates to the dowel action enabled by flexural reinforcement intersecting the shear crack; (4) Arch action, especially noticeable in deep members with a shear span-to-depth ratio less than 2.5; and (5) Residual tensile stresses within the shear crack arise from minor connections between its surfaces. The ultimate shear strength of slabs generally exceeds that of beams, a phenomenon explained by the ASCE-ACI Committee 426 [77]. This discrepancy can be attributed to several influential factors. Firstly, the allocation of bending moments within a slab differs from that in beams. Secondly, slabs lack the balancing effect present in beams. Thirdly, conventional static analysis may prove inadequate in fully capturing slab behavior. Additionally, in-plane forces exerted by supports' restraints contribute to the overall strength of slabs. Finally, the interplay between bending and shear effects further enhances the shear resistance of slabs.

Two different kinds of bending moments-radial and tangential moments-have an impact on the slab at the contact between it and the column. The first fracture usually appears as a tangential flexural crack close to the column face, where the radial moment is highest, when the material is initially exposed to vertical shear force. Following this, the tangential moment causes radial fractures to emerge from the column faces. Further tangential cracks that are located further from the column face only become visible when there is a significant increase in applied load because the radial moment rapidly decreases in the direction of the column face. On the other hand, the beginning of inclined fractures proceeds in a different way since they spread perpendicular to radial cracks. Because inclined fractures may only occur in places where flexural tangential cracks are not present, these cracks often start in the middle

of the slabs. As a result, instead of having the same characteristics as flexural-shear fractures seen in beams, they have web-shear crack features. In this case, a mechanism absent in beams governs the beginning of inclined cracks: the rigidity of the slab in the lateral direction [78].

Lenschow and Sozen [79] observed that slabs commonly employ orthogonal reinforcement mats, resulting in an intricate distribution of in-plane forces throughout the structure. A slab section with a reinforcing mat positioned at a 45-degree angle to the direction of the moment, M1, is shown in Figure 3. When there is no moment in the y direction (M2 = 0), The separate elements of the reinforcement forces, denoted as T, in the y-axis direction are counteracted by compressive forces within the concrete at the reinforcement level. As a result, if flexural fractures diverge from parallel alignment with the reinforcement, in-plane forces appear within the section of the slab where reinforcement is present. These in-plane forces increase the applied loads, which contribute to the advancement of further cracking after the first fractures.

a) Moment and reinforcement orientation   b) Internal forces at reinforcement level
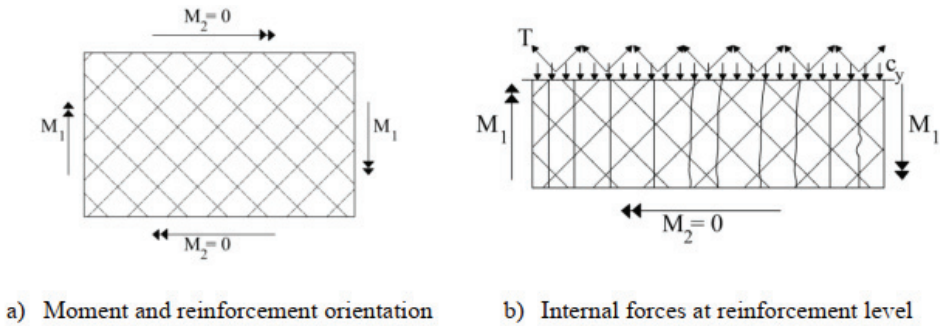
Figure 3 - The lateral forces within slabs, as described by ASCE-ACI Committee 426 [77]

Figure 4 shows the balance of internal forces along diagonal cracks within both slab and beam structures. Concerning the beam (depicted in Figure 4a), sustaining equilibrium requires the tensile force, T, in the reinforcement spanning the diagonal crack to counterbalance the compressive force, C, applied above the fracture. Conversely, in the case of the slab (Figure 4b), equilibrium doesn't demand that the compressive force, C1, beneath the inclined crack, equals the tensile force, T1, generated in the reinforcement spanning the fracture. To sustain equilibrium, it is essential for the total compressive forces across the entire width of the slab, expressed as C1+C2, to be equal the cumulative tensile forces within the reinforcement across the width of the slab, indicated as T1+T2. While fulfilling equilibrium criteria, the transfer capability of force C1 and the proportion of C1 to C2 might diminish with the reduction in uncracked concrete depth at the inclined crack location. However, there is no corresponding mechanism for decreasing shear forces at this point. Although reinforcing around the failure perimeter seems to enhance compressive force C1 by increasing the depth of uncracked concrete, the tensile force T1 within the reinforcement can be counteracted by compressive force C2 beyond the failure perimeter [77–79].

In the cracked area near the column, outward in-plane displacements are frequently observed in slabs. However, the stiffness of the surrounding slab resists these displacements, resulting in in-plane compression forces within the slab. As a result, these pressures increase both the

bending and the shear capacities of connections between slabs and columns. Conversely, they restrict the rotations of cross-sections, thus increasing susceptibility to brittle punching failure [77].

a) Beam or one-way slab   b) Two-way slab
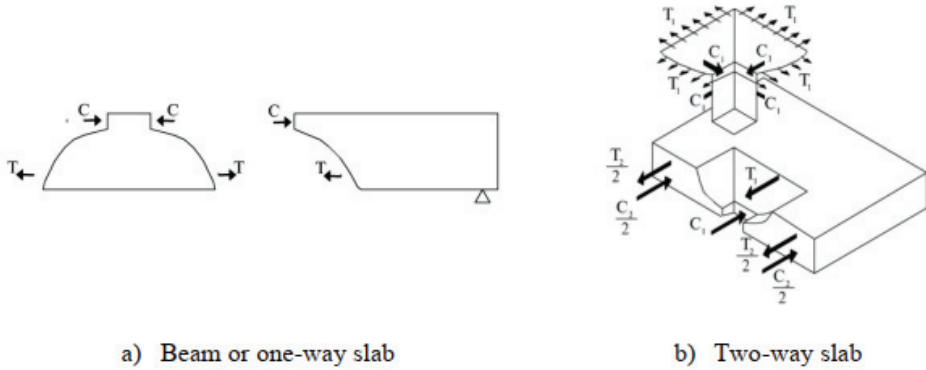
Figure 4 - Forces observed at inclined cracks, as documented by ASCE-ACI Committee 426 [77]

In slab-column connections, the regions crucial for both moment and shear are typically concentrated near the column. This convergence leads to an anticipation of moment-shear interaction, complicating the distinct classification of failures as purely flexural or punching failures in numerous instances. Typically, when the slab's reinforcement ratio increases, the failure modes shift from flexural to punching failure. [77, 78].

4. PUNCHING SHEAR STRENGTH OF FRP-RC SLAB-COLUMN CONNECTIONS WITHOUT SHEAR REINFORCEMENT

Concrete flexural cracking and steel reinforcement yielding are typical prior to punched shear failure in structural members subjected largely to flexural pressures, like reinforced concrete slab-column connections [80]. The punching shear resistance of steel-reinforced concrete (RC) slabs primarily relies on the intact concrete within the compression zone, dictated by the tensile reinforcement's resultant force [81,82]. Similar failure modes have been observed in FRP-RC slabs [16,17,19]. However, due to the superior strength of Fiber-Reinforced Polymer reinforcement as opposed to steel reinforcement and its retention of linear elastic behavior until failure, punching shear failure in slabs reinforced with FRP typically happens later than in steel-RC slabs with the same reinforcement area. In FRP-RC slabs, punching shear failure often transpires before the FRP reinforcement ruptures [18].

Banthia et al. [83] undertook a comprehensive investigation into the efficacy of FRP grid reinforcement in concrete slabs, juxtaposing its performance against that of steel-reinforced counterparts. Plots of load against load point displacement were created by careful testing under transverse loads in order to understand the behavior of the slabs. The application of fiber-reinforced concrete and variances in concrete strength were closely examined in this study, and strain measurements were methodically recorded at various grid positions. The

findings unveiled that FRP-reinforced slabs exhibited either comparable or superior ultimate loads compared to steel-reinforced slabs. However, a notable drawback surfaced: the inherent brittle fracture nature of FRP led to diminished energy absorption capacities relative to their steel counterparts. In a complementary endeavor, Matthys and Taerwe [14] investigated the punching capacity of slabs reinforced with various FRP grid configurations, directly contrasting them with steel-reinforced counterparts. Intriguingly, for FRP-reinforced slabs boasting equivalent flexural strength to their steel-reinforced counterparts, the punching load and stiffness in the cracked state experienced significant reductions. This observation underscores the pivotal role of grid bond behavior in shaping crack propagation dynamics and, ultimately, the brittleness of punching failure. El-Ghandour et al. [22] present the outcomes of a detailed two-phase experimental program aimed at investigating the punching shear behavior of fiber reinforced polymer-reinforced concrete (FRP-RC) flat slabs, both with and without carbon fiber reinforced polymer (CFRP) shear reinforcement. In the initial phase, the study identified issues related to bond slip and crack localization. Subsequent adjustments made in the second phase, particularly the reduction in spacing between flexural bars, effectively addressed these concerns, leading to the occurrence of punching shear failure in the slabs. However, despite these modifications, CFRP shear reinforcement was found to be inefficient in significantly enhancing the slab capacity due to its inherent brittleness. In a related study, Li et al. [84] investigated the behavior of flat plate slabs reinforced with CFRP rods in the punching shear zone. These slabs were subjected to constant gravity load and lateral displacements in a reversed cyclic manner. The research involved testing three specimens of interior column-slab connections: one standard specimen without shear reinforcement, a second reinforced with CFRP rods, and a third reinforced with stud rails, serving as a reference to the second specimen. While punching shear failure occurred in the standard specimens at a lateral drift ratio of approximately 5%, the specimen reinforced with CFRP rods displayed significant flexural yielding. It sustained deformations up to a drift ratio of approximately 9% without notable strength losses and did not experience punching shear failure. Additionally, displacements in this specimen were up to 1.79 times larger than those of the standard specimen, indicating a 42% superior ductile performance compared to the standard specimen, and even matching the capability of the stud rail reinforced specimen. These experimental findings suggest a promising outlook for the utilization of CFRP rods in flat slab applications.

Lee et al. [16] delved into the comparison between glass fiber-reinforced polymer (GFRP) and steel bars in terms of their impact on punching shear resistance. Their experimental findings delineated clear disparities: Due to the lower elastic modulus of GFRP bars, slabs reinforced with GFRP exhibited notably reduced punching shear capacities, decreased post-cracking stiffness, and increased deflections compared to their steel-reinforced counterparts. Additionally, GFRP-reinforced slabs showed a heightened propensity for crack formation in the immediate column region relative to those reinforced with steel bars. In a similar vein, Hussein and Rashid [85] meticulously investigated the punching-shear behavior of two-way concrete slabs reinforced with varying grades of GFRP bars. Employing monotonic concentric loading until failure, the experimental setup allowed for a comprehensive evaluation of reinforcement type and ratio effects. Notably, the tested specimens exclusively experienced punching-shear failure as the final mode, with no instances of concrete flexural crushing, rupture, or slippage failure of the reinforcing bars observed. Moreover, their study

revealed that an increase in GFRP reinforcement ratio led to enhanced punching-shear capacities, reduced strains in the reinforcement, and minimized slab deflections.
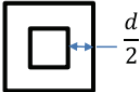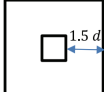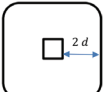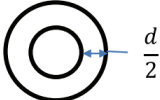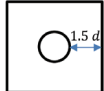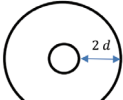
In a thorough investigation, Shill et al. [86] compared the structural behavior of extensive two-way concrete slabs reinforced with fiber-reinforced polymer (FRP) rebars to that of traditional steel-reinforced concrete. In place of steel reinforcement, basalt fiber composites (BFRP) and carbon fiber composites (CFRP) were also assessed. Comparing CFRP-RC and BFRP-RC slabs to steel-RC slabs, the testing results showed that the former had cracking moment capabilities that were around 7% and 4% greater, respectively. It is worth mentioning that the two types of FRP-RC exhibited different load capacity behaviors: CFRP-RC slabs displayed a rapid decrease in load capacity similar to steel-RC slabs, while BFRP-RC slabs demonstrated a gradual reduction beyond the peak load. Additionally, BFRP-RC slabs exhibited 1.72 times more ductility compared to CFRP-RC slabs. The collapse of FRP-RC slabs resulted from punching shear, whereas the failure of the steel-RC slab was due to flexural bending moment. Steel rebars were found to have yielded upon failure, whereas FRP rebars remained intact. Moreover, FRP-RC slabs exhibited more fractures and deflection compared to steel-RC slabs. However, FRP-RC slabs demonstrated elastic recovery after unloading, a behavior not observed in steel-RC slabs.

4.1. Punching Shear Strength of FRP-RC Slab-Column Connectors without Shear Reinforcement: Analytical Models

4.1.1. Codes Specified Formulas

The critical shear perimeter method forms the basis of various design codes, such as ACI 318-19 [87], CSA-A23.3-04 [88], BS 8110-97 [89], and CEB-FIP 90 [90]. This methodology is derived exclusively from extensive test data [91,92]. Instead of relying solely on empirical

Table 2: Critical shear perimeters as defined by various codes and standards.

Model based on perimeter	ACI 318-19 [87], CSA-A23.3-04[88] and JSCE [94]	BS 8110-97 [89]	CEB-FIP 90 [90]
Key perimeter	$\dfrac{d}{2}$ $b_c = 4(c + d)$	1.5 d $b_c = 4(c + 3d)$	2 d $b_c = 4(c + \pi d)$
	$\dfrac{d}{2}$ $b_c = \pi(c + d)$	1.5 d $b_c = 4(c + 3d)$	2 d $b_c = \pi(c + d)$

models, Model Code 2010 [21] integrates punching shear equations rooted in the mechanical concept of critical shear crack theory (CSCT) introduced by Muttoni [93]. These equations utilize the maximum shear stresses along an imaginary vertical critical perimeter surrounding the column to determine punching shear strength. Punching shear capacity in the CSCT model is dependent on the size and texture of shear fractures created by slanted compression struts that withstand shear loads. These design guidelines and standards offer distinct formulations for punching shear calculations, with significant differences in the crucial perimeter's form and placement. Various critical shear perimeters are offered, based on statistical studies and the characteristics taken into account by each design code. An overview of the essential shear perimeter anticipated for each design code is shown in Table 2. The models provided by several researchers as well as those defined by rules and standards are covered in detail in the following sections.

The ACI 318 code equation was modified with the addition of a modification factor k in ACI 440.1R-15 [95]. By incorporating this adjustment, the aim was to ensure that the punching shear strength of FRP-reinforced two-way concrete flat slabs reflects the impact of both the reinforcement ratio and the variable elastic modulus of FRP bars. The following is the equation given in ACI 440.1R-15 [95]:

$$V_R = 0.8\sqrt{f_c'}\, b_{\circ ACI} d k \tag{1}$$

$$k = \sqrt{2\rho n_t + (\rho n_t)^2} - \rho n_t \tag{2}$$

Here, n_t represents the modular ratio, defined as the ratio of the modulus of elasticity of FRP (Ef) to that of steel (Es). Meanwhile, ρ denotes the reinforcement ratio.

CSA S806-12 [96] introduced significant modifications to the punching shear equation originally designed for steel-reinforced concrete flat slabs in CSA-A23.3-04 [88], tailoring it for application in FRP-reinforced flat slabs. This revised formula takes into consideration a number of factors, including size effect, reinforcement stiffness, reinforcement ratio, and concrete compressive strength, that influencing the punching shear resistance of two-way flat slabs. The minimal value derived from the given equations is used to calculate the punching shear capacity of FRP-reinforced concrete flat slabs, per CSA S806-12 [96]:

$$V_R = \left(1 + \frac{2}{\beta}\right) 0.028\lambda \left(E_f\, \rho_f f_c'\right)^{1/3} b_{\circ CSA} d \tag{3}$$

$$V_R = \left(\frac{a_s d}{b_{\circ CSA}} + 0.19\right) 0.147\lambda \left(E_f\, \rho_f f_c'\right)^{1/3} b_{\circ CSA} d \tag{4}$$

$$V_R = 0.056\lambda \left(E_f\, \rho_f f_c'\right)^{1/3} b_{\circ CSA} d \tag{5}$$

Here, ρ_f represents the reinforcement ratio of FRP.

In JSCE 1997 [94], an equation for designing punching shear in FRP-reinforced concrete slabs was presented. This equation encompasses all primary parameters affecting punching shear strength and is structured as follows:

$$V_R = \beta_d \beta_p \beta_r f_{pcd} \, b_{\circ JSCE} d \tag{6}$$

where:

$$\beta_d = (\frac{1000}{d})^{1/4}$$

$$\beta_p = (\frac{100 \rho_f E_f}{E_s})^{1/3}$$

$$\beta_r = 1 + 1/(1 + \frac{0.25u}{d})$$

$$f_{pcd} = 0.8\sqrt{f_c'} \leq 1.2 \text{ MPa}$$

where $b_{\circ JSCE}$ the critical shear perimeter specified by JSCE [94] closely resembles that outlined in ACI 318–19 [87]. Here, u denotes the perimeter of the column.

4.1.2. Proposed or Modified Models

A comparative examination of the observed values for FRP-reinforced slabs lacking shear reinforcement available in the literature and the punched shear strength estimations obtained using the suggested formula is shown in Table 3. Rizk et al. [97] proposed a modification to the formula in ACI 318-11 for calculating the punching shear capacity of steel-reinforced concrete slabs, which can be extended to FRP-reinforced slabs by incorporating adjustments for the material properties of FRP, such as its lower stiffness and distinct tensile behavior:

$$V_R = 0.333 \sqrt{f_c'} (\frac{l_{ch}}{h})^{0.333} (100\rho)^{0.333} b_{\circ ACI} d \tag{7}$$

Here, l_{ch} denotes the characteristic length, defined as $-0.84f_c'+500$ based on the approach outlined by Zhuo et al. [98], while h represents the thickness of the slab.

Conversely, Rizk et al. [99] employed regression analysis to adjust the CSA-A23.3–04 equation used for predicting the punching shear strength of flat slabs. This adjustment takes into consideration the influence of the steel reinforcement ratio in addition to the sizes of the slabs and columns. Here is how the revised equation is put together:

$$V_R = .7 \, (f_c')^{0.333} (\frac{l_{ch}}{2h})^{0.25} (100\rho)^{0.333} b_{\circ CSA} d \tag{8}$$

Elsanadely et al. [100] formulated an empirical equation to predict the punching shear strength of flat slabs, incorporating the effects of slab depth and utilizing experimental data from the literature. The equation also accounts for the use of high-strength concrete, making it applicable to both steel- and FRP-reinforced slabs when adjustments are made for the distinct material properties of FRP. The following formula represents the equation developed by Elsanadely et al. [100]:

$$V_R = 0.127 \ (f_c')^{0.333 \ 0.333}\sqrt{\rho f_y}\left(1 + \frac{8d}{b\circ_{ACI}}\right)\sqrt{1 + \frac{125}{d}} \ b\circ_{ACI}d \tag{9}$$

El-Ghandour et al. [22] proposed an adjustment factor $(Ef/Es)^{0.333}$ to the equation in the ACI 318-95 code for estimating the punching shear strength of FRP-reinforced concrete flat slabs. The resulting equation is as follows:

$$V_R = 0.333 \ (E_f/E_s)^{0.333}\sqrt{f_c'}b\circ_{ACI}d \tag{10}$$

Matthys and Taerwe [14] proposed a modification to the BS 8110 [89] equation for calculating the punching shear strength of FRP-reinforced concrete flat slabs, resulting in the following expression:

$$V_R = 1.36 \ (1/d)^{\frac{1}{4}} \ (\frac{100\rho f_c' E_f}{E_s})^{\frac{1}{3}} \ b\circ_{BS}d \tag{11}$$

Ospina et al. [15] proposed a further adjustment to the equation introduced by Matthys and Taerwe [14], which is formulated as follows:

$$V_R = 2.77 \ (\rho_f f_c')^{\frac{1}{3}}(E_f/E_s)^{0.5}b\circ_{BS}d \tag{12}$$

El-Gamal et al.'s proposal [29] included a new factor α to the ACI 318-05 punching shear equation, which can be utilized to approximate the punching shear strength of flat slabs constructed with reinforced concrete and steel. The following is the expression for the altered equation:

$$V_R = 0.333 \ \sqrt{f_c'} \ b\circ_{ACI}da \tag{13}$$

$$a = 0.5 \ \sqrt[3]{\rho E} \ (1 + \frac{8d}{b\circ_{ACI}}) \tag{14}$$

Bompa and Onet [101] empirically determined the inclination angle of the punching shear surface through a combination of computational calculations and practical experiments gleaned from existing literature. The resulting formula for the inclination angle (θ) is contingent on factors such as the effective depth of the slab, the ratio of flexural reinforcement in the slab, and the yield strength of the reinforcement relative to the compressive strength of the concrete. The following is how this model is stated:

$$\tan\theta = 0.6 + \ \rho f_y/f_c\sqrt{d/265} \tag{15}$$

Moreover, Bompa and Onet [101] devised a punching shear model that incorporates the degree of inclination of the fracture surface, departing from the conventional approach of employing a fixed critical shear perimeter. Here is the formulation of this model:

$$V_R = 2\pi d \ (f_c)^{\frac{1}{3}}[0.4d + \rho f_y^{\frac{1}{3}}r\circ]\xi \tag{16}$$

where r_o represents the punching shear radius at the top surface of the slab.

$$r_o = d \cot\theta + c/2$$

$$\xi = 0.75 + (d/lch)^{-0.2}$$

In order to examine the punching shear behavior of two-way flat slabs, Broms [102] developed the Tangential Strain Theory (TST), which incorporates a strut-and-tie failure mechanism near the junction of the column and the slab. This approach emphasizes the importance of considering the yielding of slab reinforcement at the column edge. For slabs with reinforcement remaining within the elastic range, the punching shear strength is determined using the following equation. While originally developed for steel-reinforced slabs, the theory can be adapted for FRP-reinforced slabs by accounting for the distinct stress-strain behavior of FRP materials:

$$V_R = m_\varepsilon \frac{8\pi}{1-\ln(\frac{A}{B})-\frac{A^2}{B^2}} \tag{17}$$

As an alternative, the punching shear may be written as follows if the slab reinforcements are totally yielded:

$$V_{y2} = m_y \frac{2\pi}{1-\frac{A}{B}} \tag{18}$$

In this case, B=3π/8c, where c is the square column's side length and A is the circular test model's diameter.

$$m_\varepsilon = \rho d^2 E_s \varepsilon_s (1 - x/3d)$$

$$m_y = \rho d^2 f_y (1 - x/3d)$$

The depth of the compression zone is shown here by x.

Hassan et al. [35] introduced a punching shear formula for flat slabs reinforced with FRP by combining three suggested variables into the ACI 318-19 [87] framework: βs, βa (similar to JSCE 1997), and βc. Experiments were used to validate these parameters. This is the expression for the equation that Hassan et al. [35] proposed:

$$V_R = \beta_d \beta_p \beta_c \sqrt{f_c'} \, b_{\circ ACI} d \tag{19}$$

where:

$$\beta_d = (\frac{130}{d})^{1/4}$$

$$\beta_p = 0.55(\frac{100\rho_f E_f}{E_s})^{1/3}$$

$$\beta_c = (0.65 + \frac{4d}{b_{\circ ACI}})$$

Drawing on critical shear crack theory, Muttoni et al. [93] presented punching shear design formulations. As a minimum value derived from the above equations, the punching shear strength is offered.

$$V_R = k_b \sqrt[3]{(100\rho f_c \frac{d_{dg}}{r_s})} \, b_o d \tag{20}$$

$$V_R = 0.55 b_o d \sqrt[2]{f_c} \tag{21}$$

Here,

$$k_b = \sqrt{8a\frac{d}{b_o}} \geq 1$$

$$d_{dg} = d_{g0} + d_g.\min\left(\left(\frac{60}{f_c}\right)^2, 1\right) \leq 40mm \tag{22}$$

Here, a represents a factor fixed at 8 for interior columns. d_{dg} indicates the reference crack roughness, whereas d_{g0} and "dg" stand for the reference aggregate size, set at 16 mm, and the maximum aggregate size, respectively..

In the case of concrete slabs and footings reinforced with steel, Kueres et al. [27] revised the punching shear equations in Eurocode 2. Data testing from the literature was used to inform their revision. They promoted the unification of the two distinct equations for calculating punching shear in slabs and footings as required by Eurocode 2. The following is the suggested updated equation:

$$V_R = 2.22 \, k_d k_\lambda \sqrt[3]{(100\rho f_{ck})} \, b_{o \, revised} \, d \tag{23}$$

Here, k_d (where $k_d = 1/(1+d/200)^{0.5}$) represents the modified influence factor, while $k_\lambda = (b_o/d.a_\lambda/d)^{0.5}$, with a_λ representing the shear span.

An empirical equation obtained from substantial experimental data on FRP-reinforced concrete slabs was introduced by Hassan et al. [11]. Here is how this equation is expressed:

$$V_R = \left(\frac{4d}{b_{\circ CSA}} + 0.65\right) 0.065\lambda \left(E_f \rho_f f_c'\right)^{1/3} \left(\frac{125}{d}\right)^{1/6} b_{\circ CSA} d \tag{24}$$

Table 3 - A comparative analysis between the punching shear strength estimates derived from the proposed formula and the measured values found in the literature for FRP-reinforced slabs without shear reinforcement

Reference	$d_{(slab)}$ (mm)	$b_{(column)}$ (mm)	f_c' (MPa)	ρ (%)	E_f (GPa)	V_{Exp} (KN)	$V_{test}/V_{pred.}$
Matthys and Taerwe [14]	95 -126	80-150	32.1-36.3	0.52-3.78	40.7-95	171-347	1.032- 1.562
Hassan et al. [25]	131-281	300-375	29.6-75.8	0.73-1.61	48.1-64.9	386-1600	1.116-1.355
Hassan et al. [19]	132-281	300	34.3-75.8	0.71-1.61	48.2-64.9	329-1600	1.110-1.301
Lee et al. [16]	110	225	36.3	1.1-1.26	48.2	222-248	0.973-1.063
Zhang et al. [103]	100	250	35-71	1.05-1.18	42	218-275	1.10-1.47
Zaghloul and Razaqpur [104]	75	250	44.8	1.33	100	234	1.150
Hussien et al. [105]	100	250	26-40	0.95-1.18	42	210-249	1.205-1.262
Ospina et al. [15]	120	250	28.9-37.5	0.73-1.46	28.4-34	206-260	1.00-1.14
Ahmad et al. [106]	61	75-100	36.6-44.6	0.95	113	78-99	0.893-1.101
Nguyen-Minh and Rovnak [33]	129	200	39	0.48-0.92	48	180-244	0.867-0.946
Gouda and Elsalakawy [107]	159	300	38	0.65	68	421	1.05
Al Ajami [108]	94-191	200	35-53	0.93-1.01	52.5	168-617	0.88-1.17
Gouda and Elsalakawy [26]	160	300	38.0-70.0	0.65-1.13	68	363-425	0.77-0.87
Dulude et al. [18]	131-281	300-450	29.6-44.9	0.71-1.56	48.1-48.2	329-1248	1.08-1.39
Ramzy et al. [109]	82-112	200	33-39.7	0.81-1.54	46	165-230	0.90-1.43

4.2. Predicting Punching Shear Capacity of Punching Shear Strength of FRP-RC Slab-Column Connections without Shear Reinforcement Using Machine Learning Model

Machine learning (ML) stands as a pivotal artificial intelligence tool, adept at autonomously absorbing and refining its operations through pre-existing data [110]. In contrast to conventional regression analysis, ML boasts heightened predictive precision and adeptness in managing intricate datasets [112]. It finds extensive application across various domains, ranging from assessing concrete material properties to evaluating the load-bearing capacity of reinforced concrete elements [113–120]. Classical machine learning frameworks include

backpropagation artificial neural networks (BPANN), support vector regression (SVR), decision trees, random forests (RF), and gradient boosting regression trees (GBRT) [113, 115-119]. Although frequently used, the study of machine learning for estimating the punching shear capacity of FRP bar-reinforced concrete flat slabs is still in its early stages. Metwally [121] used an artificial neural network (ANN) to predict punching shear capacity from a dataset of 59 flat slabs, whereas Vu and Hoang [122] used the support vector machine approach in a similar attempt. Liang's recent contributions [123, 124] have increased the dataset to 154 items, using sophisticated ensemble prediction machine learning techniques and evolutionary algorithms to generate explicit expressions. These developments have significantly improved prediction accuracy and resolved application restrictions, demonstrating the superiority of machine learning models in estimating punching shear capacity over previous empirical techniques.

Yan et al. [125] performed a thorough analysis and created a complete database with 165 sets of test data, including eight critical variables required for model creation. They then developed four data-driven models—backpropagation artificial neural network (BPANN), support vector regression (SVR), random forest (RF), and gradient boosting regression tree (GBRT)-and compared their performance to conventional prediction algorithms. To improve model interpretability, the study used the Shapley Additive Explanation (SHAP) and Partial Dependence Plot (PDP) techniques to quantify the influence of parameters on anticipated outcomes. The results showed that Ju et al.'s technique beat the 25 other formulae tested, with R2, Pre/Exp, MAPE, and RMSE values of 0.76, 1.02, 22.2%, and 142.8 kN, respectively. Furthermore, machine learning methods outperformed classical formulae in prediction accuracy, with the GBRT model achieving the best precision. SHAP analysis indicated effective slab height and column section aspect ratio as important variables impacting punching shear capacity, whereas PDP analysis gave quantitative information on how punching shear capacity fluctuates with each relevant variable.

Doğan & Arslan [126] conducted a literature review and gathered experimental data from 141 slabs reinforced with GFRP bars, CFRP bars, and conventional steel bars that had undergone punching. Following data collection, meticulous parameter calibration enabled the development of prediction models for slab punching strength using five different machine learning techniques: Multiple Linear Regression (MLR), Bagging-Decision Tree Regression (Bagging-DT), Random Forest Regression (RF), Support Vector Regression (SVR), and Extreme Gradient Boosting (XGBoost). The study thoroughly examined the convergence performance of the algorithms concerning the outcomes, alongside analyzing the impact of each parameter on the data. It also critically evaluated the predicted accuracy for punching strength in the literature, including ACI 440's and other techniques. The study's most notable conclusion was that predictions, especially those derived from building codes, tended to be more conservative than experimental results. Among the methods employed, Support Vector Regression (SVR) emerged as the most efficient, particularly in estimating the strength of slabs reinforced with GFRP bars. Following analysis, SVR yielded impressive results: for slabs reinforced with GFRP bars, the R2 values, Mean Absolute Error (MAE), and Root Mean Squared Error (RMSE) performance measures significantly exceeded those of empirical correlations, reaching 96.23%, 0.16, and 0.19, respectively.

Here's the revised version of the paragraph, taking into account the note that ACI is "safe for design purposes" and should not be labeled as "least reliable". The author of this article has also clarified other aspects and ensured consistency:

In their investigation of the punching shear strength of fiber-reinforced polymer (FRP) concrete slabs, Badra et al. [127] assessed several models from the literature using a rudimentary reliability analysis, highlighting the need for more precise and consistent strength models. As a result, the study proposed two machine learning (ML) models, both of which demonstrated superior accuracy in predicting strength compared to earlier models, offering a novel approach. The study also examined the complex interplay of factors influencing punching shear strength, contrasting the impact of primary variables on strength using the proposed models with that of existing models. A more comprehensive analysis was suggested, with a streamlined reliability-based assessment that ranked CSA as the most dependable. While ACI was not the least reliable, it was considered more conservative and showed less alignment with test data trends. However, it remains a reliable approach for design purposes due to its safety focus. The study revealed that the reliability of the models deteriorated for slabs with thicknesses below 200 mm and reinforcement ratios below 1%. Interestingly, the reliability index remained consistent as concrete compressive strength, effective depth, flexural reinforcement ratio, and Young's modulus increased. Additionally, as these parameters increased, sensitivity factors decreased. Parametric experiments using an ANN model and an SVM model demonstrated enhanced accuracy, consistency, and safety. These models were capable of accommodating variable uncertainty and accurately capturing the complex behavior of FRP-reinforced concrete slabs under punching shear. The study concluded that, while the flexural reinforcement ratio had minimal impact on strength due to the reduced transverse resistance of FRP reinforcement, the size and compressive strength of the concrete significantly influenced strength, likely due to the values of Young's modulus of FRP bars and reduced dowel action effects.

In order estimate the punching shear strength of FRP-C slabs without shear reinforcement, Truong et al. [128] used machine learning (ML) approaches. Using input variables like the shear span-to-effective depth ratio, column perimeter-to-effective depth ratio, effective slab depth, concrete compressive strength, FRP reinforcement ratio, ultimate tensile strength, and elastic modulus of FRP, they created an experimental database with 104 specimens. The study evaluated the applicability of three ML techniques: extreme gradient boosting (XGBoost), random forest (RF), and support vector regression (SVR). To refine hyperparameters, ML-based models were developed using a grid search method and a 5-fold cross-validation strategy. Using a variety of statistical estimators, the effectiveness of these machine learning-based models was assessed and contrasted with the design codes and pre-existing models. The results indicated that there was no apparent bias in the predictions of punching shear strength by the three ML-based models concerning the input variables. With a coefficient of determination (R2) of 0.962, a root mean square error (RMSE) of 0.061 MN, a mean absolute error (MAE) of 0.035 MN, and a mean absolute percent error (MAPE) of 8.931% for the testing dataset, the XGBoost-based model emerged as exhibiting the most superior prediction performance. Further analysis revealed that the effective slab depth exerted the most significant impact on prediction performance. When compared to SVR- and RF-based models, as well as existing design codes and models, the XGBoost-based model demonstrated superior accuracy and robustness. These findings underscored the precision and reliability of the XGBoost-based model for FRP-RC slab design and assessment.

5. THE CAPACITY OF FRP-RC SLAB-COLUMN CONNECTIONS TO RESIST PUNCHING SHEAR WHEN INCORPORATING SHEAR REINFORCEMENT

Shear reinforcement can notably enhance punching shear capacity, despite the fact that many slabs are frequently constructed without it due to relatively lenient code requirements and challenges associated with anchoring and installation [87]. Similar to RC slab-column connections with shear reinforcement, punching shear failure in FRP-RC slab-column connections with FRP shear reinforcement may be categorized into three main failure modes depending on the amount and detailing of the FRP shear reinforcement: (1) failure at the level of maximum punching shear capacity, (2) failure outside the shear-reinforced zone, and (3) failure within the shear-reinforced zone [27, 129]. The first mode, shown in Figure 5(a), happens when there is not enough shear reinforcement to stop shear cracks from spreading across the FRP shear reinforcement. This is frequently the result of inadequate shear reinforcement-concrete interaction or anchorages coming loose. Conversely, the second mode, illustrated in Figure 5(b), occurs when there is an excess of shear reinforcement or when the spacing between the shear reinforcement is dense enough. Here, the shear reinforcement halts the propagation of the shear crack, leading to punching shear failure at the maximum punching shear capacity level. This typically transpires at the critical section, positioned between the innermost perimeter of the FRP shear reinforcement and the column edge. In cases where the shear-reinforced zone is relatively short in length, the third mode (depicted in Figure 5(c)) may manifest.
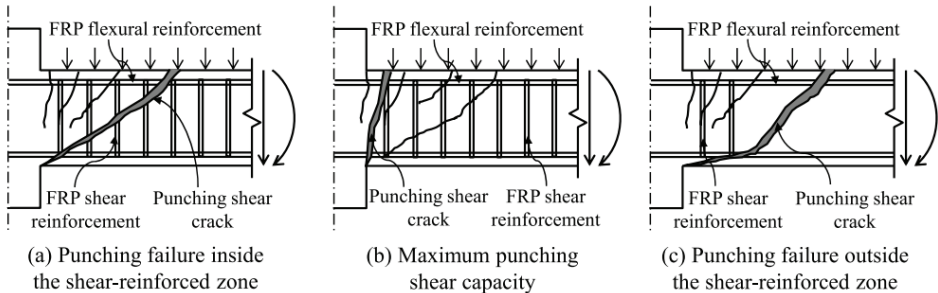
Figure 5 - FRP-RC slab-column connections with FRP shear reinforcement show punching shear failure mechanisms [27].

El-Ghandour et al. [22] investigated eight internal connections between circular slabs and columns, with three incorporating CFRP shear bands as shear reinforcement at varying flexural reinforcement ratios. The introduction of CFRP shear bands enhanced deformability compared to unreinforced slabs, with a significant 13.9% increase in punching capacity observed in slabs featuring 0.38% GFRP flexural reinforcement. The authors suggested a strain limit of 0.0045 for shear reinforcement and advocated for a maximum spacing of 0.5d. Furthermore, they recommended relying on only 50% of concrete resistance, consistent with the provisions of the ACI 318-95 code. Similarly, Hassan et al. [25] investigated 10 full-scale slab-column connections categorized into 200 mm or 350 mm series based on thickness. While the flexural reinforcement of all slabs was GFRP, only seven of them incorporated FRP stirrups for shear reinforcement. FRP stirrups notably enhanced shear capacity by 23%

for series II and reduced failure brittleness by 29% for series I. However, in specimens with low reinforcement ratios, flexural reinforcement primarily governed punching shear capacity, suggesting that FRP stirrups could only offer a modest enhancement.

Gouda and El-Salakawy [26] investigated the utilization of a distinctive type of headed-end GFRP studs as shear reinforcement in internal connections. These studs were meticulously positioned in eight lines encircling the central column, creating five and seven parallel peripheral rows of studs, respectively, with 120 mm and 80 mm (0.75d and 0.50d) spacing between stud rows in Connections R-15-75 and R-15-50. The critical segment was situated 3.90d from the column face, beyond the shear-reinforced zone in both configurations, where the studs extended into the slab. Despite the authors' observations of improved rigidity and load-bearing capability in the shear-reinforced connections, the GFRP studs failed to avert the occurrence of brittle punching shear failure, resulting in both connections collapsing within the shear-reinforced zone. Additionally, there was evidence of damage to the shear stud heads. El-Gendy and El-Salakawy [30] employed a comparable arrangement of GFRP shear reinforcement in GFRP-RC slab-column edge connections in a related study. Their analysis revealed that the joint equipped with seven parallel rows of studs along the periphery (spaced at 0.50d) encountered a failure mode characterized by significant deformations due to bending. Conversely, a connection outfitted with merely five parallel rows of studs along the periphery, with a spacing of 0.75 inches between them, experienced failure due to a combined flexural and punching mode.Table 4 displays the test outcomes for interior slabs constructed with FRP reinforcement, specifically featuring FRP shear reinforcement.

Table 4 - The existing test data for interior slabs reinforced with FRP, particularly focusing on the inclusion of FRP shear reinforcement.

Reference	$d_{(slab)}$ (mm)	$b_{(column)}$ (mm)	f_c' (MPa)	ρ (%) (Flexural rein.)	E_f (GPa) (Flexural rein.)	A_s (mm²) (Shear rein.)	E_f (GPa) (Shear rein.)	V_{Exp} (KN)	$V_{test}/V_{pred.}$
Hassan et al. [25]	131-284	300	29.5-40.2	0.34-1.61	68	71-129	44.6-130.4	514-2024	0.93-1.12
Gouda and El-Salakawy [26]	160	300	42	0.65	63.1-68	113	60	385-401	0.96-0.97
Zaghloul [24]	100	250	45.7-57.6	0.87-1.48	100	100	100	318-328	1.16
Hussein [130]	160	300	43	0.98-1.93	65	71-127	52-68	527-595	1.01-1.08

5.1. Analytical Models for Predicting the Punching Shear Strength of FRP-Reinforced Concrete Slab-Column Connections with Shear Reinforcement

Present design standards lack precise directives for integrating FRP shear reinforcement in FRP-RC slab-column connections. Additionally, there is a scarcity of analytical models for forecasting the punching shear resistance of FRP-RC slab-column connections devoid of shear reinforcement, as delineated in Table 5.

Hassan et al. [25] introduced an equation aimed at assessing the contribution of FRP stirrups, denoted as, to the punching shear capacity in two-way slabs. This suggested equation, which

is shown below, is a modification of the shear design equation for steel specified in CSA/A23.3-04:

$$v_s = 0.7 \frac{\emptyset_f A_{vs} f_{fs}}{b_o s} \tag{23}$$

Incorporating ϕ_f, the factor representing the resistance of FRP reinforcement, the area of the shear reinforcement's cross-section, and the minimum stress in the shear reinforcement f_{fs}, as delineated in the subsequent two equations:

$$f_{fs} = \frac{\left(0.05 \frac{r_o}{d_b} + 0.5\right) f_{fu}}{1.5} \leq f_{bend}$$

$$f_{fs} = 0.004 \, E_{fs}$$

In this scenario, where E_{fs} represents the modulus of elasticity of FRP shear reinforcement, b_r indicates the bend radius, d_b stands for the diameter of the bars, f_{fu} denotes the tensile strength of the unstressed section of the stirrup, and f_{bend} characterizes the ability of the FRP stirrup to resist bending.

Gouda and El-Salakawy [26], as well as El-Gendy and El-Salakawy [30], proposed an equation designed to evaluate the role of FRP stirrups. Their method is based on the similarities between the recommendations for steel-reinforced concrete connections between slabs and columns featuring stud shear reinforcement as detailed in CSA/A23.3-14 and ACI 318-14, respectively.

$$v_s = \frac{\emptyset_f A_{vs} f_{fs}}{b_o s} \tag{24}$$

$$v_s = \frac{A_{vs} f_{fs}}{b_o s} \tag{25}$$

Salama et al. [31] presented an equation tailored to assess the function of FRP stirrups. Their method is informed by the similarities observed in the guidelines for steel-reinforced concrete slab-column connections featuring stud reinforcement against shear, as outlined in CSA S806-12 and ACI 440.1R-15, respectively.

$$v_s = \frac{\emptyset_f A_{vs} (0.005 \, E_{fs})}{b_o s} \tag{26}$$

$$v_s = \frac{\emptyset_f A_{vs} (0.004 \, E_{fs})}{b_o s} \tag{27}$$

Truong et al. [131], in their study, formulated a design equation for FRP shear reinforcement based on the design principles specified in ACI 440.1R-15 and the methodology established by El-Gendy and El-Salakawy [30]. This equation is represented as follows:

$$v_s = \frac{0.7\, A_{vs}\, \varepsilon_s\, E_{fs}\, (d-c_u)}{s} \tag{28}$$

In the context of this research article, ε_s denotes the strain effectiveness of FRP shear reinforcement, c_u represents the depth of the neutral axis, and d signifies the effective depth of the slab.

Table 5 - Design approaches for slabs reinforced with FRP and featuring FRP shear reinforcement

Model	Equation
Hassan et al. [25]	$v_s = 0.7 \dfrac{\emptyset_f A_{vs} f_{fs}}{b_o s}$
Gouda and El-Salakawy [26]	$v_s = \dfrac{\emptyset_f A_{vs} f_{fs}}{b_o s}$
El-Gendy and El-Salakawy [30]	$v_s = \dfrac{A_{vs} f_{fs}}{b_o s}$
Salama et al. [31]	$v_s = \dfrac{\emptyset_f A_{vs} \left(0.005\, E_{fs}\right)}{b_o s}$ $v_s = \dfrac{\emptyset_f A_{vs} \left(0.004\, E_{fs}\right)}{b_o s}$
Truong et al. [131],	$v_s = \dfrac{0.7\, A_{vs}\, \varepsilon_s\, E_{fs}\, (d-c_u)}{s}$

6. SUMMARY, CONCLUSIONS AND LIMITATIONS

Interest in reinforcing concrete slabs with Fiber Reinforced Polymer (FRP) bars is increasing, particularly for their advantageous properties in harsh environments where conventional steel reinforcement is prone to corrosion. Understanding the punching shear behavior of flat slabs reinforced with FRP bars is crucial because punching shear is a critical failure mode in flat slab floor systems. A review of approximately one hundred studies, both recent and historical, indicates that FRP reinforcement can effectively replace steel reinforcement, addressing the issue of corrosion. Experimental results suggest that while the basic failure mechanism of slab-column connections reinforced with FRP in concrete (FRP-RC) shares similarities with those reinforced with steel, unique strength prediction models are required due to substantial variations in the elastic modulus and stress-strain characteristics of FRP. Moreover, the punching shear resistance of FRP-RC slab-column connections is enhanced with the incorporation of shear reinforcement. In specimens featuring shear reinforcement, the occurrence of brittle punching shear failure is less frequent, and fractures are more evenly distributed. FRP stirrups effectively distribute the shearing forces across the punched shear zone, providing adequate confinement and resistance to hinder the development of significant shear fractures. This ensures that failure predominantly occurs within or outside the shear-reinforced zone, rather than at a singular point. Despite considerable research on FRP, its

widespread adoption in the construction sector, especially in slab-column connections, remains in its infancy, with limited large-scale implementation:

1. While FRP materials offer excellent resistance to corrosion and other environmental factors, long-term performance data, particularly in real-world conditions, is still limited.

2. Although there is growing research on the use of FRP in concrete reinforcement, there are still no universally accepted design codes or guidelines specifically for FRP-reinforced slab-column connections with shear reinforcement.

3. While FRP bars exhibit favorable properties under normal conditions, their behavior under extreme conditions such as high temperatures, fire, or severe seismic events is not as well-documented as that of steel reinforcement.

4. Most existing studies are based on laboratory-scale tests, which may not fully capture the complexities and constraints of actual construction environments. Scaling up these findings to real-world applications involves uncertainties that need to be addressed.

5. Although the use of FRP can reduce the environmental footprint of reinforced concrete structures, the environmental impact of producing FRP materials themselves, including the energy consumption and emissions associated with their manufacture, needs more comprehensive evaluation.

7. FUTURE RESEARCH DIRECTIONS

Based on the evaluation, the following areas are suggested for further research:

1. The bond between FRP bars and concrete differs from that of steel bars, potentially affecting the overall performance of slab-column connections. Further research is needed to understand and improve this interfacial bond behavior to ensure structural integrity.

2. Conducting tests on FRP-reinforced slab-column connections in flat plates with drop panels or column capitals will provide insights into their structural behavior and potential improvements in punching shear strength.

3. Examining the punching shear strength of FRP pre-stressed slab-column connections will help determine the benefits and limitations of pre-stressing techniques in enhancing structural performance.

4. Studying the behavior and strength of FRP-reinforced slab-column connections under quasi-static dynamic loads is essential to evaluate their seismic response and ensure their reliability in earthquake-prone areas.

5. Conduct experimental and field studies to assess the long-term performance of FRP-RC slab-column connections under various environmental conditions, including exposure to freeze-thaw cycles, chlorides, and UV radiation.

6. Explore the punching shear performance of FRP-RC connections under dynamic and cyclic loading, such as seismic or wind-induced forces, to understand their behavior in regions prone to such events.

7. Study the effect of various FRP stirrup configurations and spacing on punching shear resistance to develop optimized design guidelines for shear reinforcement.

References

[1] N. Özyurt, T. A. Söylev, T. Özturan, A. O. Pehlivan, and A. Niş, "Corrosion and Chloride Diffusivity of Reinforced Concrete Cracked under Sustained Flexure", Teknik Dergi, vol. 31, no. 6, pp. 10315–10337, 2020, doi: 10.18400/tekderg.430536.

[2] M. Benredouane, N. Bourahla, A. Ghodbane, and H. Khalfaoui, "Corrosion Rate-Based Adjustment of Plastic Hinge Parameters of Corroded RC Elements", TJCE, vol. 35, no. 2, pp. 103–123, 2024, doi: 10.18400/tjce.1214088.

[3] A.A. Almusallam, "Effect of degree of corrosion on the properties of reinforcing steel bars," Construct. Build. Mater., vol. 15, pp. 361–368, 2001.

[4] H. Yiğiter, A. Beglarıgale, S. Aydın, and B. Baradan, "Corrosion Behavior of Rebars Embedded in Alkali-Activated and Conventional Reactive Powder Concretes", Teknik Dergi, vol. 31, no. 6, pp. 10359–10378, 2020, doi: 10.18400/tekderg.478154.

[5] Goksu, C., Inci, P., & Ilki, A., "Effect of corrosion on bond mechanism between extremely low-strength concrete and plain reinforcing bars," *J. Perform. Constr. Facil.*, vol. 30, no. 3, 04015055, 2016.

[6] R. Patel, "Prevention of corrosion of steel reinforcement in concrete," in: AIP Conference Proceedings, vol. 2158, 2019, pp. 020035-1~7, https://doi.org/10.1063/1.5127159.

[7] A. Zaki, M.A.M. Johari, W.M.A.W. Hussin, Y. Jusman, "Experimental assessment of rebar corrosion in concrete slab using ground penetrating radar (GPR)," Intern.J. Corrosion, vol. 2018, 5389829, 10 pages, https://doi.org/10.1155/2018/5389829.

[8] M. Zaki, A. Tobaa, A. Shehata, F. Mohamed, R. Khalef, Y. Hagras, R. Abou-Ali, M. Farag, A. Ghaly, M. Madi, E.S. Ahmed, Y. El-Maghraby, M. Abou-Zeid, "Potential advantages of basalt FRP bars compared to carbon FRP bars & conventional steel," Aust. J. Civ. Eng., vol. 19, no. 1, pp. 107–122, 2021.

[9] Seyhan, E. C., Goksu, C., Saribas, I., & Ilki, A., "Hybrid use of externally embedded FRP reinforcement for seismic retrofitting of substandard RC columns," *J. Compos. Constr.*, vol. 27, no. 3, 04023022, 2023.

[10] M. A. Çankaya and Ç. Akan, "An Experimental and Numerical Investigation on the Bending Behavior of Fiber Reinforced Concrete Beams", TJCE, vol. 34, no. 1, pp. 59–78, 2023, doi: 10.18400/tjce.1209152.

[11] M. Hassan, E.A. Ahmed, B. Benmokrane, "Punching shear strength of glass fiber-reinforced polymer reinforced concrete flat slabs," Can. J. Civ. Eng., vol. 40, pp. 951–960, 2013.

[12] T.H.-K. Kang, J.W. Wallace, "Punching of reinforced and post-tensioned concrete slab-column connections," ACI Struct. J., vol. 103, no. 4, pp. 531–540, 2006.

[13] J.-W. Kim, C.-H. Lee, T.H.-K. Kang, "Shearhead reinforcement for concrete slab to concrete-filled tube column connections," ACI Struct. J., vol. 111, no. 3, pp. 629–638, 2014.

[14] S. Matthys, L. Taerwe, "Concrete slabs reinforced with FRP grids. II. Punching resistance," J. Compos. Construct., vol. 4, no. 3, pp. 154–161, 2000.

[15] C.E. Ospina, S.D.B. Alexander, J.J. Roger Cheng, "Punching of two-way concrete slabs with fiber-reinforced polymer reinforcing bars or grids," ACI Struct. J., vol. 100, no. 5, pp. 589–598, 2003.

[16] J.H. Lee, Y.S. Yoon, W.D. Cook, D. Mitchell, "Improving punching shear behavior of glass fiber-reinforced polymer reinforced slabs," ACI Struct. J., vol. 106, no. 4, pp. 427–434, 2009.

[17] J.H. Lee, J.M. Yang, Y.S. Yoon, "Rational prediction of punching shear strength of slabs reinforced with steel or FRP bars," Mag. Concr. Res., vol. 62, no. 11, pp. 821–830, 2010.

[18] C. Dulude, M. Hassan, E.A. Ahmed, B. Benmokrane, "Punching shear behavior of flat slabs reinforced with glass fiber reinforced polymer bars," ACI Struct. J., vol. 110, no. 5, pp. 723–734, 2013.

[19] M. Hassan, E.A. Ahmed, B. Benmokrane, "Punching-shear strength of normal and high-strength two-way concrete slabs reinforced with GFRP bars," J. Compos. Construct., vol. 17, pp. 04013003-1~12, 2013.

[20] T.H.-K. Kang, J.W. Wallace, "Seismic performance of reinforced concrete slab-column connections with this plate stirrups," ACI Struct. J., vol. 105, no. 5, pp. 617–625, 2008.

[21] T.H.-K. Kang, J.D. Lee, B.-S. Lee, M.-J. Kim, K.-H. Kim, "Punching and lateral cyclic behavior of slab-column connections with shearbands," ACI Struct. J., vol. 114, no. 5, pp. 1075–1087, 2017.

[22] A.W. El-Ghandour, K. Pilakoutas, P. Waldron, "Punching shear behavior of fiber reinforced polymers reinforced concrete flat slabs: experimental study," J. Compos. Construct., vol. 7, no. 3, pp. 258–265, 2003.

[23] R. Li, Y.S. Cho, S. Zhang, "Punching shear behavior of concrete flat plate slab reinforced with carbon fiber reinforced polymer rods," Composites Part B, vol. 38, no. 5–6, pp. 712–719, 2007.

[24] A. Zaghloul, "Behaviour and Strength of CFRP Reinforced Flat Plate Interior Column Connections Subjected to Shear and Unbalanced Moments," Master Thesis, Department of Civil and Environmental Engineering, Carleton Univ., Ottawa, Canada, 2002.

[25] M. Hassan, E.A. Ahmed, B. Benmokrane, "Punching shear behavior of two-way concrete slabs reinforced with FRP shear reinforcement," J. Compos. Construct., vol. 19, no. 1, pp. 04014030-1~13, 2015.

[26]   A. Gouda, E. El-Salakawy, "Behavior of GFRP-RC interior slab-column connections with shear studs and high-moment transfer," J. Compos. Construct., vol. 20, no. 4, pp. 04016005-1~12, 2016.

[27]   D. Kueres, P. Schmidt, J. Hegger, "Two-parameter kinematic theory for punching shear in reinforced concrete slabs with shear reinforcement," Eng. Struct., vol. 181, pp. 216–232, 2019.

[28]   J.-M. Yang, K.H. Min, Y.-S. Yoon, "Effect of anchorage and strength of stirrups on shear behavior of high-strength concrete beams," Struct. Eng. Mech., vol. 41, no. 3, pp. 407–420, 2012.

[29]   S. El-Gamal, E. El-Salakawy, B. Benmokrane, "Behavior of concrete bridge deck slabs reinforced with fiber-reinforced polymer bars under concentrated loads," ACI Struct. J., vol. 102, no. 5, pp. 727–735, 2005.

[30]   M. El-Gendy, E. El-Salakawy, "Effect of shear studs and high moments on punching behavior of GFRP-RC slab–column edge connections," J. Compos. Construct., vol. 20, no. 4, pp. 04016007, 2016.

[31]   A. Salama, M. Hassan, B. Benmokrane, "Effectiveness of glass fiber-reinforced polymer stirrups as shear reinforcement in glass fiber-reinforced polymer reinforced concrete edge slab–column connections," ACI Struct. J., vol. 116, no. 5, pp. 97–112, 2019.

[32]   D.D. Theodorakopoulos, R.N. Swamy, "Analytical model to predict punching shear strength of FRP-reinforced concrete flat slabs," ACI Struct. J., vol. 104, no. 3, pp. 257–266, 2007.

[33]   L. Nguyen-Minh, M. Rovnak, "Punching shear resistance of interior GFRP reinforced slab-column connections," J. Compos. Construct., vol. 17, no. 1, pp. 2–13, 2013.

[34]   Canadian Standard Association (CSA), "Design and Construction of Building Structures with Fibre-Reinforced Polymer, CSA/S806-12), Canada, Toronto, 2017.

[35]   M. Hassan, E.A. Ahmed, B. Benmokrane, "Punching-shear design equation for two-way concrete slabs reinforced with FRP bars and stirrups," Construct. Build.Mater., vol. 66, pp. 522–532, 2014.

[36]   Garden HN, Hollaway LC. "An experimental study of the influence of plate end anchorage of carbon fibre composite plates used to strengthen reinforced concrete beams," Compos Struct, vol. 42, no. 2, pp. 175–188, 1998.

[37]   Hollaway LC. "A review of the present and future utilisation of FRP composites in the civil infrastructure with reference to their important in-service properties," Constr Build Mater, vol. 24, no. 12, pp. 2419–245, 2010.

[38]   Gdoutos EE, Pilakoutas K, Rodopoulos CA. "Failure analysis of industrial composite materials." New York: McGraw-Hill Professional Engineering; 2000. p. 51–108.

[39]   Taerwe Luc. "Non-metallic (FRP) reinforcement for concrete structures." Proceedings of the Second International RILEM Symposium vol. 29. CRC Press; 1995.

[40] ACI 440 1R-15. "Guide for the design and construction of structural concrete reinforced with FRP bars." Farmington Hills, MI: American Concrete Institute (ACI); 2007.

[41] ACI 440 Part 6–8. Specification for carbon and glass fiber-reinforced polymer bar materials for concrete reinforcement. Farmington Hills, MI: American Concrete Institute (ACI); 2008.

[42] Al-Sunna Raed, Pilakoutas Kypros, Hajirasouliha Iman, Guadagnini Maurizio.Deflection behaviour of FRP reinforced concrete beams and slabs: an experimental investigation. Compos Part B Eng 2012;43(5):2125–34.

[43] Teng JG, Chen Jian-Fei, Smith Scott T, Lam L. FRP: strengthened RC structures.Front Phys 2002:266.

[44] Burgoyne C. FRP reinforcement in RC structures. Switzerland: International Federation for Structural Concrete (FIB); 2007.

[45] Canadian Standards Association. Specification for fibre-reinforced polymers, (CAN/CSA S807-10). Mississauga, Ont, Rexdale, ON, Canada: Canadian Standards Association; 2010. p. 27.

[46] Bakis CE, Bank LC, Brown V, Cosenza E, Davalos JF, Lesko JJ, et al. Fiber-reinforced polymer composites for construction—state-of-the-art review. J Compos Constr 2002;6(2):73–87.

[47] Aashto L. Bridge design guide specifications for GFRP—reinforced concrete bridge decks and traffic railings. Washington (DC): American Association of State Highway and Transportation Officials; 2009.

[48] Calvi GM, Pavese A, Rasulo A, Bolognini D. Experimental and numerical studies on the seismic response of RC hollow bridge piers. Bull Earthq Eng 2005;3(3):267–97.

[49] Cheng C-T, Mo Y, Yeh Y-K. Evaluation of as-built, retrofitted, and repaired shearcritical hollow bridge columns under earthquake-type loading. J Bridg Eng 2005;10(5):520–9.

[50] Dawood M. Bond characteristic sand environmental durability of CFRP materials for strengthening steel bridges and structures Ph.D thesis Raleigh, NC: North Carolina State Univ.; 2008.

[51] Delgado Pedro, Rocha Patrício, Pedrosa João, Arêde António, Pouca Nelson Vila,Santos Miguel, et al. Retrofitting of bridge hollow piers with CFRP. Proceedings of ECCOMAS Thematic Conference Quot; Computational Methods in StructuralDynamics and Earthquake Engineering 2007.

[52] Dong ZH, Han Q, Du XL, Zhang DJ. Experimental study on seismic performance of CFRP confined RC rectangular hollow section bridge piers. International efforts in lifeline earthquake engineering. 2014. p. 457–64.

[53] Han Qiang, Wen Jianian, Du Xiuli, Jia Junfeng. Experimental and numerical studies on seismic behavior of hollow bridge columns retrofitted with carbon fiber reinforced polymer. J Reinf Plast Compos 2014;33(24):2214–27.

[54] Matta F. Bond between steel and CFRP laminates for rehabilitation of metallic bridges Master's thesis Padua, Italy: Faculty of Engineering, Univ. of Padua; 2003.

[55] Miller Trent C, Chajes Michael J, Mertz Dennis R, Hastings Jason N. Strengthening of a steel bridge girder using CFRP plates. J Bridg Eng 2001;6(6):514–22.

[56] Breña Sergio F, Bramblett Regan M, Benouaich Michaël A, Wood Sharon L, Kreger Michael E. Use of carbon fiber reinforced polymer composites to increase the flexural capacity of reinforced concrete beams. The University Of Texas at Austin; 2001. Research Report no. 1776-1.

[57] Ning Huiming, Li Yuan, Hu Ning, Arai Masahiro, Takizawa Naoya, Liu Yaolu, et al. Experimental and numerical study on the improvement of interlaminar mechanical properties of Al/CFRP laminates. J Mater Process Technol 2015;216:79–88.

[58] Ammar MA. Bond durability of basalt fibre-reinforced polymers (BFRP) bars under freeze-and-thaw conditions Ph.D thesis Dept. of Civil Engineering, Université Laval; 2014. p. 125.

[59] Banibayat P, Patnaik A. Creep rupture performance of basalt fiber-reinforced polymer bars. J Aerosp Eng 2013;28(3):04014074.

[60] Brothers H. Glass fiber reinforced polymer (GFRP) rebar Aslan 100. Seward, Neb. 2001.

[61] Davies Peter, Reaud Yvan, Dussud Loic, Woerther Patrice. Mechanical behavior of HMPE and aramid fibre ropes for deep sea handling operations. Ocean Eng 2011;38(17):2208–14.

[62] Sahu NP, et al. Study on aramid fibre and comparison with other composite materials. Int J 2014;1:303–6.

[63] Palmieri A, Matthys S, Taerwe L. Experimental investigation on fire endurance of insulated concrete beams strengthened with near surface mounted FRP bar reinforcement. Compos Part B Eng 2012;43(3):885–95.

[64] Zhou Jikai, Bi Fengtong, Wang Zhiqiang, Zhang Jian. Experimental investigation of size effect on mechanical properties of carbon fiber reinforced polymer (CFRP) confined concrete circular specimens. Constr Build Mater 2016;127:643–52.

[65] Liu H, Zhao X, Al-Mahaidi R. Effect of fatigue loading on bond strength between CFRP sheets and steel plates. Int J Struct Stab Dyn 2010;10(01):1–20.

[66] Abdelrahman K, El-Hacha R. Cost and ductility effectiveness of concrete columns strengthened with CFRP and SFRP sheets. Polymer 2014;6(5):1381–402.

[67] Das S. The cost of automotive polymer composites: a review and assessment of DOE's lightweight materials composites research. Springfield, VA: American Department of Energy; 2001. p. 1–47.

[68] Delgado Pedro, Arêde António, Vila Pouca Nelson, Rocha Patrício, Costa Aníbal, Delgado Raimundo. R

[69] J. Custo´dio, J. Broughton, H. Cruz, A review of factors influencing the durability of structural bonded timber joints, Int. J. Adhes. Adhes. 29 (2009) 173–185.

[70] R.M. Guedes, J.L. Morais, A.T. Marques, A.H. Cardon, Prediction of long-term behavior of composite materials, Comput. Struct. 76 (2000) 183–194.

[71] R.M. Guedes, Lifetime prediction of polymers and polymer matrix composite structures: failure criteria and accelerated characterization, in: Creep and Fatigue in Polymer Matrix Composites, Elsevier, 2019.

[72] A. Movaghghar, G.I. Lvov, An energy model for fatigue life prediction of composite materials using continuum damage mechanics, Appl. Mech. Mater. 110–116 (2011) 1353–1360

[73] A. Al-Saoudi, R. Kalfat, R. Al-Mahaidi, Investigation into the fatigue life of FRP strengthened concrete structures, Mater. Struct. 55 (6) (2022), https://doi.org/10.1617/s11527-021-01839-y.

[74] Shaaban, A.M., and Gesund, H., "Punching Shear Strength of Steel Fiber Reinforced Concrete Flat Plates," Structural Journal, vol. 91, no. 4, pp. 406-414, Jul. 1994.

[75] E. H. Rochdi, D. Bigaud, E. Ferrier, and P. Hamelin, "Ultimate behavior of CFRP strengthened RC flat slabs under a centrally applied load," Composite Structures, vol. 72, no. 1, pp. 69-78, 2006.

[76] A. Torabian, B. Isufi, D. Mostofinejad, and A. P. Ramos, "Behavior of thin lightly reinforced flat slabs under concentric loading," Engineering Structures, vol. 196, p. 109327, 2019.

[77] ASCE-ACI Committee 426, "The shear strength of reinforced concrete members - slabs," *J. Struct. Div.,* vol. 100, no. 8, pp. 1543–1590, 1974.

[78] American Concrete Institute, "Guide to seismic design of punching shear reinforcement in flat plates," ACI 421.2R, Farmington Hills, MI, ACI, 2010.

[79] R. Lenschow and M. Sozen, "A yield criterion for reinforced concrete slabs," ACI J. Proc., vol. 64, no. 5, pp. 266–273, 1967.

[80] M.D. Kotsovos and M.N. Pavlovic, "Ultimate Limit-State Design of Concrete Structures: A New Approach," Thomas Telford, London, 1998, p. 208.

[81] H.-G. Park, K.-K. Choi, and L. Chung, "Strain-based strength model for direct punching shear of interior slab-column connections," Eng. Struct., vol. 33, pp. 1062–1073, 2011.

[82] P.D. Zararis and G.C. Papadakis, "Diagonal shear failure and size effect in RC beams without web reinforcement," J. Struct. Eng., vol. 127, no. 7, pp. 733–742, 2001.

[83] Banthia, N., Al-Asaly, M., & Ma, S. "Behavior of concrete slabs reinforced with fiber-reinforced plastic grid." Journal of Materials in Civil Engineering, vol. 7, no. 4, pp. 252-257, 1995.

[84] Li, R., Cho, Y. S., & Zhang, S. "Punching shear behavior of concrete flat plate slab reinforced with carbon fiber reinforced polymer rods." Composites Part B: Engineering, vol. 38, no. 5-6, pp. 712-719, 2007.

[85] Hassan, M., Ahmed, E., & Benmokrane, B. "Punching-shear strength of normal and high-strength two-way concrete slabs reinforced with GFRP bars." Journal of Composites for Construction, vol. 17, no. 6, p. 04013003, 2013.

[86] S. K. Shill, E. O. Garcez, R. Al-Ameri, and M. Subhani, "Performance of two-way concrete slabs reinforced with basalt and carbon FRP rebars," Journal of Composites Science, vol. 6, no. 3, p. 74, 2022.

[87] ACI Committee 318-19. Building Code Requirements for Structural Concrete andCommentary. American Concrete Institute; 2019.

[88] CSA-A23.3- 04. Design of concrete structures for buildings. Canadian Standards Association 2004.

[89] British Standards Institution. Structural use of concrete, part 1: code of practice for design and construction. BS 8110-1; 1997.

[90] CEB–FIP. 1990. Model Code: Bulletin D'Information No. 203– 305. Comit´e Euro– International Du B´ eton – F´ed´ eration de la Pr´econtrainte; 1990.

[91] FIB 2001. Punching of structural concrete slabs. Lausanne: InternationalFederation for Structural Concrete; 2001.

[92] Lantsoght E. Literature Review of Punching Shear in Reinforced Concrete Slabs. Research Report No. 09-10; 2009, Georgia Institute of Technology.

[93] Muttoni A, Schwartz, J. Behaviour of Beams and Punching in Slabs without Shear Reinforcement. IABSE Colloquium 1991; 62: 703-08, Zurich, Switzerland.

[94] Japan Society of Civil Engineers (JSCE). Recommendation for design and construction of concrete structures using continuous fibre reinforcing materials. Concrete Engineering, Series 23, A. Machida, ed., 1997.

[95] ACI Committee 440. Guide for the design and construction of concrete reinforced with FRP bars (ACI 440.1R-15). American Concrete Institute; 2015.

[96] CAN/CSA S806-12. Design and construction of building structures with fibre reinforced polymers. Canadian Standards Association; 2012.

[97] Rizk E, Marzouk H, Hussein A. Punching shear of thick plates with and without shear reinforcement. ACI Struct J 2011;108(5):581–91.

[98] Zhou P, Barr B, Lydon F. Fracture properties of high strength concrete with varying silica fume content and aggregates. Cem Conc Res 1995;25(3):543– 52. https://doi.org/10.1016/0008-8846(95)00043-C.

[99] Rizk E, Marzouk H, Hussein A, Hossin M. Effect of reinforcement ratio on punching capacity of RC plates. Can J Civ Eng 2011;38:729–40. https://doi.org/10.1139/L11-053.

[100] Elsanadedy HM, Al-Salloum YA, Alsayed SH. Prediction of punching shear strength of HSC interior slab-column connections. KSCE J Civil Eng 2013;17(2):473–85. https://doi.org/10.1007/s12205-013-1971-8.

[101] Bompa DV, Oneț T. Punching shear strength of RC flat slabs at interior connections to columns. Mag Concr Res 2016;68(1):24–42. https://doi.org/10.1680/macr.14.00402

[102] Broms CE. Tangential strain theory for punching failure of flat slabs. ACI Struct J2016;113(1):95–104. https://doi.org/10.14359/51687942.

[103] Zhang Q, Marzouk H, Hussein A. A Preliminary Study of High-Sstrength concrete two-way slabs reinforced with GFRP bars. Proc., 33rd CSCE Annual Conf.: General Conference and International History Symposium, Canadian Society of Civil Engineers; Toronto, ON, Canada; 2005.

[104] Zaghloul A, Razaqpur A. Punching Shear Strength of Concrete Flat Plates Reinforced with CFRP Grids. Proc., 4th Int. Conf. on Advanced Composite Materials in Bridges and Structures, CSCE, Calgary, AB, Canada; 2004

[105] Hussein A, Rashid I, Benmokrane B. Two-Way Concrete Slabs Reinforced with GFRP Bars. Proc., 4th Int. Conf. on Advanced Composite Materials in Bridges and Structures, Canadian Society of Civil Engineers; Calgary, AB, Canada; 2004.

[106] Ahmad SH, Zia P, Yu TJ, Xie Y. Punching shear tests of slabs reinforced with 3-D carbon fiber fabric. Conc Int 1993;16(6):36–41.

[107] Gouda A, El-Salakawy E. Behaviour of GFRP-RC interior slab-column connections with shear studs and high-moment transfer. J Comp Constr (ASCE) 2016;20(4). https://doi.org/10.1061/(ASCE)CC.1943-5614.0000663.10.1061/(ASCE) CC.1943-5614.0000663.

[108] Ajami AL. Punching shear of concrete flat slabs reinforced with fiber reinforced polymer bars. University of Bradford; 2018. PhD thesis

[109] Ramzy ZZ, Salma MT. Punching behavior and strength of two-way concrete slab reinforced with glass-fiber reinforced polymer (GFRP) rebars. Structural Composites for Infrastructures Applications Conference. 2007

[110] Y. Yu, G.H. Fang, R. Kurda, et al., An agile, intelligent and scalable framework for mix design optimization of green concrete incorporating recycled aggregates from precast rejects, Case Stud. Constr. Mat. (2024) e03156.

[111] V. Shobeiri, B. Bennett, T.Y. Xie, et al., Mix design optimization of waste-based aggregate concrete for natural resource utilization and global warming potential, J. Clean. Prod. (2024) 141756.

[112] H. Xue, H. Guan, B.P. Gilbert, X. Lu, Y. Li, Simulation of punching and post-punching shear behaviours of RC slab–column connections, Mag. Concr. Res. 73 (22) (2021) 1135–1150.

[113] Y. Yu, T.Y. Hu, Machine learning based compressive strength prediction model for CFRP-confined columns, KSCE J. Civ. Eng. 28 (1) (2024) 315–327.

[114] T. Liu, Z. Wang, Z. Long, J. Zeng, J. Wang, J. Zhang, Direct shear strength prediction for precast concrete joints using the machine learning method, J. Bdg Eng.27 (5) (2022) 04022026.

[115] Y.X. Shen, L.F. Wu, S.X. Liang, Explainable machine learning-based model for failure mode identification of RC flat slabs without transverse reinforcement, Eng.Fail Anal. 141 (2022) 106647.

[116] L. Lin, J.J. Xu, J.C. Yuan, et al., Compressive strength and elastic modulus of RBAC: an analysis of existing data and an artificial intelligence based prediction, Case Stud. Constr. Mat. 18 (2023) e02184.

[117] S.X. Liang, Y.X. Shen, X.D. Ren, Comparative study of influential factors for punching shear resistance/failure of RC slab-column joints using machine-learning models, Struct 45 (2022) 1333–1349.

[118] D.C. Feng, W.J. Wang, S. Mangalathu, E. Taciroglu, Interpretable XGBoost-SHAP machine-learning model for shear strength prediction of squat RC walls, J. Struct. Eng. 147 (11) (2021) 04021173.

[119] S.X. Liang, Y.Q. Cai, Z.Y. Fei, et al., Multi-objective optimization design of FRP reinforced flat slabs under punching shear by using NGBoost-based surrogate model, Buildings 13 (11) (2023) 2727.

[120] Y. Yu, X.Y. Zhao, J.J. Xu, S.C. Wang, T.Y. Xie, Evaluation of shear capacity of steel fiber reinforced concrete beams without stirrups using artificial intelligence models, Mater 15 (7) (2022) 2407.

[121] I.M. Metwally, Prediction of punching shear capacities of two-way concrete slabs reinforced with FRP bars, HBRC J. 9 (2013) 125–133

[122] D.T. Vu, N.D. Hoang, Punching shear capacity estimation of FRP-reinforced concrete slabs using a hybrid machine learning approach, Struct. Infrastruct. Eng. 12 (9) (2016) 1153–1161.

[123] S.X. Liang, Y.X. Shen, X.L. Gao, et al., Symbolic machine learning improved MCFT model for punching shear resistance of FRP-reinforced concrete slabs, J. Build. Eng. 69 (2023) 106257.

[124] Y.X. Shen, J.H. Sun, S.X. Liang, Interpretable machine learning models for punching shear strength estimation of FRP reinforced concrete slabs, Crystals 12 (2022) 259.

[125] J. Yan, J. Su, J. Xu, K. Hua, L. Lin, and Y. Yu, "Explainable Machine Learning Models for Punching Shear Capacity of FRP Bar Reinforced Concrete Flat Slab without Shear Reinforcement," *Case Studies in Construction Materials*, vol. e03162, 2024.

[126] G. Doğan and M. H. Arslan, "Determination of punching shear capacity of concrete slabs reinforced with FRP bars using machine learning," *Arabian Journal for Science and Engineering*, vol. 47, no. 10, pp. 13111-13137, 2022.

[127] N. Badra, S. A. Haggag, A. Deifalla, and N. M. Salem, "Development of machine learning models for reliable prediction of the punching shear strength of FRP-reinforced concrete slabs without shear reinforcements," *Measurement*, vol. 201, p. 111723, 2022.

[128] Truong, G. T., Hwang, H. J., & Kim, C. S. (2022). Assessment of punching shear strength of FRP-RC slab-column connections using machine learning algorithms. Engineering Structures, 255, 113898.

[129] S. Lips, M. Fernandez ´ Ruiz, A. Muttoni, Experimental investigation on punching strength and deformation capacity of shear-reinforced slabs, ACI Struct. J. 109 (2012) 889–900

[130] A.M.H. Hussein, Punching Shear Behaviour of GFRP-RC Slab-Column Interior Connections with High Strength Concrete and Shear Reinforcement, Master Thesis, University of Manitoba, Canada, 2017.

[131] G. T. Truong, K. K. Choi, and C. S. Kim, "Punching shear strength of interior concrete slab-column connections reinforced with FRP flexural and shear reinforcement," *Journal of Building* Engineering, vol. 46, p. 103692, 2022.

Impact Angle-Based Section Design and Optimization of the C Post in Order to Improve the Safety and Structural Performance of Guardrails

Sedat ÖZCANAN[1*]
Özgür ÖZCAN[2]

ABSTRACT

This study focuses on enhancing the performance of the C post in H1 containment-level guardrail systems by optimizing its design to better withstand angular impacts, common in roadside safety applications. Since the post plays a crucial role in transferring impact loads to the ground, modifications were made by adjusting the angle of the post edge that aligns with the impact direction, while keeping the perpendicular side constant. Two key test angles from EN1317 standards were used: a 20-degree angle (TB11) to assess safety metrics like the Acceleration Severity Index (ASI) and theoretical Head Impact Velocity (THIV), and a 15-degree angle (TB42) to evaluate structural performance, including working width and exit angle. Finite element modelling in LS-DYNA, followed by model validation and calibration, showed that aligning the C post angle more closely with crash angles improved both safety and structural integrity, resulting in a transition of the C post design toward a Z post shape with enhanced rigidity and performance.

Keywords: Guardrail systems, post performance, EN1317, finite element analysis, LS-DYNA.

1. INTRODUCTION

Steel guardrail systems are the most preferred barrier type on highways due to their high energy absorption capability and low impact severity during collisions. The safe end of the collision event in steel guardrails depends on the proper functioning of the guardrail system elements. In a simple steel guardrail system composed of rails and posts, it is first requested that the rails meet the load and energy resulting from the collision with flexural resistance

and transfer them to the posts in order to minimize the sudden impact effects. Afterwards, for the guardrail system to remain stable and prevent the vehicle from leaving the road, the posts must meet this load and energy with bending resistance and transfer it to the ground [1]. Posts are the elements of the guardrail system that directly affect the factors such as the guardrail providing a reasonable working width and its integrated behavior with the ground. The fact that the crash tests are carried out by considering a certain angle makes the choice of post type important in guardrails. There are many types of posts used in steel guardrails such as C, H, I, T, U, S, Z, box and circular profile. While C-shape post is the most preferred post type in steel guardrails; since Z-shape post gives an angular dimension to the use of posts, its use in steel guardrails is increasing day by day.

Guardrail systems are subjected to crash tests based on certain parameters (speed, angle of impact, vehicle mass) within the framework of standards such as EN 1317 and MASH in order to determine their safety levels and structural performances [2], [3]. As a result of full-scale crash tests, within the scope of EN 1317, safety criteria such as ASI and THIV and structural performance criteria such as working width (W) and exit angle (α) can be determined. Dynamic collision effects can also be observed with the help of programs that can perform finite element (FE) analysis, if verified by full-scale crash tests. There are many studies aiming to improve the crash severity level and structural performance criteria of guardrails.

In guardrail systems, posts are the most important element that affects guardrail performance. In this sense, the post-soil interaction of sigma (S) post was investigated [4]. In another study, the performances of S and T posts were compared [5]. Post height and its embedment depth are important parameters that affect post behaviour. How post height and its embedment depth affect post performance and their interaction with the soil have been revealed by [6], [7]. In addition, the geometric cross-sections of the posts affect their mechanical performance. In this sense, the performances of C, H and S posts in dense, medium and loose soils were investigated and the best performing posts and their optimum depths were determined [7-9]. In addition, a study investigating the performance of posts with different geometric cross-sections in case of head-on and angular impact was determined the best performing post for the mentioned cases [10].

Another important element in the guardrail system is the rail. Marzougui et al. [11] investigated the effect of different heights of the W-rail on the barrier performance, and the optimum rail height was determined. Also, the effect of different rail geometries on barrier performance was investigated and superior rail types were given [12-14]. Moreover, there are studies about guardrail part such as blockout which placed between the rail and the post. In studies on how the blockout placed between the rail and the post affect the barrier performance, the performances of different blockout types are given [15, 16]. It is known that the material used in the barrier affects the guardrail performance as well as the rail and post affect the barrier performance. In studies related to this, Klasztorny et al. [17] investigated the barrier performance of the coating by placing a foam composite coating (rubber/foam/composite overlay) on a steel guardrail system formed from Sigma-100 post and type B rail, and shared the details in the study. Ozcanan and Atahan [18] performed RBF-based metamodel optimization over the parameters of post width and rail thickness with the combination of different steel materials (S235JR, S275JR and S355JR) for H1W4 and H2W4 types of guardrails with C post.

In addition to the issues mentioned above, ASI-THIV-based optimization of barriers [19], improving of continuous motorcyclists' protection barrier system [20], standards-based performance analysis of different safety systems [21], hybrid barriers developed with wooden materials [22, 23] and, of course, there are studies [24] investigating the deficiencies in the EN1317 standard. Moreover, in addition to the above-mentioned cross-sectional performances and geometric structures of steel guardrail elements, it was shown in the given study [25] that the impact point is important in terms of guardrail performance.

As mentioned above, the post behaviour significantly affects the barrier performance. In many studies, the performance of posts with different geometries has been investigated and compared. Angular collisions are often the case in systems that provide roadside safety. In this study, it is aimed to improve the performance of the C post, which is the most used in guardrail systems, in H1 containment-level guardrail by reshaping the edge in the impact direction according to the impact angle. Therefore, the perpendicular side of the C post to the impact direction was kept constant and only the angular variations of the side parallel to the impact direction were tried, and the optimum angle was investigated.

The impact angles specified for H1-level tests in the EN1317 standard are chosen to simulate the real-world impact conditions that roadside safety barriers may encounter. In the TB11 and TB42 tests, the angles of 20 degrees for TB11 and 15 degrees for TB42 are designed to analyse the effects of different vehicle types and collision scenarios on the barrier. The TB11 test represents situations where smaller vehicles collide with barriers at lower speeds, and a 20-degree angle is considered suitable for examining vehicle dynamics and the barrier's ability to safely redirect the vehicle without altering its direction significantly. The TB42 test, on the other hand, simulates impacts with larger, heavier vehicles, which tend to strike barriers at narrower angles. The 15-degree impact angle in this case accounts for the tendency of large vehicles to slide along the barrier, thus evaluating the barrier's capacity to safely absorb the vehicle's energy. These angles play a critical role in determining the safety performance and structural resilience of the barrier, ensuring it can provide effective protection under various impact conditions.

For this purpose, firstly, the guardrail system was constructed in the LS-DYNA finite element environment, and then validation and calibration of models were done. Finally, on the model, which was calibrated and validated, analyses were made for different body angles of the C post, and the results were presented in the study.

2. MATERIALS AND METHODS

2.1. EN1317 Safety and Performance Criteria

The EN1317 standard uses two factors, also referred to as safety criteria, to represent the seriousness of an injury. These are the theoretical head impact velocity and the acceleration (injury) severity index (ASI) (THIV). The impact of occupant restraint systems, such as seat belts, is taken into consideration by the injury parameter ASI. It is calculated using the ASI Equation (1),

$$ASI(t) = \sqrt{\left(\frac{a_x}{\hat{a}_x}\right)^2 + \left(\frac{a_y}{\hat{a}_y}\right)^2 + \left(\frac{a_z}{\hat{a}_z}\right)^2} \tag{1}$$

The components in the denominator indicate the threshold values applied in accordance with the standard, which are, respectively, $\hat{a}_x = 12g$, $\hat{a}_y = 9g$, and $\hat{a}_z = 10g$. The components a_x, a_y, and a_z include the vehicle acceleration values in the $Ox, Oy,$ and Oz axes, respectively. The gravitational acceleration is denoted by g. The scalar value indicated by Equation (2) represents the estimated value of ASI.

$$ASI = \max[ASI(t)] \tag{2}$$

The theoretical head impact velocity is the second element that the EN1317 standard specifies (THIV). This parameter assumes that any injuries to the occupant of the car are directly attributable to the occupant's contact with the car's interior. Equation (3) can be used to determine the THIV value under the assumption that the head speed of the driver or passenger inside the car is equal to the car's speed in the horizontal plane.

$$THIV = \left[V_{head\,x}{}^2(T) + V_{head\,y}{}^2(T)\right]^{0.5} \tag{3}$$

Here, the head velocities in the longitudinal and lateral directions relative to the vehicle axis passing through its center are denoted as $V_{head\,x}$ and $V_{head\,y}$, respectively. T is the point at which the fictitious passenger head moves 300 mm in the O y axis or 600 mm in the O x axis. Table 1 lists the maximum values for the ASI and THIV safety parameters.

Table 1 - Impact severity levels in EN1317 [2].

Impact severity level	Index values		
A	ASI ≤ 1.0		
B	ASI ≤ 1.4	and	THIV ≤ 33 km/h
C	ASI ≤ 1.9		

The locations of the accelerometer and test subject utilized to measure ASI and THIV during the TB11 crash test are shown in Figure 1.

The performance evaluation standards for the H1W4-A barrier system are listed in Table 2. The test scenario in accordance with EN1317 requirements is shown in Figure 2. The working width (W), which is seen in the picture, is where the guardrail is most likely to move/displaced during an impact. A vehicle leaves the guardrail from an exit point after colliding with it. The vehicle exit point, the width (A), and the length (B) of the impacting vehicle can be used to compute the dimensions of the exit box, which can be constructed as a rectangular box. When leaving the barrier, a vehicle must stay inside the short edge of the departure box, which is one of the EN1317 evaluation criteria for a crash test. To stop errant vehicles from joining the traffic after an accident is the goal here. As a result, determining a

vehicle's exit angle is crucial for test acceptability. The upper limit of W4 level, or the maximum allowable lateral displacement or working width (W), is 1.3 m. Additionally, the maximum exit angle (α) in relation to the guardrail is limited to 19 degrees for the test conditions of TB11 and TB42.
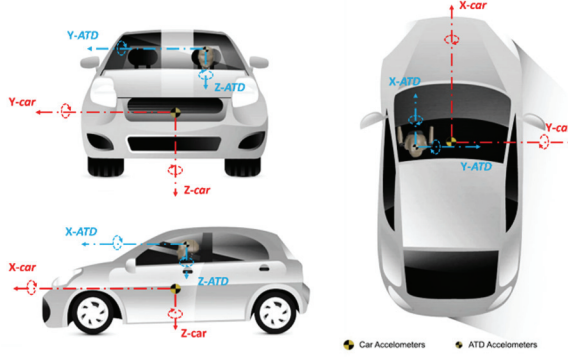

Figure 1 - Accelerometer and dummy positions for ASI and THIV calculation.

Table 2 - EN1317 test evaluation criteria for H1 and H2 guardrail systems.

System Type	Test	Working width (W) (m)	Exit box (width(A)x length(B)) (m)*	Exit angle (α) (°)**
H1W4A	TB11	≤1.3	4.4x10	≤19
	TB42	≤1.3	8.22x20	≤17

*Calculated based on EN1317/2
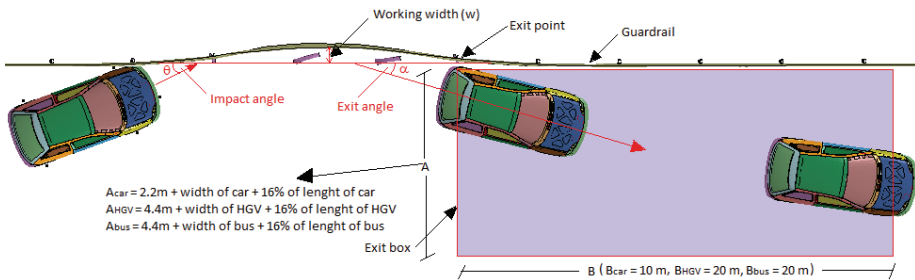**Calculated based on exit box length

Figure 2 - Illustration of crash test condition of EN1317 and exit box calculation [18].

In Turkey, road safety design evaluations are conducted in accordance with EN1317 standards. Table 3 lists the test acceptance criteria for the H1 containment level as described in EN1317. The FE models of the cars used in the TB11 and TB42 experiments are shown

in Figure 3. In EN1317 part 2 [2], specifics on vehicle crash test descriptions and containment levels are provided.

Table 3 - EN1317 test acceptance criteria for H1 and H2 guardrail systems [2].

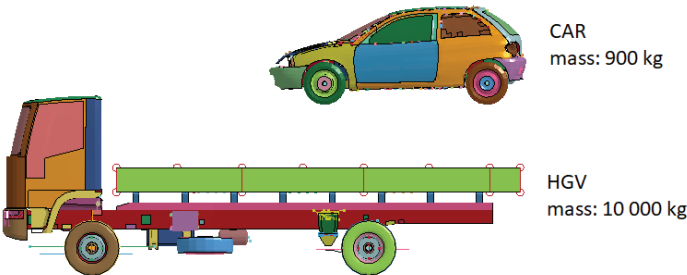| System type	Test	Impact speed (km/h)	Impact angle (Θ) (°)	Total mass (kg)	Type of vehicle
H1	TB11	100	20	900	Car
	TB42	70	15	10000	Rigid HGV*

*Heavy Goods Vehicle

Figure 3 - The FE models of vehicles used in TB11 and TB42 tests [26].

2.2. Virtual Testing Tolerance in European Norm (EN) 16303

Validation and calibration are required in order to be able to analyze with numerical models of crash tests conducted within the scope of EN1317. For this, there are acceptance criteria and error tolerances specified in EN16303 [27]. Allowable tolerances regarding safety and performance parameters are given in Table 4. In the quantitative comparison of the numerical models made with the real models, the allowed error tolerances must remain within the given deviation values.

Table 4 - EN16303 virtual test tolerance for validation process [27].

Parameter	Tolerance
ASI	±0.1
THIV (km/h)	±3
W (m)	±0.1
Exit angle (α)	*

* Calculation and acceptance criterion is given in EN1317. Limit values are given in Table 2.

2.3. The Details and FE Models of H1W4-A Guardrail System and Test Vehicles

Crash test results for the H1W4-A barrier system were used in this investigation. One of the most often used barrier systems overall is H1W4-A. The W-beam rail and C-type post are the guardrail's primary building components. Additionally, S235JR graded steel is used for the guardrail. The H1W4-A system's geometrical details and FE models are shown in Figure 4. The rail and post sections are "Shell" modeled in the LS-DYNA, with "MAT24" serving as the material for both. "Beam" is defined as bolt connections between rail and posts. In this study, materials and models that have been validated by other studies [7], [18], and [19] were employed.
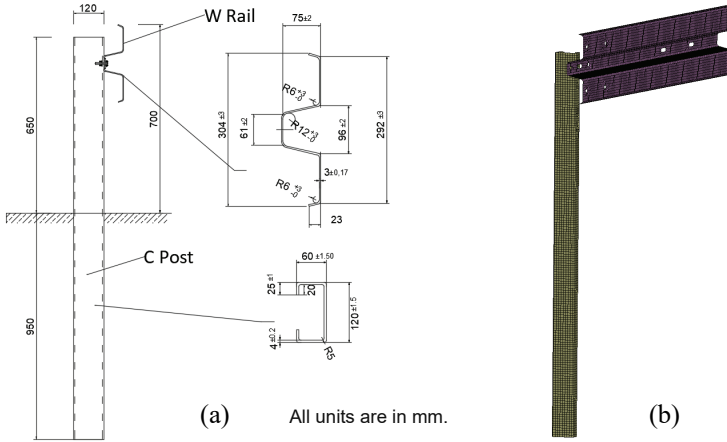
Figure 4 - (a) H1W4 guardrail system details and (b) FE model of the design [18].

The meanings of the symbols that make up the name of the guardrail system that is categorized in accordance with EN 1317 standards are shown in Figure 5.
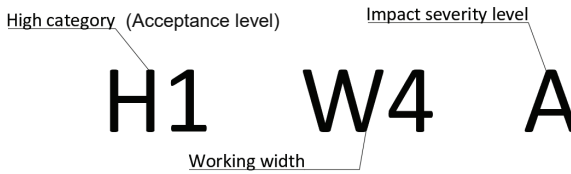
Figure 5 - Symbol meanings of H1W4-A system.

Commonly used materials and technical specifications of H1W4A system is given in Table 5. As can be seen from the technical drawings of the H1W4 system in Figure 4, the names rail and post come from their geometric structures resembling W and C, respectively. Additionally, as can be seen from the figure, the numerical values in the post are the measurements of the geometric structure of the C post.

Table 5 - Technical details of guardrail systems used in this study.

System	Rail	Post (mm)	Material	Rail thickness (mm)	Post thickness (mm)
H1W4A	W	C120X60X20	S235JR	3.0	4.0

2.4. Validation of the FE Models

In the above section, the tests to be performed for H1 system is given in Table 2. Previous studies have included actual test data [28] for TB11, and TB42 tests. Using LS-DYNA software, full-scale finite element models of the H1 system were produced based on these tests. When compared to actual crash test data, these models developed in the FE environment were found to be valid. The quantitative comparison of the FE model and the crash test is given in Table 6. The difference between the ASI, THIV, W and α values obtained for the FE model and the crash test as a result of the TB11 and TB42 tests remains within the limits specified in the EN16303 and EN1317 standards. In addition, the qualitative comparison of FE model and crash test is given in Figures 6 and 7. Figures 6 and 7 illustrate the good agreement between the FE model and actual crash test [28] results. As a result of the validation, it was understood that the FE model could be used in this study.

Table 6 - Quantitative comparison of data obtained from real tests [28] and FE models.

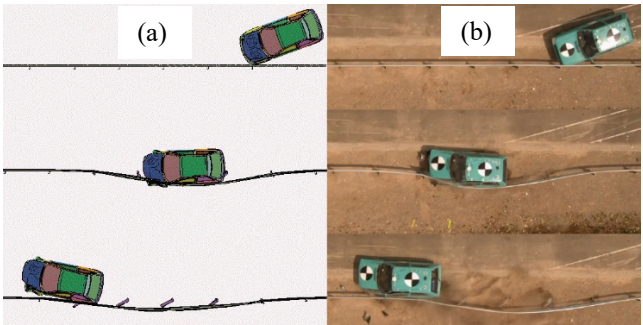| Tests	Parameters	Real crash tests	FE models	Tolerance	Inside limits?
TB11	ASI	0.86	0.79	±0.1	Yes
	THIV (km/h)	22	21	±3	Yes
TB42	W (m)	1.12	1.20	±0.1	Yes
	α (°)	8	10	≤19	Yes

Figure 6 - Visual comparison of (a) FE model of TB11 and (b) Real test of TB11 [18],[28].
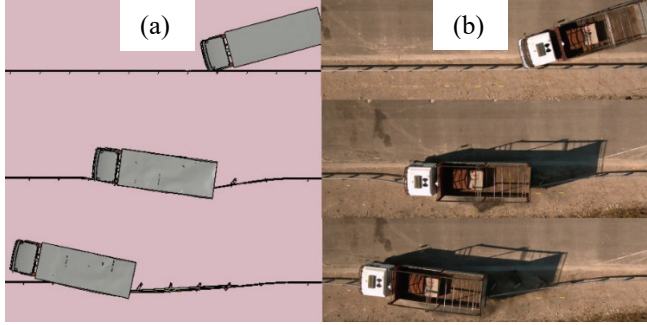
Figure 7 - Visual comparison of (a) FE model of TB42 and (b) Real test of TB42 [18],[28].

3. RESULTS AND DISCUSSION

3.1. FE Test Setup

It is known that the perpendicular edge of the C post, detailed in Figure 4, to the rail is the edge that meets the main load during impact. However, in guardrails built on the side of the road, the impact is usually angular during a traffic accident. For this reason, in the tests defined in EN1317, vehicles crashed the guardrail angularly as test detail given in Table 3. In this case, for the C post, angularly changing the perpendicular edge to the rail in the impact direction during impact will mean that the moment of inertia is increased in the impact
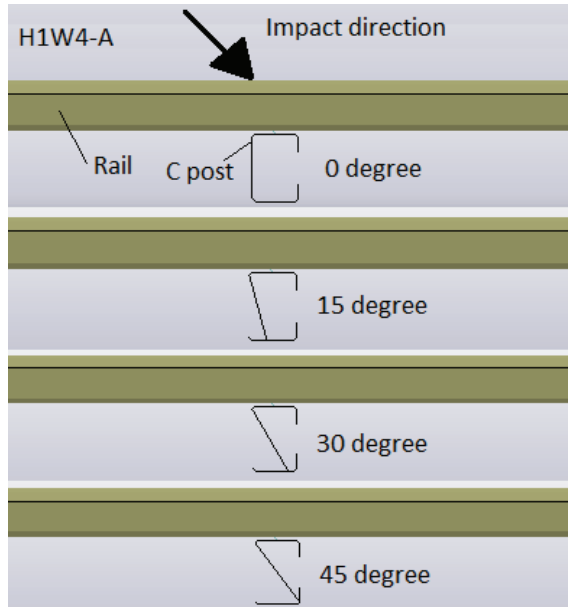

Figure 8 - The perpendicular edge of the C post that changed angularly in the direction of impact.

direction. Therefore, it is thought that the performance of post will improve. Hence, in this study, it is aimed to improve the performance of the C post in the H1 system based on the impact angles in the TB11 and TB42 tests. The perpendicular edge of the C post to the rail has been changed to 0-15-30-45 degree in the impact direction, and the optimum angle has been optimized based on the safety and structural performance of the guardrail. For this, using the validated model, the perpendicular edge of the C post was changed angularly in the direction of impact as shown in Figure 8 and subjected to TB11 and TB42 tests.

3.1. FE Analysis and Results

A total of 8 analyses were performed for 4 variations of C post. Four of them are TB11 test and four of them are TB42 test. Safety and structural performance data from TB11 (ASI-THIV) and TB42 (W, α) tests are given in Table 7.

Table 7 - Quantitative comparison of data obtained from TB11 and TB42 tests in FE.

Tests	Parameters	Degree			
		0°	15°	30°	45°
TB11	ASI	0.79	0.83	0.85	0.88
	THIV (km/h)	21	23	24	26
TB42	W (m)	1.20	1.10	1.04	0.95
	α(°)	10	31	40	41

In Figure 8, the impact direction and the angular change of the C post body are given. Looking at the values in Table 7, it can be seen that as the angle of impact increases, guardrail safety values such as ASI-THIV increase. This means that the rigidity of the guardrail system increases. The increase in the ASI value means the increase in the impact severity and acceleration values. In fact, it is not desirable for security parameters like ASI-THIV to be large. However, in this study, it is aimed to increase the load impact performance of the C post, and it can be seen with the ASI values given in Figures 9 and 10 that as the angular value in the body of the C post increases in the impact direction, its rigidity increases, because increasing rigidity allow more economical design.

Parameters such as the working width (W) and the exit angle (α), which also show the structural performance, are other parameters that show the rigidity of the guardrail. W value is small in rigid guardrails. In Figure 11, the variation of W value depending on the angular value is given. It is seen that the W value decreases as the body angle of C post increases in the direction of impact. This means that the rigidity of the guardrail increases. Different studies support this finding. For example, in a study [10], the mechanical performances of guardrail posts with different cross-sections such as rigidity, displacement, and rotation at different impact angles were investigated, and it was determined that the weakest cross-section post among S, I, Z, C, circular, and rectangular cross-section posts for head-on and angular impacts was the C post, and the best performing posts were closed cross-section

posts, as well as I and Z cross-section posts. The increase in rigidity in terms of posts means that a more rigid post can perform the same as a weak post with less material. From here we can deduce: The post (Z) obtained with a 45-degree angle can show the performance of the C post with more economical sections. Therefore, for more economical guardrail design, posts that perform in the impact direction (such as Z-type) should be used.
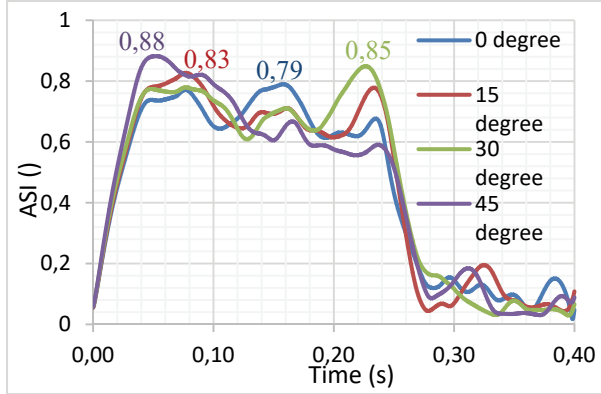

Figure 9 - ASI maximum and graphical values for different degrees from TB11 test.

The proposed Z post in the study has been developed with the assumption that it will be positioned in the direction of traffic flow, similar to the C post. Currently, Z posts in use are also positioned this way. However, in future studies, optimization of the specific placement angle of the Z post for different impact angles can be investigated. Additionally, existing Z posts are produced through cold forming/bending processes. It is well known that welded production can lead to residual stresses and cause time delays during the manufacturing process. Therefore, cold forming/bending is recommended, especially for guardrail components.
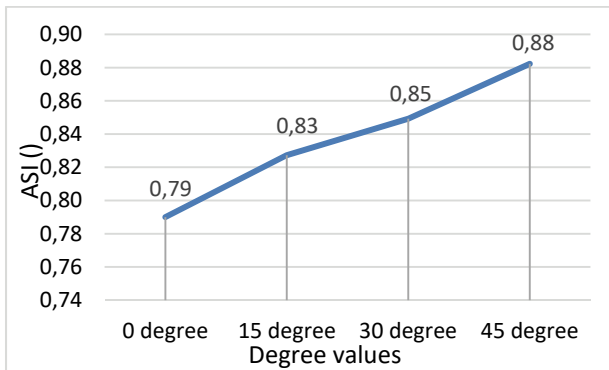

Figure 10 - Increase in ASI values depending on degrees.

In this study, it was aimed to redesign and optimize the body section of the C post section, based on the safety and structural performance of the H1W4-A guardrail. From the results obtained, it was understood that the cross-section of the C post evolved to Z and the body angle closest to the impact angle showed the best performance. In future studies, it will be investigated how many (%) more economical guardrails can be designed with Z post compared to C post for the same safety and structural performance situation. The economical investigation here is the comparison of the production material (steel) per meter of two posts in kg, and the decrease in the Z post is expressed as a percentage (%).
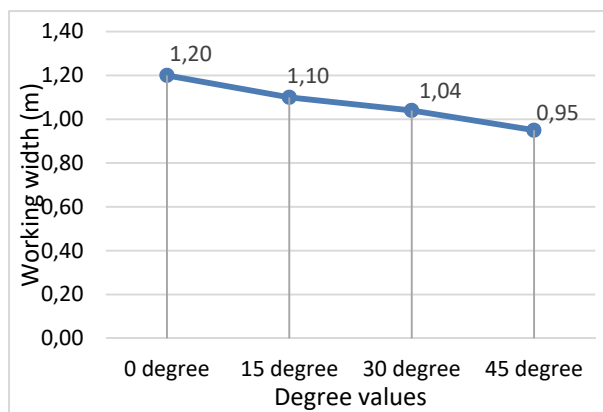

Figure 11 - Decrease in W values depending on degrees.

4. CONCLUSION AND RECOMMENDATIONS

In this study, it is aimed to improve the performance of the C post with the help of finite elements (FE). For this, the H1W4-A guardrail system, which has been applied and crash-tested, has been used. The FE model was calibrated and validated using crash test data. Then, using the validated model, 8 analyses were performed by increasing the perpendicular edge of the C post to the guardrail angularly in the direction of impact. The analyses showed that both the safety and the structural performance parameters increased with the increase of the body angle of the C post. This shows that the rigidity of the guardrail system has increased. The C post body angle closest to the crash angle showed the best performance in terms of safety and structure. From the results obtained, it has been seen that the C post has evolved into a post with a 45-degree body (Z type). It was understood that the obtained Z type post performed better than C. Therefore, it is thought that the new post will offer more economical sections under the same safety and structural design condition. To advance this study in the future, the following suggestions could be considered:

- It is recommended to develop a placement guide for Z-profile posts based on impact angles, optimize the design of the connection with W-beams, and thoroughly analyze manufacturing challenges in cold forming processes. Additionally, investigating performance improvements with alternative materials, validating findings through field tests, and exploring modular and adjustable designs to enhance flexibility are crucial.

Ensuring compliance with international standards and evaluating economic and environmental impacts will further support the large-scale applicability of the design.

- Conduct a comprehensive economic analysis to assess the cost advantage of the Z post compared to the C post. Factors such as steel cost, production processes, ease of installation, and maintenance expenses could be considered to evaluate the economic sustainability of the Z post in more detail.

- Evaluate the performance of the Z post at different impact angles. Crash tests conducted at varying speeds and angles could better reveal the system's adaptability to different scenarios.

- Consider using alternative materials to improve the performance of the Z post. For example, high-strength steel alloys or lightweight composite materials could enhance performance while reducing costs.

- Test the developed Z post in real road conditions under various climate, traffic, and environmental circumstances. Collecting and analyzing field data would help validate theoretical results in practical scenarios.

Funding

Authors' Contribution

The authors contributed equally to the study.

The Declaration of Conflict of Interest/ Common Interest

No conflict of interest or common interest has been declared by the authors.

The Declaration of Ethics Committee Approval

This study does not require ethics committee permission or any special permission.

The Declaration of Research and Publication Ethics

The authors of the paper declare that they comply with the scientific, ethical and quotation rules of Turkish Journal of Civil Engineering in all processes of the paper and that they do not make any falsification on the data collected. In addition, they declare that Turkish Journal of Civil Engineering and its editorial board have no responsibility for any ethical violations that may be encountered, and that this study has not been evaluated in any academic publication environment other than Turkish Journal of Civil Engineering.

References

[1] T.-L. Teng, C. Liang, C. Hsu, C. Shih, and T. Tran, "Impact Performance of W-beam Guardrail Supported by Different Shaped Posts," *International Journal of Mechanical Engineering and Applications*, vol. 4, no. 2, p. 59, 2016, doi: 10.11648/j.ijmea.20160402.14.

[2] EN1317-2, *Road restraint systems - Part 2: Performance classes, impact test acceptance criteria and test methods for safety barriers including vehicle parapets Dispositifs*. 2010.

[3] American Association of State Highway and Transportation Officials, *Manual for assessing safety hardware, 2009.* 2009, p. 259.

[4] W. Wu and R. Thomson, "A study of the interaction between a guardrail post and soil during quasi-static and dynamic loading," *Int J Impact Eng*, vol. 34, no. 5, pp. 883–898, 2007, doi: 10.1016/j.ijimpeng.2006.04.004.

[5] O. Prentkovskis, A. Beljatynskij, E. Juodvalkiene, and R. Prentkovskiene, "A study of the deflections of metal road guardrail post," *Baltic Journal of Road and Bridge Engineering*, vol. 5, no. 2, pp. 104–109, 2010, doi: 10.3846/bjrbe.2010.15.

[6] N. M. Sheikh and R. P. Bligh, "Finite Element Modeling and Validation of Guardrail Steel Post Deflecting in Soil at Varying Embedment Depths," *11th International LS-DYNA® Users Conference*, no. 4, 2011.

[7] S. Ozcanan and A. O. Atahan, "Radial basis function surrogate model-based optimization of guardrail post embedment depth in different soil conditions," *Proceedings of the Institution of Mechanical Engineers, Part D: Journal of Automobile Engineering*, vol. 234, no. 2–3, pp. 739–761, Feb. 2020, doi: 10.1177/0954407019848548.

[8] M. Örnek, A. O. Atahan, Y. Türedi, M. M. Erdem, and M. Büyük, "Soil based design of highway guardrail post depths using pendulum impact tests," *Acta Geotechnica Slovenica*, vol. 16, no. 2, pp. 77–89, 2019, doi: 10.18690/actageotechslov.16.2.77-89.2019.

[9] A. O. Atahan, M. Büyük, M. Örnek, M. Erdem, and Y. Turedi, "Determination of optimum post embedment depth for C120 steel posts using field and full scale crash test," *International Journal of Crashworthiness*, vol. 24, no. 5, pp. 533–542, 2019, doi: 10.1080/13588265.2018.1479499.

[10] Ozcanan S. Head-on and angular impact-based investigation of mechanical behavior of guardrail post types with finite element analysis. *Proceedings of the Institution of Mechanical Engineers, Part C: Journal of Mechanical Engineering Science*. 2024;238(4):1112-1124. doi:10.1177/09544062231179990

[11] D. Marzougui, P. Mohan, and S. Kan, "Evaluation of Rail Heights Effects on the Safety Performance of W - Beam Barriers," *FHWA/NHTSA National Crash Analysis Center*, no. November, pp. 1–30, 2007.

[12] K. S. Tan, W. Tan, and S. v. Wong, "Design of motorcyclist-friendly guardrail using finite element analysis," *International Journal of Crashworthiness*, vol. 13, no. 5, pp. 567–577, 2008, doi: 10.1080/13588260802293186.

[13] M. R. Ferdous, A. Abu-Odeh, R. P. Bligh, H. L. Jones, and N. M. Sheikh, "Performance limit analysis for common roadside and median barriers using LS-DYNA," *International Journal of Crashworthiness*, vol. 16, no. 6, pp. 691–706, 2011, doi: 10.1080/13588265.2011.623023.

[14] Z. Li, H. Fang, J. Fatoki, M. Gutowski, and Q. Wang, "A numerical study of strong-post double-faced W-beam and Thrie-beam guardrails under impacts of vehicles of multiple size classes," *Accid Anal Prev*, vol. 159, no. June, p. 106286, 2021, doi: 10.1016/j.aap.2021.106286.

[15] H. A. Whitworth, R. Bendidi, D. Marzougui, and R. Reiss, "Finite element modeling of the crash performance of roadside barriers," *International Journal of Crashworthiness*, vol. 9, no. 1, pp. 35–43, 2004, doi: 10.1533/ijcr.2004.0270.

[16] C. E. Hampton and H. C. Gabler, "Crash performance of strong-post W-beam guardrail with missing blockouts," *International Journal of Crashworthiness*, vol. 17, no. 1, pp. 93–103, 2012, doi: 10.1080/13588265.2011.626931.

[17] M. Klasztorny, D. Nycz, and R. Romanowski, "Rubber / Foam / Composite Overlay Onto Guide B of Barrier Located on Road Bend," *Archiwum Motoryzacji*, vol. 69, no. November, pp. 65–86, 2015.

[18] S. Ozcanan and A. O. Atahan, "RBF surrogate model and EN1317 collision safety-based optimization of two guardrails," *Structural and Multidisciplinary Optimization*, vol. 60, no. 1, pp. 343–362, Jul. 2019, doi: 10.1007/s00158-019-02203-z.

[19] S. Ozcanan and A. O. Atahan, "Minimization of Accident Severity Index in concrete barrier designs using an ensemble of radial basis function metamodel-based optimization," *Optimization and Engineering*, vol. 22, no. 1, pp. 485–519, Mar. 2021, doi: 10.1007/s11081-020-09522-x.

[20] İ. Yılmaz, İ. Yelek, S. Özcanan, A. O. Atahan, and J. M. Hiekmann, "Artificial neural network metamodeling-based design optimization of a continuous motorcyclists protection barrier system," *Structural and Multidisciplinary Optimization*, 2021, doi: 10.1007/s00158-021-03080-1.

[21] M. Y. Apak *et al.*, "Finite element simulation and failure analysis of fixed bollard system according to the PAS 68:2013 standard," *Eng Fail Anal*, vol. 135, no. February, p. 106151, 2022, doi: 10.1016/j.engfailanal.2022.106151.

[22] H. I. Yumrutas, S. Ozcanan, and M. Y. Apak, "Experimental and numerical comparative crashworthiness analysis of innovative renewable hybrid barrier with conventional roadside barriers," *International Journal of* Crashworthiness, vol. 0, no. 0, pp. 1–17, 2022, doi: 10.1080/13588265.2022.2075124.

[23] Yorur, H., Ozcanan, S., Yumrutas, H. I., and Birinci, E. "Renewable hybrid roadside barrier: Optimization of timber thickness," *BioResources* 18(1), 2023, 804-82. DOI: 10.15376/biores.18.1.804-826

[24] S. Ozcanan and O. Ozcan, "Criteria inadequacy of the vehicles used for the calculation of safety parameters in the EN1317-TB11 test," 2022, doi: 10.1177/09544070221115010.

[25] Ozcanan, S. (2023). Finite Element Analysis and Investigation of Critical Impact Point of Steel Guardrails Affecting Safety and Structural Performance. *Turkish Journal of Civil Engineering*, 34(2), 125-144. https://doi.org/10.18400/tjce.1238657

[26] NCAC (2008) Finite element model archive, George Washington University FHWA/NHTSA National Crash Analysis Center, http://www.ncac.gwu.edu/vml/models.html, Virginia (Accessed 2008)

[27] Europan Norm, "BS EN 16303:2020 BSI Standards Publication Road restraint systems - Validation and verification process for the use of virtual testing in crash testing against vehicle restraint system," 2020.

[28] CSI (2017) Crash testing of H1 and H2 guardrails systems. 0021\ME\HRB\17, Bollate, Italy

Evaluation of Wind Power Plants from the Aspect of Earthquake Design

Cüneyt TÜZÜN[1]*
Murat ERÖZ[2]
Tolga CIMILLI[3]
Mustafa ERDIK[4]

ABSTRACT

In recent years, Türkiye has steadily invested in renewable energy including wind turbines Conseqently their share in the total generation of energy in the country has been increasing every year. Considering the cost of wind power plants, together with the targeted amount of energy generation, earthquake planning for these systems becomes crucial. Earthquakes are one of the principal risks of wind energy investments, especially when considering the earthquake hazard level in a large portion of the country. Under the present circumstances, the companies producing wind turbines conduct the analysis and planning they deem necessary and forward these to the investors in our country. The extent to which manufacturers consider earthquake parameters and analysis methods in the design of wind turbines for earthquake resistance is not well-defined. The lack of clarity makes it difficult for investors to accurately evaluate the suitability of wind turbine tower and foundation designs for the specific conditions of the country.

This study evaluates earthquake design methods by investigating the regulations used in the design of wind turbines around the world. The magnitude of ground motion considered in the earthquake design, the method of analysis used, the load combinations on which the designs are based, and the criteria for the designs have been inspected. Moreover, the design documents for a wind turbine that is being constructed have been examined in detail, with the earthquake design stage being especially scrutinized.

Assessments and recommendations have been made regarding the design specifications, analysis methods and criteria used in the analysis and design of the wind turbines currently being built in our country. Subsequently, obtained recommendations have been taken into consideration to propose an earthquake design procedure for the earthquake design of wind turbines.

Keywords: Wind power, seismic design, design criteria.

1. INTRODUCTION

The implementation of wind power plants has been continuously increasing in Türkiye in recent years. Consequently, their share in the total generation of energy in the country is also increasing every year. Considering the cost of wind power plants, together with the targeted amount of energy generation, earthquake planning for these systems becomes crucial. Earthquakes are one of the principal risks of wind energy investments, especially when considering the earthquake hazard in a large part of the country. Under the present circumstances, the companies producing wind turbines conduct the analysis and planning they deem necessary and forward these to the investors in the country. The extent to which manufacturers consider earthquake parameters and analysis methods in the design of wind turbines for earthquake resistance are not well-defined. The lack of clarity makes it difficult for investors to accurately evaluate the suitability of wind turbine tower and foundation designs for the specific conditions of the country.

This study evaluates earthquake design methods by reviewing the regulations used in the design of wind turbines around the world. The magnitude of ground motion considered in the earthquake design, the method of analysis used, the load combinations on which the designs are based, and the criteria for the designs have been examined. Moreover, the design documents for a wind turbine that is being constructed has been examined in detail, with the earthquake design stage being especially scrutinized.

Assessments and recommendations have been made regarding the design specifications, analysis methods and criteria used in the analysis and design of the wind turbines currently being built in the country. Subsequently, obtained recommendations have been taken into consideration to propose an earthquake design procedure for the earthquake design of wind turbines.

2. TYPES OF DAMAGE IN WIND POWER PLANTS (WPP) DUE TO EARTHQUAKE

The current literature does not contain any information on damages caused by earthquakes to WPPs. The primary reason for this is that the average period in which earthquakes of a certain high magnitude recur is typically quite long, while at the same time, the number and geographic distribution of the relevant systems have only begun to increase in the last twenty years.

However, considering the geometric and construction specifications of WPP-type structures, the locations and types of damage expected due to the impact of an earthquake can be listed as follows:

i.   Tower - Crushing and cracking in the concrete at the connection of the tower to the foundation.

ii.   Tower - Local bending and buckling in the tower components at the connection of the tower to the foundation.

iii. Tower - Shear and bending damages in the tower components at the connection of the tower to the foundation

iv.   Bending and shear damage in the flanges and bolts at the joints of the tower components

v.   Bending damage in the reinforced concrete component of the foundation

vi.   Damage to the load-bearing system due to excessive deformation on the ground under the foundation

vii. Damage to the moving mechanisms of the nacelle due to a high degree of horizontal ground motion and acceleration.

Figure 1 - Damage at the connection of the tower and the foundation of a WPP

Figure 2 - Possible damage of WWP due to earthquake [16]

After the site visits of existing WPPs Kahramanmaras Earthquakes that occurred on 6 February 2023, it has been observed that the most common structural problems in turbines in Türkiye occur at the foundation and/or the tower and at the foundation connections. The sources of these problems encountered in the foundations are primarily related to the quality of reinforced concrete construction, reinforcement layout and arrangement, reinforcement concrete covers, and concrete curing. The most common problem among them is the separation of the base-tower connection over time. Problems that may arise in the tower-base connection are mostly because of bending. In some cases, permanent bending deformations may also occur in the tower. Moreover, general internal-external foundation controls that are primarily evaluated by visual inspection and conducted rapidly pose significant risks. Microcracks that may occur can be a precursor to a serious problem in the future.

The problems in the foundation generally stem from design errors and workmanship issues in the application. In particular, the lack of sufficient inspection in Türkiye, coupled with rapid manufacturing processes, results in problems in the foundation.

To identify the types of damage mentioned above, a systematic examination and observation is the most appropriate approach. To this end, the following activities are recommended:

i.   Monitor and compare horizontal displacement and acceleration values in the support system of the WPP with the design parameters.

ii.   Continuously measure the tilt and deformations occurring at the transition between the tower and the foundation of the WPP tower.

iii. In the event of an earthquake that occurs within 30 km of the WPP, torque control should be performed on the foundation connection bolts.

iv.   Inspect the foundation concrete, including the junction between the tower and the concrete, both inside and outside the tower, for cracks resulting from crushing, as well as possible deformations on the concrete surface.

v.   Inspect non-structural elements inside the tower.

3. DESIGN REGULATIONS FOR WIND POWER PLANTS (WPPS)

The main regulations and specifications widely accepted and used worldwide for the design of WPPs that form the basis of this study have been examined. The main components of the analysis include the loads considered in the structural design, load combinations, structural analysis methods, structural modeling rules, design criteria, and methods. In the examination, the latest versions of the regulations that are widely used both in our country and in the world have been considered. These regulations are as follows:

i.   Turkish Standards, TS EN 61400 -1 (April 2006), Wind Turbines - Part 1: Design requirements (Wind Turbines - Part 1: Wind turbine generator systems, Safety requirements, (IEC 61400-1:1999, modified)

ii.   INTERNATIONAL STANDARD IEC 61400-1, Wind turbines – Part 1: Design requirements 2005

iii. ACP 61400-1-202x, Wind Energy Generation Systems – Part 1: Design requirements – Modified Adoption of IEC 61400-1

iv. SASO IEC 61400-3-1: 2020, IEC 61400-3-1: 2019, Wind energy generation systems – Part 3-1: Design requirements for fixed offshore wind turbines

v. Germanischer Lloyd: Guideline for the Certification of Wind Turbines, Basic Principles for Design and Construction, 2010

vi. DNVGL-ST-0437 Edition November 2016, Loads and site conditions for wind turbines

vii. ASCE/AWEA RP2011, Recommended Practice for Compliance of Large Land-based Wind Turbine Support Structures

viii. DNV GL AS, DNVGL-ST-0437 Edition, November 2016, Loads and site conditions for wind turbines

ix. ASCE/AWEA RP2011, Recommended Practice for Compliance of Large Land-based Wind Turbine Support Structures

Some of the regulations comprise expanded versions of some main regulations and others compromise modified versions consistent with the dissimilar conditions of various countries.

The most important point to be emphasized here is that, since these regulations are used widely in the world, it is necessary to refer to the specifications and guidelines in local regulations and engineering practices both in analysis and design processes, or to leave the relevant design decisions to the approach of the engineer responsible for the design.

The earthquake design approaches in the examined regulations contain quite general expressions and approaches, and parameters to be used in WPP seismic design are left to countries' local regulations.

In the light of the above-mentioned issues, in the design of WPP in regions where earthquake hazard is high in Türkiye, the most rational and current data and methods focused on practical implementation have been determined by conducting a detailed evaluation of the most frequently used documents (i), (iii) and (viii) from these regulations, with the aim of establishing a more rational design approach.

3.1. Turkish Standards, TS EN 61400 -1 (April 2006)

This regulation, *Turkish Standards, TS EN 61400-1 (April 2006), Wind turbines - Part 1: Design requirements, Wind turbine generator systems, Part 1: Safety requirements, (IEC 61400-1:1999, modified)*, has been accepted as a Turkish Standard by the Turkish Standards Institute, based on the relevant European standard.

In the section related to definition of seismic input definition of the relevant regulation, it is clearly stated that "*there are no earthquake resistance requirements for standard class turbines*". However, the regulation also stated that in regions with high earthquake hazard, the section referred to as "*Annex C*" can be used. It is noted here that earthquake loads can be considered together with significant and frequently occurring operating loads. The ground movement sets, and response spectra set out in the local regulations may be used in the determination of the earthquake loads. For the determination of earthquake loads, the ground

motion level with a 10% probability of exceedance within a 50-year period (average recurrence period of 475 years) is considered. Earthquake loads are combined with (a) normal operating loads and (b) the larger of the loading that occurs during emergency shutdowns. In addition, the load factors for design are considered as 1.0 in load combinations where earthquake loading is considered. When considering earthquake loading in the time domain, enough ground motions are required to be taken into account and combined with operating loads. For the determination of the resistance under earthquake loading, the structure should exhibit limited ductile and elastic behavior.

3.2. ACP 61400-1-202x, Wind Energy Generation Systems – Part 1: Design requirements – Modified Adoption of IEC 61400-1

The document is one of the most current documents used for wind turbine design and was created by the updating of IEC 61400-1 document. This document primarily proposes 2 approaches for ensuring the safety and integrity of the support structure:

- Verifying the safety of the system by considering the largest expected impacts during the operational process of the WPP design

- Verifying the structural integrity by considering the largest values of the effects in the region where the system is located

The document does not specifically mention the design of WPPs under earthquake effects. It is noted that earthquake hazards should be considered in the design stages in the regions where seismic activity is high, and the design steps are explained. The fundamental approach in the earthquake design is to combine seismic loads with significant and frequent operating loads arise during the wind turbine operation period.

3.3. DNV GL AS, DNVGL-ST-0437 Edition, November 2016, Loads and Site Conditions for Wind Turbines

The DNV - GL document is a standard where the design principles, technical requirements, loads to be considered and site conditions of the wind turbines are fundamentally set out. The principal purpose of this standard is to specify the loads that are to be considered in the design of wind turbines under an acceptable level of safety, as well as to determine the principles of design under different load conditions, for designers, manufacturers and administrators. Taking into consideration the standards in practice and engineering practices, the document also serves as a guide for the design of wind turbines.

The earthquake effect in the document is referenced to the latest version of IEC 61400-1 regulation [1]. It is stated that local earthquake codes should be considered in regions where earthquake hazard is high, and in the absence of appropriate local codes, Eurocode 8 [2] and/or API 2RP [3] documents can be used. Combining the earthquake loads corresponding to ground motion level with an average recurrence period of 475 years and wind loads in the earthquake design of wind turbines is recommended.

The rules required for the determination of the design loads to be used during structural analysis are defined in this document. It is stated that linear analysis methods are to be used

in the structural calculations, but that non-linear methods may also be used where the ground conditions may result in excessive deformations. It is emphasized that it is important for the structural model to be used, both in linear and non-linear analyses, to be established in a manner to reflect the dynamic behavior in the most rational way possible. The definitions of the load components to be used under all these loading conditions and the design are set out in the form of tables.

4. EVALUATION OF THE REGULATIONS IN EFFECT FROM THE ASPECT OF EARTHQUAKE DESIGN APPROACHES

The highlighted aspects compiled from evaluations made within the framework of analysis and design rules specified for the design of wind turbines in the examined regulations are presented below in bullet points.

- Due to the application of WPPs in many different regions of the world, earthquake effect is not initially considered as a priority in the relevant design codes.

- The conditions regarding the earthquake loading are specified in the sections of the regulations referred to as "extreme loading".

- For WPPs that are installed in regions where the earthquake risk is high, it is indicated that the effect of earthquakes should be considered.

- No specific limit parameter has been defined for the criteria of high earthquake hazard, and the local regulations that are applicable in the relevant region has been referenced.

- The regulations recommend that in case of considering the earthquake effect in the design, the earthquake loads should be considered along with operation, emergency stop, restart, and extreme wind loads.

- Considering an earthquake ground motion with a 10% probability of exceedance in 50 years is recommended in the earthquake design.

- Although a specific target is not given for the earthquake performance level, definitions such as maintaining the integrity and stability of the system under operational loads during the earthquake are provided, and no specific value is given for performance criteria. However, it is required to ensure that the units comprising the structural system should remain within elastic limits.

- The recommended analysis methods include the time-domain analysis and mode combination methods, which are specified in all regulations, and the mathematical model of the structural system is considered using the packed mass approach.

- Particularly in the current regulations, emphasis is placed on the need for more detailed modeling and analysis approaches for the earthquake analysis and design, as well as the control of the system integrity and verification of the structural elements' behavior remains within elastic limits.

- It is recommended to perform structural analysis to obtain the displacement and acceleration values generated in the rotor and other moving components on the tower during the earthquake effect, and to compare them with the limit values defined by

the manufacturer for the safe operation of the system. However, there is no control or suggestion mechanism regarding whether these elements exhibit nonlinear behavior under the design earthquake level.

- In earthquake analysis, it is recommended to use a structural damping ratio of 1%.

- It is stated that for the design of the foundation system of WPPs under the earthquake effect, not only the stress distribution that will occur at the foundation but also the deformations in the soil should be determined. For this purpose, it is stated that experiments and analyses should be carried out to determine the dynamic properties of the soil within the scope of local soil investigations.

- In only one regulation [7], it is stated that the acceleration values affecting the non-structural elements of a WPP should be determined and possible negative effects on the integrity and operation of the system under the occurring displacements should be controlled.

5. THE EVALUATION OF WPP DESIGN APPLICATION PRACTICE IN TÜRKIYE

After reviewing analysis reports of a WPP currently being applied to evaluate the analysis and design stages of wind turbine applications constructed in Türkiye, the following points have emerged:

5.1. Soil Investigation Practices

Geotechnical investigation studies carried out in the scope of the earthquake design mainly intend to determine the soil bearing capacity. The soil investigation and analysis activities specified in Section 16 of the Turkish Building Seismic Regulation (2018) are not adequately carried out within the scope of soil investigation studies. Insufficient number and depth of borehole drilling and geophysical surveys are being carried out to determine the distribution of the shear wave velocity (V_{s30}) that is required to determine the parameters for the earthquake design, and this prevents the correct determination of the soil class as stated in the earthquake regulation.

5.2. The Determination of the Earthquake Parameters

In the earthquake design of WPPs, the earthquake parameters taken into consideration in practice are based on the Türkiye Seismic Hazard Map (TSHM) published in 2018. As known, during the preparation phase of the aforementioned map, effects such as "*effect of near-fault*", "*directional effect*", "*orientation effect*" and "*topographic conditions*" were not taken into account in determining the earthquake parameters.

Additionally, another important point is that the high natural frequencies of WPPs require a specific examination of the earthquake spectrum provided within the scope of TSHM (2018) for high-period systems.

5.3. The Modelling of the Structural System

The mathematical models considered in the seismic analysis of WPPs in practice are greatly simplified models. The support systems of WPP-type structures are quite simple, and the packed mass modeling approach with the mass concentrated at the top point provides a sufficient modeling in the seismic analysis. However, this simple approach is not used in practice and the structural analysis is only used to determine stress distribution occurring below the foundation system. In practice, the tower system is not considered in the mathematical model, and fictitious forces provided by the WPP manufacturer at a certain height in the superstructure are used for the foundation analysis and design. In determining the stresses on the foundation, no special or detailed modeling work related to the soil is performed, and simple support approaches are applied.

Existing literature regarding modeling wind turbines for seismic loading is divided between two types of models; models that focus on the tower by accounting for the mass of the nacelle and rotor as a point mass at the top of the tower; and models that describe the full turbine including the nacelle and rotor with some level of detail. Simplified models are preferable because they remove the complexity of modeling the rotor. But it should be emphasized that the simplified approach in which the turbine is considered as a SDOF system and may be unreliable for modeling behavior that arises from modes other than the first tower mode.

5.4. The Methods of Earthquake Response Analysis

In practice, no calculation or analysis is carried out to determine the section forces occurring in WPPs under the effect of earthquakes. In the design phase, internal forces resulting from earthquake effects are provided by the manufacturer, and the earthquake parameters and analysis methods used to obtain these values are not specified.

The analysis methods used in the earthquake design of structures, namely "*equivalent earthquake load* ", "*mode superposition*", and "*time-domain analysis*" methods, can also be applied to WPPs. In case the performance-based design approach is applied as an advanced earthquake analysis method, then "*the non-linear analysis*" can also be used in the earthquake design. In practice, the rational approach from an engineering standpoint is to obtain the section forces related to the earthquake loading by considering all the characteristics of the structure by the design engineer, rather than receiving them from the manufacturers and using without analysis. These values should then be compared with those provided by the manufacturer before being utilized.

In terms of consistency in design, conducting an earthquake analysis using the locally applicable earthquake parameters and monitoring the displacements and deformations occur in the event of an earthquake is recommended.

5.5. The Analysis and Design of the Foundation

During the foundation analysis and design phase of WPPs, simple approaches are used for soil modeling to determine the stresses and cross-sectional forces that emerge at the foundation base. To determine the stress distribution occurring on the foundation in the most rational way, modeling the soil behavior efficiently is required. Especially due to the

occurrence of tensile effects in the stress distribution that will occur below the foundation, the calculation of the primary loads that form the basis of tension distribution and soil modeling are of great importance.

In practice, the approaches used for the analysis and design of the soil and the foundation system contain inadequacies in determining both the soil tension distribution and the internal forces and soil deformations essential to the design. Adopting a more feasible modeling approach for the soil characteristics to determine the stress distribution of soil, deformation, and cross-sectional forces is required.

The reinforced concrete calculation of foundation section shall be performed within the framework of the TS500 requirements in effect in Türkiye, while the ACI-318 and EC 2 reinforced concrete design regulations accepted in the international arena may also be used.

5.6. Recommendations for Earthquake Analysis and Design Practice for WPP Systems

Distinctively different approaches and design procedures can be seen when the stages of the analysis and design of wind turbines in practice in Türkiye are examined. One of the main reasons for this situation is the lack of regulations for existing designs that can be followed in Türkiye.

Certain approaches and criteria for a more rational consideration of the impact of earthquakes at the analysis and design stages are recommended because of the investigations and evaluations which have been conducted. These recommendations are as follows:

- Evaluating the behavior of the WPP support system under the effect of the earthquakes (*limiting the relative displacement*)

- Analyzing and evaluating the effect of horizontal displacement and acceleration limits occurring in the system during the power production stage of WPP systems on operational efficiency

- Controlling the behavior of the non-structural systems in the WPP systems under the effect of earthquakes (*detecting the displacement and acceleration levels of the systems that can affect production*)

- The realization of the design of the WPP support system considering the post-elastic behavior *(including the determination of the deformations occurring at the tower and connection points by considering the material-based and geometrical post-elasticity situations)* under the effect of earthquakes.

- Defining a specific performance criterion to be determined by the manufacturer at different earthquake levels for the design of WPP support systems *(determining economic and downtime loss within the framework of performance-based design)*

6. AN ALTERNATIVE APPROACH TO THE EARTHQUAKE DESIGN OF WIND TURBINES

The adequacy of the designs created by WPP manufacturers under the effect of earthquakes should be reviewed based on the latest data, adopting the most up-to-date approaches. Considering the costs of these investments and the benefits they will provide throughout their service life, the importance of the earthquake design of these systems becomes evident once again.

In case of constructing such systems in areas with high earthquake hazard, it is recommended that the designer, manufacturer, and investor confer to determine the expected performance under the effect of earthquakes and establish the necessary design criteria to achieve this performance. Potential economic losses and operational continuity must also be considered during the performance assessment.

It is recommended that the following factors should be included within the scope of these special technical specifications:

- Conducting a site-specific earthquake hazard analysis and preparing the design acceleration spectrum of the design and ground motion records to be used in analysis for the relevant magnitudes of earthquake.

- Conducting a sufficient soil investigation and analysis to determine the aerodynamic characteristics of the soil.

- The use of mathematical models that consider the system behavior more appropriately according to the soil and earthquake conditions in which the system is located (soil, superstructure, and soil-structure interaction)

- Realization of nonlinear analysis in the time domain to demonstrate that the behavior of the system's current section, size, and connection details exhibit linear elastic behavior under the effect of earthquakes.

- The definition of required checks for non-structural elements for earthquake safety in the systems

- The checking of deformations expected to occur in the foundation during the operating lifespan of the systems by conducting structure - soil interaction analyses which consider soil deformations as well as the stress distribution in the soil

- Taking into consideration the second degree (P-delta) effects occurring as a result of the high level of horizontal displacements in the elements of the system.

For the WPPs which are designed with the knowledge that the risk of earthquakes in Türkiye is high in a large portion of the country, the most rational approach is determining the behavior of the wind turbine systems during operation and under the impact of earthquakes compatible with the conditions of the country and the expectations of investors.

All strategies recommended for every step throughout the design phase, including their scope, are summarized below.

6.1. The Determination of the Parameters for Soil Exploration and Design

Investigating the soil characteristics of the region where the WPP systems are located, directly impacts determining the earthquake parameters and the foundation design. Even though these systems are not classified as buildings, it will be appropriate for the scope of Part 16 of the Building Earthquake Regulations of Türkiye (2018) to be used to determine the framework of the ground investigation to be conducted in the relevant areas and the parameters that are relevant for the design.

When design soil surveys, the characteristics related to the special conditions of the project, the local soil structure, the seismicity of the region and the environmental conditions should be considered. The collection, recording and reporting of the data concerning the soil survey should be conducted in accordance with the relevant national and/or generally accepted international legislation, norms and standards.

6.2. Site-specific Earthquake Hazard Assessment

When the importance of these structures within the power generation system and their operational continuity is considered, the use of the parameters set out in the Earthquake Hazard Map of Türkiye published in 2018 in determining the parameters which will constitute a basis for earthquake design is not sufficient. The principal reason for this has been set out below in the form of main headings.

- The Near-Fault Directionality Effect

- The Directivity Effect

- Topographical Features

- High WPP natural vibration period

Near-fault and directionality effects, which are among the principal inputs in calculation of the earthquake risk, have not been considered when creating the Earthquake Hazard Map of Türkiye. Similarly, the current Seismic Regulation does not include the evaluation of the adverse topographical conditions. Additionally, due to significant free vibration periods of the WPP structures, the spectral acceleration levels stated in the current Seismic Regulation need to be examined. Lastly, the average renewal period (of earthquake levels), which is considered for the design of WPP structures, may vary from those provided within the scope of the earthquake regulations.

6.3. Structural Modeling Approaches

Horizontal-axis wind turbines consist of three main components: the tower, the nacelle, and the hub. (Figure 3) The tower supports the nacelles and raises the hub to the desired height. The nacelle contains the generator, gearbox, and the other mechanical components of the turbine, essential to supporting the hub. A typical structure used in a WPP is shown in Figure 3.
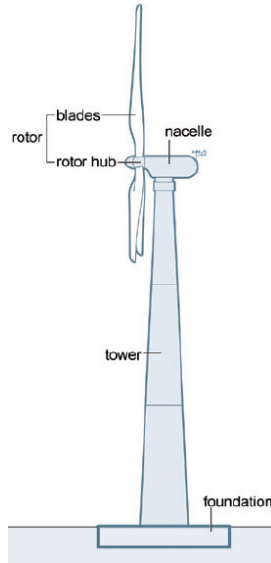
Figure 3 - The main components of the wind turbine

Two models are used in analyzing the reaction of wind turbines, the components of which are stated above, under external loads. The first is the simplified model in which the mass of the nacelle and rotor is regarded as a mass stacked on the top of the tower. This first modeling approach is called a single degree of freedom system, which only considers the tower to determine the behavior of wind turbines under the external effects by regarding the nacelle and rotor as a stacked mass on top of the tower. Simplified models are the most preferred models due to the complexity of the components at the top of the wind turbine.

The other approach, on the other hand, is a more complex and advanced modelling approach where all the parts constituting the turbine are modeled in a more detailed manner.

6.4. Design Loading and Load Combinations

The behavior of the turbine under different operating conditions, under wind and earthquake loads, is considered at the stage of the analysis of the wind turbines. Different effects occurring under different circumstances, including where the ground movement has an effect while the turbine is operating, where the ground movement has an effect while the turbine is parked and where the ground movement does and does not have an effect while the turbine is in idle mode, under the normal operational state of the turbine, are taken into consideration.

It is recommended that the earthquake loads equivalent to the ground movement levels in earthquakes with recurrence periods of 475 years and the wind loads are combined in the earthquake design of wind turbines. There are two principal loading conditions to be considered to ensure the integrity and safety of the wind turbines such as "Normal Loading Case which consists of the loadings affected by the design wind loads occurring under normal

operating conditions between the periods where the wind turbine is operating, and it is shut down and "Maximum Loading Case that consists of loading conditions with an expected recurrence period of 1 (one) and 50 (fifty) years during the operating life of the wind turbine.

6.5. Earthquake Analysis Methods

Either the equivalent earthquake load method, the response spectrum method or the time domain analysis shall be used as the earthquake analysis method. It is necessary for the "nacelle" effective mass to be packed together in the center of gravity of the wind turbine and for all the systems (stairs, platform, etc.) connected to the tower to be considered when calculating the effective earthquake mass in the model to be used for the earthquake analysis.

The earthquake behavior of the structural systems of WPP systems display an "inverted pendulum" type of behavior. With this behavior, the largest sectional effects and deformations arise at the foundation level. Even if a value for the wind turbine has not been implicitly defined for R values, the "seismic load reduction coefficient" which is to be used at the earthquake analysis and design stage in line with this behavior, R value is accepted as 1.5 - 2.5 for these types of structures, in practice (for the design).

It should be stated that linear methods of calculation are to be used in the structural analysis of these systems, but that non-linear methods may also be used under circumstances where the foundation conditions may cause excessive deformations. The importance of establishing the structural model to be used in a manner which will reflect the dynamic behavior in the most rational way possible, in both linear and non-linear analyses, should be emphasized.

In practice, two methods are mostly used in the earthquake analysis of wind turbines as; Mode Superposition Analysis and Time Domain Analysis.

6.6. Earthquake Performance Targets and Criteria

The shutdown of WPPs and damages at a level which can be repaired economically under the effect of a design earthquake are permitted.

While the permitted damage should not pose a threat to human life, depending on the number of WPPs in the field, it should also be noted that the direct or indirect economic loss caused by the damage may reach an unacceptable level for the operator.

Due to the second case mentioned above, the objective of maintaining operational continuity under a higher level of design earthquake is an approach that can be determined because of the owner's requests. However, the difference between the conditions required for "life safety", which is the minimum performance objective specified in the regulations, and the high-performance level should be clearly defined.

The current design philosophy in the effective regulations define the two performance levels set out below:

- The occurrence of very little damage and disruption in normal operations under the Design Earthquake Level (with a mean recurrence period of 475 years).

- The occurrence of no severe health, safety and environmental issues in rare earthquakes which are referred to as the Maximumt Earthquake Level, even if they do cause irreparable damage and economic loss to the WPP.

Deformation tolerances are generally expressed in terms of the permanent rotation angle allowed to occur at the base of the turbine, and it is recommended that earthquake-induced permanent slope should not exceed 0.5°. Considering this performance criterion, detailed analysis tools will be required to estimate the permanent slope of the foundation during design earthquake.

6.7. Limiting Horizontal Displacement in Application

No limit has been defined for the relative displacement value used in earthquake design for wind turbine systems. The determination of the value should be decided through the joint evaluation of the wind turbine manufacturer and the designer in accordance with the effective operation of the system and the targeted earthquake performance. On the other hand, it is more appropriate to determine this value by consulting with the manufacturer instead of using the limits given in the regulations for similar types of structures used in the relevant region.

6.8. Design of the Foundation System

International regulations are used in the design of the foundations of these towers as the rules and limits set out in the regulations for local structures are not extensive in the design of the foundations of wind turbines. However, in practice, the use of local regulations in the foundations of wind turbines is only possible where they have been approved by the authority which issues certifications.

The following parameters need to be examined for the analysis and design of the foundation:

- Uplift stress in soil
- Load-bearing capacity of soil
- Deformation of soil
- Rotation of foundation

Tensile stress that occurs during the calculation of ground uplift is allowed up to 50% of the foundation ground.

7. GENERAL EVALUATION AND CONCLUSION

This study has presented the current status of consideration of seismic loads for wind turbines. This subject is attracting more interest as the use of wind power grows, particularly in seismic regions.

A preliminary analysis based on existing guidelines has been conducted to understand how tower moment demand scales with rated power. The literature shows a development from simple models that focus on predicting tower loads to full system models that illuminate loads

for other components. The published analyses show that seismic loading may impact more than just the tower and suggest that full system models are important in analyzing seismic demand for turbines.

The important points revealed in the course of an assessment of the regulations and guidelines on the design of WPP systems in the world and an investigation into the design documents for the real practices in Türkiye have been set out in detail in the above sections.

The most fundamental conclusion which emerges in the light of these assessments is that the preparation of regulations or guidelines for the earthquake analysis and design stages of WPP systems shall be a rational approach.

Due to the reasons listed in the study, it is extremely important in a country like Türkiye, where earthquakehazard is high, that regulations based on the consensus that the size and power production of the investment to be undertaken should be high, that the parameters of the WPP systems to be used in earthquake design need to be determined and that the use of appropriate design procedures is the rational approach, are prepared, in order that the wind energy investments throughout the country can be realized in a consistent manner and in line with the current technical rules.

Approaches to design and criteria that should be prepared within the scope of "the earthquake design regulations for wind energy systems" as a result of activities to be conducted in this area in cooperation with investors in Wind Energy Systems and the authorities and institutions leading the sector, will thus become more suitable for implementation.

Lastly, it is considered that this document, which is to be referenced in the investments to be undertaken by investors, who hold an important position and share in the sector, will be an important step towards ensuring a certain standard within the sector and earthquake safety.

References

[1] IEC 61400-1 Wind Energy Generation Systems - Part 1: Design Requirements

[2] EUROPEAN STANDARD NORME EUROPEENNE EUROpAISCHE NORM EN 1998-1 December 2004

[3] API Recommended Practice 2A-WSD Planning, Design, and Constructing Fixed Offshore Platforms—Working Stress Design

[4] International Building Code, 2018

[5] Minimum Design Loads and Associated Criteria for Buildings and Other Structures, ASCE/SEI 7-16

[6] Minimum Design Loads and Associated Criteria for Buildings and Other Structures, ASCE/SEI 7-05

[7] Turkish Standards, TS EN 61400 -1 (April 2006), Wind turbines - Part 1: Design requirements, Wind turbine generator systems, Part 1: Safety requirements, (IEC 61400-1:1999, modified)

[8]   INTERNATIONAL STANDARD IEC 61400-1, Wind turbines - Part 1: Design requirements 2005

[9]   ACP 61400-1-202x, Wind Energy Generation Systems – Part 1: Design requirements – Modified Adoption of IEC 61400-1

[10] SASO IEC 61400-3-1: 2020, IEC 61400-3-1: 2019, Wind energy generation systems – Part 3-1: Design requirements for fixed offshore wind turbines

[11] Germanischer Lloyd: Guideline for the Certification of Wind Turbines, Basic Principles for Design and Construction, 2010

[12] DNVGL-ST-0437 Edition November 2016, Loads and site conditions for wind turbines

[13] ASCE/AWEA RP2011, Recommended Practice for Compliance of Large Land-based Wind Turbine Support Structures

[14] DNV GL AS, DNVGL-ST-0437 Edition, November 2016, Loads and site conditions for wind turbines

[15] ASCE/AWEA RP2011, Recommended Practice for Compliance of Large Land-based Wind Turbine Support Structures

[16] Li-Xin Duan, Wen-Da Wang, Long Zheng, Yan-Li Shi, "Dynamic response analysis of monopile CFDST wind turbine tower system under wind-wave-seismic coupling action", Thin-Walled Structures, Volume 202, September 2024, 112089

Turkish Journal of Civil Engineering (formerly Teknik Dergi)
Manuscript Drafting Rules

1. The manuscript (text, charts, equations, drawings etc.) should be arranged in Word and submitted in ready-to-print format. The article should be typed on A4 (210 x 297 mm) size paper using 10 pt (main title 15 pt) Times New Roman font, single spacing. Margins should be 40 mm on the left and right sides and 52.5 mm at the top and bottom of the page.

2. Including drawings and tables, articles should not exceed 25 pages, technical notes 10 pages. Drawings and tables should be clear and legible; should not use characters smaller than 8 pt.

3. A correct language conforming to the grammar rules should be used in drafting the manuscript. Third singular person and passive tense must be used, and no inverted sentences should be contained. Line numbers should be used throughout the text.

4. Title must be short (10 words maximum) and clear, and reflect the content of the paper.

5. Sections should be arranged as: (i) abstract and keywords, (ii) main text, (iii) symbols, (iv) acknowledgements and (v) references.

6. The abstract should briefly describe the object, scope, method and conclusions of the work and should not exceed 100 words. If necessary, abstract may be modified without consulting the author. At least three keywords must be given. Manuscript title, full names of authors, their affiliations and e-mail addresses should appear in the first page.

    An English abstract accompanied by English title and English keywords must be given before the abstract in manuscripts in Turkish.

7. Symbols must conform to the international rules; each symbol must be defined where it appears first, additionally, a list of symbols must be given in alphabetic order (first Latin, then Greek alphabets) at the end of the text, before References.

8. Equations must be numbered using numbers given in brackets at the end of the line.

9. Tables, drawings and photographs must be placed inside the text, each one should have a number and title. Titles should be written above the tables and below the drawings and photographs.

10. Only SI units must be used in the manuscripts.

11. Quotations must be given between inverted commas and the source must be indicated with a reference number.

12. Acknowledgement must be short and mention the people/ institutions contributed or assisted the study.

13. References must be numbered (in brackets) in the text referring to the reference list arranged in the order of appearance in the text. References must include the following information:

    If the reference is an article: Author's surname, his/her initials, other authors, full title of the article, name of the journal, volume, issue, starting and ending pages, year of publication.

    Example: Naghdi, P. M., Kalnins, A., On Vibrations of Elastic Spherical Shells. J. Appl. Mech., 29, 65-72, 1962.

    If the reference is a book: Author's surname, his/her initials, other authors, title of the book, volume number, editor if available, place of publication, year of publication.

    Example: Kraus. H., Thin Elastic Shells, New York. Wiley, 1967.

    If the reference is a conference paper: Author's surname, his/her initials, other authors, title of the paper, title of the conference, location and year.

    If the source is a thesis: Author's surname, his/her initials, thesis title, level, university, year.

    If the source is a report: Author's surname, his/her initials, other authors, title of the report, type, number, institution it is submitted to, publication place, year.

14. Discussions to an article published in Turkish Journal of Civil Engineering should not exceed two pages, must briefly express the addressed points, must criticise the content, not the author and must be written in a polite language. Authors' closing remarks must also follow the same rules.

15. Copyright has to be transferred to UCTEA Turkish Chamber of Civil Engineers. The standard "copyright form" signed by the authorised author and the standard "statement of originality" signed by all authors should be submitted together with the manuscript.

16. A separate note listing authors' names, business and home addresses and phone numbers and their brief resumes should accompany the manuscript.

17. The manuscript must be submitted through the DergiPark system. (https://dergipark.org.tr/tekderg)

CONTENTS